NASA TECHNICAL NOTE

NASA TN D-2536

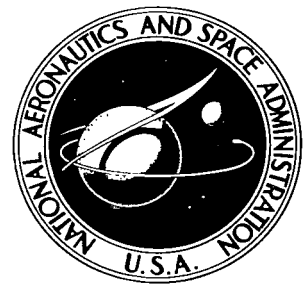

NASA TN D-2536

GRAPHICAL RESULTS FOR LARGE-AMPLITUDE UNSTEADY ONE-DIMENSIONAL WAVES IN MAGNETIZED COLLISION-FREE PLASMAS WITH DISCRETE STRUCTURE

by Wm. Prichard Jones and Vernon J. Rossow

Ames Research Center
Moffett Field, Calif.

NATIONAL AERONAUTICS AND SPACE ADMINISTRATION • WASHINGTON, D. C. • JANUARY 1965

GRAPHICAL RESULTS FOR LARGE-AMPLITUDE UNSTEADY ONE-DIMENSIONAL WAVES IN MAGNETIZED COLLISION-FREE PLASMAS WITH DISCRETE STRUCTURE

By Wm. Prichard Jones and Vernon J. Rossow

Ames Research Center
Moffett Field, Calif.

NATIONAL AERONAUTICS AND SPACE ADMINISTRATION

For sale by the Office of Technical Services, Department of Commerce,
Washington, D.C. 20230 -- Price $3.00

GRAPHICAL RESULTS FOR LARGE-AMPLITUDE UNSTEADY ONE-DIMENSIONAL WAVES IN MAGNETIZED COLLISION-FREE PLASMAS WITH DISCRETE STRUCTURE

By Wm. Prichard Jones and Vernon J. Rossow

Ames Research Center
Moffett Field, Calif.

SUMMARY

Structure of the compressed layer of gas behind one-dimensional time-dependent large-amplitude waves moving across a collisionless fully ionized magnetic plasma is studied by means of electronic computer codes developed by Auer, Hurwitz, and Kilb. Data from these codes are processed by an automatic digital-to-analog plotter and presented graphically in several formats that make it possible to observe special characteristics of the development of collisionless shock waves.

Cases considered in the first sequence of solutions illustrate the variation of the structure of the flow field with Alfvén Mach number of the shock front. Changes brought about in these flow fields when the driving and ambient magnetic fields are assumed to be of opposite sign are then studied. Wave forms that result when two identical collisionless shock waves collide are presented for two special situations. The effect of the mass ratio of the two charged species and the temperature of the ambient plasma on the structure of the magnetic field in the flow field is also considered.

These graphical results indicate that a smooth, orderly wave form is achieved only for compression waves in which the Alfvén Mach number of the front is less than approximately 2 but greater than 1 and the ambient plasma temperature is very small. When the Alfvén Mach number is greater than 2 or the initial temperature of the gas is not negligible, the disturbance produces a field that has a spatially irregular and disorganized form. The structure and velocity of the wave front is then markedly time dependent. Solutions in the strong-disturbance regime appear to be so individualistic that only gross features are attributable to the strong-family solutions as a whole.

INTRODUCTION

Theoretical studies of the structure of shock waves and of the compressed layer behind them, in one dimension, provide information for investigating more complex flow fields that involve the same physical phenomena. Although the structure of the compressed layer is usually simple in continuum fluid mechanics, such is not the case when the gas is a rarefied plasma.

Of interest here are the changes that take place when a compression wave propagates across a fully ionized magnetic plasma at a density so low that the particles make neither single large-angle nor multiple small-angle encounters, but interact collectively through their electromagnetic fields on a scale of the order of the electron Larmor radius; that is, the relative position and motion of the particles contribute to or determine the electric and magnetic fields present in the fluid. These fields, added to those impressed by external sources, cause the particles to be accelerated. Hence, a history of the changes brought about in the fluid as it passes from its undisturbed state into and through the compressed layer provides a description of the shock structure and the compressed layer. Previous investigations show that under such circumstances the shock layer behind a relatively weak magnetic compression wave consists of a wave train that is orderly and smooth in shape; see for example reference 1. For strong disturbances, however, the flow field behind the wave is highly irregular and time dependent as was discovered in reference 2.

Numerous other papers that also treat nonlinear waves of this type, sometimes called collisionless compression waves, collision-free shock waves, hydromagnetic shock waves, etc., are cited in the list of references. Most of this research is devoted to weak nonlinear waves in a magnetic plasma having continuous structure. References that pertain to waves in a non-magnetic plasma but employing a physical model with discrete structure are also cited since it is just such a model that Auer, Hurwitz, and Kilb employed (refs. 1 and 2) to examine the propagation of both weak and strong nonlinear disturbances across a magnetic plasma. In the appendix, the literature related to the present work is grouped according to: (1) that bearing directly on the compression waves studied here (refs. 1 through 26); (2) that concerning large-amplitude waves moving along or canted to a magnetic field (refs. 27 through 30); (3) that concerning discrete models of collisionless plasmas but without a magnetic field (refs. 31 through 36). Also, several papers are noted that describe physical situations wherein these waves are known to occur or may occur (refs. 37 through 45). References 37 through 41 discuss the possibility that collisionless shock waves occur a few Earth radii ahead of the Earth's magnetosphere and cite data from space experiments that suggest the presence of such waves. The interaction of colliding waves is described in reference 42, the radiation from collision-free or nearly collision-free shocks in references 43 and 44, and a way in which a plasma can be heated to high temperature, in reference 45.

The wealth of experimental data from satellites in regions where highly nonlinear waves are thought to occur (refs. 37 through 41) has accentuated the need for more theoretical information of collisionless compression waves in order to organize and classify the observed data. Therefore, the present investigation was undertaken to gain added insight into the motion and structure of large-amplitude, unsteady waves and of the plasma behind them for a number of different physical situations by utilizing numerical techniques and graphical presentation. Because of the complexity of the flow field revealed in the study of the strong case (ref. 2), it was felt that such a display of numerical data would make it possible to identify any orderliness, flow patterns or regular structure, that is characteristic of these waves.

As a minimum, a compilation of shock-wave solutions should provide a physical feeling for their properties and a reference with which experimental data can be compared. To achieve this, the results of a systematic study of the Auer-Hurwitz-Kilb discrete plasma model are exhibited graphically for a variety of parameters, initial conditions, and boundary conditions.

The numerical results are obtained by means of a digital computer and the majority of the figures are produced by a high-speed digital-to-analog data plotter. The two computer programs used to generate the data were given to the NASA Ames Research Center by the authors of references 1, 2, and 21. For this, the authors wish to acknowledge and thank the General Electric Co. of Schenectady, New York, and in particular Dr. Henry Hurwitz, Jr., and Dr. R. W. Kilb.

PRINCIPAL SYMBOLS

A	y component of magnetic vector potential in dimensionless form (see eq. (17d))
b_o	dimensionless magnetic induction ahead of wave (see eqs. (11))
B	magnetic induction
B_∞	magnetic induction ahead of wave
c	velocity of light, $\frac{1}{\sqrt{\epsilon\mu}}$
e	unit charge
e_o	dimensionless electric field intensity at left boundary (see eq. (27b))
E	electric field intensity
E_o	electric field intensity at left boundary, that is, $x = 0$
EX,EY	dimensionless electric field intensity in X and Y directions
j	electric current density
J	dimensionless electric current density (see eqs. (15))
m	mass of particle
M_A	Alfvén Mach number of wave front, $\frac{U_s}{U_A}$

n	number density of particles
N	$\frac{n}{n_o}$
N_s	number of slabs of plasma in flow field
p	pressure
rms	root mean square
R	$\frac{m_i}{m_e}$
R_f	$\frac{(\text{ion plasma frequency})^2}{(\text{ion cyclotron frequency})^2} = \frac{\frac{n_o e^2}{\epsilon m_i}}{\left(\frac{eB_\infty}{m_i}\right)^2} = \frac{R}{R+1}\frac{c^2}{U_A{}^2}$
$\mathcal{R}, S$	see equations (31)
t	time
T	temperature
u, v	velocity components in x and y directions
U, V	$\frac{u}{U^*}$, $\frac{v}{V^*}$
U_A	Alfvén velocity, $\frac{B_\infty}{\sqrt{\mu n_o (m_e + m_i)}}$
U_D	electric drift velocity, $\frac{E_o}{B_\infty}$
x_m	extent of flow field in x direction
x, y, z	rectangular Cartesian coordinates, x in direction of wave motion
X	$\frac{x}{\lambda}$
X_m	$\frac{x_m}{\lambda}$
X_{vav}	rms velocity of particles in X direction at $\tau = 0$
Y_v	rms Y velocity of particles at $\tau = 0$
α	constant that regulates rate of rise of electric field e_o (see eq. (27b))
β	ratio of gas pressure to magnetic pressure

γ	ratio of specific heats, $\frac{c_p}{c_v}$
ϵ	electric permittivity of free space
λ	$\frac{U_A}{\omega_{ch}}$
μ	magnetic permeability of free space
ξ	Lagrangian coordinate variable
ρ_c	charge density
τ	$\frac{t}{t^*}$
ω_{ch}	hybrid cyclotron frequency, $\frac{eB_\infty}{\sqrt{m_e m_i}}$
ω_{ci}	ion cyclotron frequency, $\frac{eB_\infty}{m_i}$
ω_{pi}	ion plasma frequency, $\sqrt{\frac{e^2 n_o}{\epsilon m_i}}$
$(\ )_e$	electron
$(\ )_{eg}$	motion of electron relative to guiding center
$(\ )_g$	guiding center of electron
$(\ )_i$	ion
$(\ )_{o,\infty}$	value at $\tau = 0$ or unshocked plasma region
$(\ )_s$	shock wave or shocked plasma region
$(\ )_v$	vacuum-plasma contact surface or vacuum (piston) region
$(\ )_{x,y,z}$	coordinate components
$(\ )^*$	quantity used to make variables dimensionless (see eqs. (10) and (11))
$\hat{(\ )}$	unit vector
$(\ )^-$	electron
$(\ )^+$	ion
$(\ )^k, (\ )_k$	kth fluid element or sheet

DEVELOPMENT OF EQUATIONS FOR NUMERICAL ANALYSIS

A description is given in references 1, 2, and 21 of the theory and of the electronic computer codes that were used to generate the solutions presented in this paper. A résumé of each code is also presented in the following sections. After a physical description of the one-dimensional flow field is presented, the governing differential equations are introduced. Physical and mathematical idealizations that are applied in order to develop the computer programs define the separate cases that the codes represent. The equations for the two cases are developed in two sections that bear the titles assigned to the program. For further discussion of the assumptions made in these codes, the reader is referred to the original papers given as references 1, 2, and 21.

Plasma Model With Continuous Structure

Physical description.- As shown in sketch (a), the flow field is taken as the space between $x = 0$ and $x = x_m$ and all dependent variables are to be a function of one space dimension and time. All fields and particle motions are referred to the origin which is fixed in the left-hand plane at $x = 0$. A fully ionized plasma, embedded in a steady uniform magnetic field in the positive z direction, is situated between the two planes. At $t = 0$ an electric field is established at $x = 0$ in the positive y direction. This field is the disturbance that accelerates and compresses the plasma near the wall in the x direction.

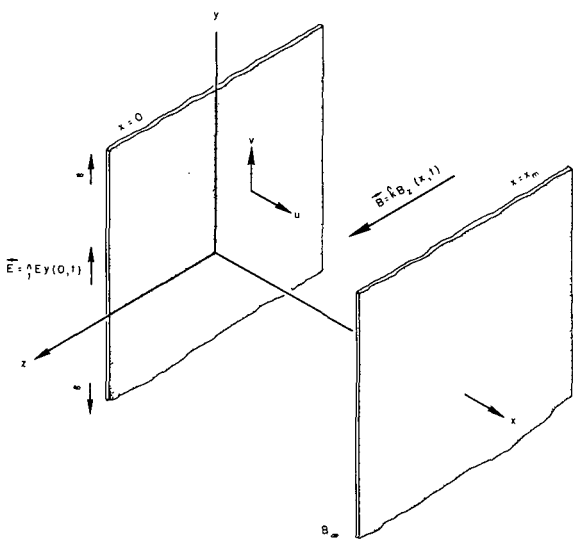

Sketch (a)

The surface at x_m can be regarded as a plane of symmetry separating an identical flow that emanates from $x = 2x_m$. No motion of the gas is permitted in the z direction. Although particles may move vertically, that is, in the y direction, variations in the y and z directions are not allowed ($\partial/\partial y = \partial/\partial z = 0$). It is assumed that the number density of the particles is so low that the particles interact on a collective basis through the electric and magnetic fields only, that is, the single, strong interactions at short range and the multiple, weak interactions at intermediate ranges are sufficiently rare that their effect on the flow field is negligible. The ion and electron Larmor radii are less than the mean free path based on the Coulomb cross section. Under these circumstances, the gas can be considered as collision-free.

The plasma is assumed to consist of equal numbers of ions and electrons that have equal but opposite charge of unit magnitude e. Positively charged particles, ions, are assumed to have a mass m_i, and negatively charged particles m_e, so that their mass ratio is $R = m_i/m_e$. These particles are assumed to be embedded in a magnetic field that has only a + z component that is a function of only the one space dimension x and time t; that is, $\vec{B} = \hat{k}B_z(x, t)$. An idealized flow field extending indefinitely in the y direction bypasses the need to consider return circuits for the electric currents in that direction. Finally, the initial state of the plasma is assumed to be known. The differential equations governing the flow field in which the ambient plasma is cold are developed in the next subsection, and in the subsection following the difference equations for a computer program, Code I, which generates the solutions for cold plasma, are examined in detail. Following that, a subsection is devoted to a review of additional physical idealizations and modifications to the basic differential equations that permit the effects of an initial finite temperature to be incorporated into a second machine program, Code II, which generates solutions for warm ambient plasma.

Two-fluid equations for cold plasma.- Differential equations in Eulerian form for the problems under consideration are listed in vector notation as follows (see table of symbols).

Conservation of momentum

$$\frac{\partial \vec{U}_i}{\partial t} + (\vec{U}_i \cdot \nabla)\vec{U}_i = \frac{e}{m_i}(\vec{E} + \vec{U}_i \times \vec{B}) \tag{1a}$$

$$\frac{\partial \vec{U}_e}{\partial t} + (\vec{U}_e \cdot \nabla)\vec{U}_e = -\frac{e}{m_e}(\vec{E} + \vec{U}_e \times \vec{B}) \tag{1b}$$

where $\vec{U} = u\hat{i} + v\hat{j} + w\hat{k}$, and $w = 0$ for the problems to be considered here.

Conservation of mass or charge

$$\frac{\partial n_i}{\partial t} + \nabla \cdot n_i\vec{U}_i = 0 \tag{2a}$$

$$\frac{\partial n_e}{\partial t} + \nabla \cdot n_e\vec{U}_e = 0 \tag{2b}$$

If the charge and current densities are introduced at this point by the defining relations

$$\rho_c = e(n_i - n_e) \tag{3a}$$

$$\vec{j} = e(n_i\vec{U}_i - n_e\vec{U}_e) \tag{3b}$$

then from equations (2) and (3) the following relation is obtained,

$$\nabla \cdot \vec{j} = - \frac{\partial \rho_c}{\partial t} \tag{3c}$$

Electromagnetic field equations

$$\nabla \times \vec{B} = \mu \vec{j} \tag{4a}$$

$$\nabla \times \vec{E} = - \frac{\partial \vec{B}}{\partial t} \tag{4b}$$

subject to the field conditions

$$\nabla \cdot \vec{B} = 0 \tag{4c}$$

$$\nabla \cdot \vec{E} = \frac{\rho_c}{\epsilon} \tag{4d}$$

where the term $\mu\epsilon(\partial\vec{E}/\partial t)$ in equation (4a) has been assumed to be negligible in comparison with $\mu\vec{j}$.

When the preceding equations are reduced to their component forms that are applicable to the one-dimensional unsteady problems considered here, they become:

Conservation of x momentum

$$\frac{\partial u_i}{\partial t} + u_i \frac{\partial u_i}{\partial x} = \frac{e}{m_i} (E_x + v_i B_z) \tag{5a}$$

$$\frac{\partial u_e}{\partial t} + u_e \frac{\partial u_e}{\partial x} = - \frac{e}{m_e} (E_x + v_e B_z) \tag{5b}$$

Conservation of y momentum

$$\frac{\partial v_i}{\partial t} + u_i \frac{\partial v_i}{\partial x} = \frac{e}{m_i} (E_y - u_i B_z) \tag{6a}$$

$$\frac{\partial v_e}{\partial t} + u_e \frac{\partial v_e}{\partial x} = - \frac{e}{m_e} (E_y - u_e B_z) \tag{6b}$$

Conservation of mass or charge

$$\frac{\partial n_i}{\partial t} + \frac{\partial n_i u_i}{\partial x} = 0 \tag{7a}$$

$$\frac{\partial n_e}{\partial t} + \frac{\partial n_e u_e}{\partial x} = 0 \tag{7b}$$

Equations (3b) and (3c) become

$$j_x = e(n_i u_i - n_e u_e) \tag{8a}$$

$$j_y = e(n_i v_i - n_e v_e) \tag{8b}$$

$$\frac{\partial j_x}{\partial x} = -e \frac{\partial (n_i - n_e)}{\partial t} \tag{8c}$$

Electromagnetic field equations

$$\frac{\partial B_z}{\partial x} = -\mu j_y = -e\mu(n_i v_i - n_e v_e) \tag{9a}$$

$$\frac{\partial E_y}{\partial x} = -\frac{\partial B_z}{\partial t} \tag{9b}$$

subject to the field condition

$$\frac{\partial E_x}{\partial x} = \frac{e}{\epsilon}(n_i - n_e) \tag{9c}$$

In any numerical analysis, it is convenient to reduce the equations to a dimensionless form by dividing each of the flow variables by a quantity that has the same dimensions and is characteristic of the flow field. Any number of combinations of parameters could be used to carry this out but the system used here will be that employed previously in references 1 and 2, namely,

$$U^* = (U_A U_D)^{1/2} = \text{"snowplow" velocity}$$

where

U_A $\quad B_\infty/[\mu n_o(m_i + m_e)]^{1/2}$ = Alfvén velocity

U_D $\quad E_o/B_\infty$ = electric drift velocity

B_∞ ambient magnetic induction ahead of wave

E_o electric field at $x = 0$ that excites disturbance magnetic field

n_o number density of particles in ambient field

$$B^* = B_\infty U^*/U_A = B_\infty \sqrt{U_D/U_A}$$

$$\lambda = U_A/\omega_{ch} = \text{characteristic length}$$

$$V^* = (m_e + m_i)U^*/\sqrt{m_e m_i}$$

$$t^* = \lambda/\sqrt{U_A U_D}$$

When these quantities are combined with the various flow variables, a set of dimensionless quantities to be used in the calculations are defined as,

$$\left.\begin{aligned} X &= x/\lambda \\ \tau &= t/t^* \end{aligned}\right\} \tag{10}$$

$$\left.\begin{aligned} N_i(X,\tau) &= n_i(x,t)/n_o\,, \quad & N_e(X,\tau) &= n_e(x,t)/n_o \\ U_i(X,\tau) &= u_i(x,t)/U^*\,, \quad & U_e(X,\tau) &= u_e(x,t)/U^* \\ V_i(X,\tau) &= v_i(x,t)/V^*\,, \quad & V_e(X,\tau) &= v_e(x,t)/V^* \\ B(X,\tau) &= B_z(x,t)/B^* \\ EY(X,\tau) &= E_y(x,t)/E_o = E_y(x,t)/(U^*B^*) \\ EX(X,\tau) &= E_x(x,t)/(V^*B^*) \\ b_o &= B_\infty/B^* \end{aligned}\right\} \tag{11}$$

Equations (5) through (9) then become,

$$\frac{\partial U_i}{\partial \tau} + U_i \frac{\partial U_i}{\partial X} = \frac{R+1}{R}(EX + V_i B) \tag{12a}$$

$$\frac{\partial U_e}{\partial \tau} + U_e \frac{\partial U_e}{\partial X} = -(R+1)(EX + V_e B) \tag{12b}$$

$$\frac{\partial V_i}{\partial \tau} + U_i \frac{\partial V_i}{\partial X} = \frac{1}{R+1}(EY - U_i B) \tag{13a}$$

$$\frac{\partial V_e}{\partial \tau} + U_e \frac{\partial V_e}{\partial X} = - \frac{R}{R + 1} (EY - U_e B) \tag{13b}$$

$$\frac{\partial N_i}{\partial \tau} + \frac{\partial N_i U_i}{\partial X} = 0 \tag{14a}$$

$$\frac{\partial N_e}{\partial \tau} + \frac{\partial N_e U_e}{\partial X} = 0 \tag{14b}$$

$$\frac{\partial J_X}{\partial X} = \frac{\partial (N_i - N_e)}{\partial \tau} \tag{15a}$$

where

$$J_X = N_i U_i - N_e U_e \approx 0 \tag{15b}$$

$$J_y = N_i V_i - N_e V_e \tag{15c}$$

$$\frac{\partial B}{\partial X} = N_e V_e - N_i V_i \tag{16a}$$

$$\frac{\partial EY}{\partial X} = - \frac{\partial B}{\partial \tau} \tag{16b}$$

and

$$\frac{\partial EX}{\partial X} = \frac{R_f}{R + 1} b_o^2 (N_i - N_e) \tag{16c}$$

where

$$R_f = \frac{\frac{n_o e^2}{\epsilon m_i}}{\left(\frac{eB_\infty}{m_i}\right)^2} = \frac{(\text{ion plasma frequency})^2}{(\text{ion cyclotron frequency})^2} = \frac{R}{R + 1} \frac{c^2}{U_A^2} \tag{16d}$$

Subsequent development of the governing equations is simplified by introducing at this point the magnetic vector potential, $\vec{A}$, defined in such a way that, in dimensionless form,

$$B(X, \tau) = \frac{\partial A}{\partial X} \tag{17a}$$

$$EY(x, \tau) = - \frac{\partial A}{\partial \tau} \tag{17b}$$

The choice of components for $\vec{A}$ that accomplish this are $A_X = 0$, $A_Z = 0$, and

$$A(X,\tau) = -\int_0^\tau EY(0,\tau')d\tau' + \int_0^X B(X',\tau)dX' - b_0X_m \tag{17c}$$

where

$$A = A_y/B^*\lambda \tag{17d}$$

Plasma Model With Discrete Structure

Until now the flow field has been regarded as a continuous, fully ionized gas, for which all dependent variables are smooth functions of the Eulerian variable, X, and time. If this continuous plasma structure is replaced by a plasma having discrete structure, the analysis of the nonsteady flow field is simplified. Therefore, the plasma contained between the planes at $X = 0$ and $X = X_m$ is subdivided into many slabs, each containing equal numbers of electrons or ions. Two slabs that are coincident at a given time, one containing ions and the other containing a like number of electrons, constitute a fluid slab or a fluid element of plasma. The Eulerian coordinate, X, of such a plasma element can be related to the Lagrangian variables, ξ_i and ξ_e, which are defined as the amount of fluid, ion or electron, to the left of the position, X, to which it is assigned, in dimensionless notation. Thus,

$$\xi_i(X,\tau) = \int_0^X N_i(X',\tau)dX' \qquad \xi_e(X,\tau) = \int_0^X N_e(X',\tau)dX'$$

or

$$N_i = \frac{\partial \xi_i}{\partial X}\Big|_\tau \qquad N_e = \frac{\partial \xi_e}{\partial X}\Big|_\tau$$

At $\tau = 0$, $\xi_i = \xi_e$, $N_i = N_e$, and charge slabs are uniformly distributed so that $\xi(X,0) = NX$. After the plasma is set into motion, ion slabs and electron slabs move differently because of their different masses. In fact it can be seen that ion slabs can overtake one another leaving their former electron slab companions behind and that electron slabs do not overtake one another except under extreme conditions. (See ref. 26.) This is the principal feature that severely complicates the use of the Eulerian coordinate system. Conversion of the differential equations to the Lagrangian coordinate system affords a means by which ion and electron slab motions can be followed separately regardless of whether or not overtaking occurs, yet permits a description of the flow field in terms of the Eulerian coordinate. Flow field variables U_i, U_e, V_i, V_e, EY, and B can be found as functions of X and τ by means of the following identities:

$$U_i = \left.\frac{\partial X}{\partial \tau}\right|_{\xi_i} \qquad U_e = \left.\frac{\partial X}{\partial \tau}\right|_{\xi_e}$$

and

$$\left.\frac{\partial}{\partial X}\right|_{\tau} = \left.\frac{\partial \xi_i}{\partial X}\right|_{\tau} \left.\frac{\partial}{\partial \xi_i}\right|_{\tau} = N_i \left.\frac{\partial}{\partial \xi_i}\right|_{\tau}, \qquad \text{etc.}$$

The acceleration of a given segment of the plasma is then

$$\left.\frac{\partial U_i}{\partial \tau}\right|_{\xi_i} = \left.\frac{\partial^2 X}{\partial \tau^2}\right|_{\xi_i} = \left.\frac{\partial U_i}{\partial \tau}\right|_{X} + \left.\frac{\partial X}{\partial \tau}\right|_{\xi_i} \left.\frac{\partial U_i}{\partial X}\right|_{\tau}$$

so that equations (12) to (16) can be rewritten with the aid of the potential A as

$$\left.\frac{\partial U_i}{\partial \tau}\right|_{\xi_i} = \frac{R+1}{R}(EX + V_i B) \tag{18a}$$

$$\left.\frac{\partial U_e}{\partial \tau}\right|_{\xi_e} = -(R+1)(EX + V_e B) \tag{18b}$$

$$\left.\frac{\partial V_i}{\partial \tau}\right|_{\xi_i} = \frac{1}{R+1}(EY - U_i B) = \frac{-1}{R+1}\left(\frac{\partial A}{\partial \tau} + U_i \frac{\partial A}{\partial X}\right) = \left.\frac{-1}{R+1}\frac{\partial A}{\partial \tau}\right|_{\xi_i}$$

or

$$\left.\frac{\partial}{\partial \tau}\left(V_i + \frac{A}{R+1}\right)\right|_{\xi_i} = 0 \tag{19a}$$

and

$$\left.\frac{\partial}{\partial \tau}\left(V_e - \frac{AR}{R+1}\right)\right|_{\xi_e} = 0 \tag{19b}$$

$$\frac{\partial}{\partial \tau}\left(\frac{1}{N_i}\right) = \left.\frac{\partial U_i}{\partial \xi_i}\right|_{\tau} \tag{20a}$$

$$\frac{\partial}{\partial \tau}\left(\frac{1}{N_e}\right) = \left.\frac{\partial U_e}{\partial \xi_e}\right|_{\tau} \tag{20b}$$

$$\left.\frac{\partial B}{\partial \xi_i}\right|_{\tau} = \frac{N_e}{N_i} V_e - V_i \tag{21a}$$

$$\left.\frac{\partial B}{\partial \xi_e}\right|_{\tau} = V_e - \frac{N_i}{N_e} V_i \tag{21b}$$

$$\left.\frac{\partial EY}{\partial \xi_i}\right|_{\tau} = \frac{-1}{N_i}\left.\frac{\partial B}{\partial \tau}\right|_{X} \tag{21c}$$

$$\left.\frac{\partial EY}{\partial \xi_e}\right|_{\tau} = \frac{-1}{N_e}\left.\frac{\partial B}{\partial \tau}\right|_{X} \tag{21d}$$

$$\left.\frac{\partial EX}{\partial X}\right|_{\tau} = \frac{R_f}{R+1} b_o^{\,2}\left(\left.\frac{\partial \xi_i}{\partial X}\right|_{\tau} - \left.\frac{\partial \xi_e}{\partial X}\right|_{\tau}\right) \tag{21e}$$

or, at a given time,

$$EX = \frac{R_f}{R+1} b_o^{\,2}(\xi_i - \xi_e) \tag{21f}$$

since $\xi_i = \xi_e$ ahead of the wave and at $X = X_m$.

Effects of Charge Separation and Temperature

Characteristics of the flow fields represented by the two machine codes considered in this paper (and referred to hereinafter as Code I and Code II) can now be discussed by means of equations (18) to (21). As mentioned previously, it is assumed that the number density is so low that the particles interact only collectively. A single charge slab is accelerated by the long-range forces of the electric and magnetic fields brought about by the relative positions and motions of all other ion and electron charge slabs. Also, the foregoing equations do not contain pressure or viscous terms. In addition to this restriction, both codes assume that the plasma properties and the ambient magnetic field are such that the parameter R_f is large. Then from equation (21e)

$$\frac{1}{R_f}\frac{\partial EX}{\partial X} = (N_i - N_e)\frac{b_o^{\,2}}{R+1} \approx 0$$

or in the limit as $R_f \to \infty$

$$N_i = N_e \equiv N \tag{22a}$$

It then follows by conservation of mass of both species (eqs. (20)) that

$$U_i = U_e \equiv U \tag{22b}$$

Since $R_f \approx 10^3 - 10^8$ in both laboratory fusion devices and in the vicinity of the earth's magnetosphere, such an approximation appears to be quite reasonable. Development of the code requires several additional assumptions regarding the ordering of the charge slabs at each instant of time. The order assumed at $t = 0$ is not necessarily preserved for strong compression waves passing through the plasma because the trajectories of slabs can cross. In such situations, it is physically reasonable to require that the electron slabs, because of their smaller mass, retain their original order. Only the ion slabs will take on a new position sequence as predicted by the equations of motion.

A computer code, developed at Ames Research Center as an extension of Code I and presented in reference 26, does not assume the parameter R_f to be large and therefore treats the plasma as a medium with two separate fluids. Flow-field elements that contain either ions or electrons but never both are followed as individuals and are permitted to interchange order in the manner indicated by their respective equations of motion. The role of the electric field comes about because inertial forces tend to separate the ions and electrons. Counteracting this tendency to separate is the electric field EX (eq. (21f)). Some compromise position or separation distance between slab pairs will then result and an oscillation about this relative position may occur. The flow fields analyzed by this code had a fine structure that would not be observable in those analyzed by Code I of the present paper. It was found in reference 26 that as $R_f \to \infty$, the assumptions referred to above are valid and, in fact, adequate for $R_f \geq 100$.

In Code I, which is dealt with next, the particles ahead of the compression wave are assumed to be stationary, that is, at zero temperature. Code II, developed by Kilb in reference 21 as an extension of Code I, treats a compression wave passing into a gas that has a small temperature. In both codes, I and II, charge separation is not allowed. When the particles move at random in the undisturbed region, the gas is referred to as being thermalized. Since several idealizations were required in order to make Code II a reasonable numerical calculation, the temperature, or magnitude of the random velocities permitted, is restricted to moderate values so that the ambient gas is referred to as "warm" or "tepid" rather than "hot." Modifications that are made to equations (18) to (21) to account for the effects brought about by such an initial temperature are elaborated upon in a subsequent section of this paper.

CODE AMBIENT GAS: CODE I

As pointed out previously the defining characteristics of the flow field represented in this computer program are the assumptions that the initial temperature of the plasma is zero and that the parameter R_f is infinite. Therefore, the number density and the X velocities of the ions at a particular X location must be the same as the electrons at that location; that is,

$$N_i = N_e \equiv N \tag{22a}$$

so that at any instant

$$\xi_i = \xi_e \equiv \xi$$

and

$$U_i = U_e \equiv U \tag{22b}$$

Even though $(1/R_f)(\partial EX/\partial X)$ is zero, EX itself is not zero but is of such a magnitude that paired ion and electron slabs at a given location and specified time satisfy equation (22b). Since the X velocity in equations (18a) and (18b) is the same, it can be eliminated from those equations to yield

$$EX = - \frac{R}{R + 1} \left(\frac{V_i}{R} + V_e \right) B \tag{23}$$

Equation (21f) does not contradict equation (23). The Lagrangian variables ξ_i and ξ_e are equal because the product $R_f(\xi_i - \xi_e)$ must be finite. For situations in which R_f is not infinite equations (21f) and (23) can be used to calculate the charge separation distance; thus,

$$\xi_i - \xi_e = - \frac{R}{R_f b_o^2} \left(\frac{V_i}{R} + V_e \right) B$$

If the X momentum equations are now employed to eliminate EX with the aid of equations (16a), (22), and (23), the following relation is obtained, namely,

$$\left. \frac{\partial U}{\partial \tau} \right|_{\xi} = (V_i - V_e)B = - \frac{1}{N} B \frac{\partial B}{\partial X}$$

or

$$\left. \frac{\partial U}{\partial \tau} \right|_{\xi} = - \frac{\partial}{\partial \xi} \left(\frac{B^2}{2} \right) \Bigg|_{\tau} \tag{24}$$

When the equations for the y momentum (eqs. (19)) are integrated once,

$$V_i + \frac{A}{R+1} = V_i^o + \frac{A^{o+}}{R+1} \qquad \xi_i^o = \text{constant} \tag{25a}$$

$$V_e - \frac{AR}{R+1} = V_e^o - \frac{A^{o-}R}{R+1} \qquad \xi_e^o = \text{constant} \tag{25b}$$

where V_i^o, V_e^o, ξ_i^o, ξ_e^o, and A^{o+}, A^{o-} are the values of these parameters that the particles ξ_i and ξ_e in the fluid element ξ under consideration had at time $\tau = 0$. A distinction must be made here between ions and electrons. Even though the local value of ξ at a given time is the same for both species, the original (i.e., at $\tau = 0$) location (ξ_i^o and ξ_e^o) of each can be quite different for strong waves. On the physical grounds (see ref. 2) that the ions have a large inertia compared to that of the electrons, it is assumed that the ion trajectories can cross one another so that ξ_i^o is not always equal to ξ. Conversely, it is assumed that the electrons always retain their original order; that is, $\xi_e = \xi = \xi_e^o$. To illustrate this point consider two ion-electron pairs as they assume successive positions in time. Sketch (b) represents the initial ordering of charge pairs, their positions just prior to interchange and their ordering after interchange. At $\tau = 0$, two fluid elements are shown labelled k and $k+1$. They each consist of an ion and electron layer labelled ξ_k^{o+}, ξ_k^{o-} and ξ_{k+1}^{o+}, ξ_{k+1}^{o-}, respectively. Before the ion orbits cross, for example, at τ_1, the kth ion and electron slab still travel together, and similarly for the $(k+1)$th pair. The next computed location for the two fluid elements, $\tau = \tau_2$, illustrates the new ordering as a consequence of interchange of ion partners which is equivalent to the requirement that electrons do not lose their initial spatial ordering. Therefore, at $\tau = \tau_2$

$$\xi_k^- = \xi_k^{o-} = \xi_k$$

but

$$\xi_k^{o+} \neq \xi_k$$

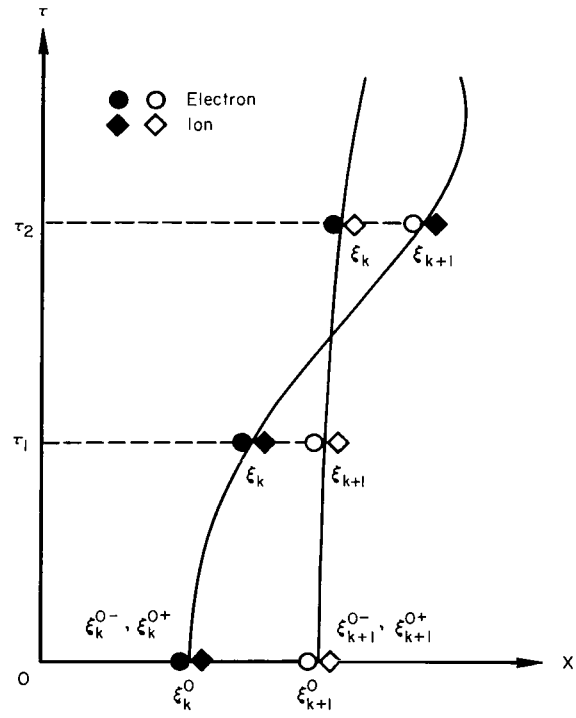

Sketch (b)

The equations for the conservation of mass, the magnetic field and the y component of the electric field, become

$$\left.\frac{\partial}{\partial\tau}\left(\frac{1}{N}\right)\right|_{\xi} = \left.\frac{\partial U}{\partial\xi}\right|_{\tau} \tag{26a}$$

$$\left.\frac{\partial B}{\partial\xi}\right|_{\tau} = V_e - V_i \tag{26b}$$

$$\left.\frac{\partial EY}{\partial\xi}\right|_{\tau} = -\frac{1}{N}\left.\frac{\partial B}{\partial\tau}\right|_{X} \tag{26c}$$

The boundary conditions imposed on the flow field may be divided into the initial and the wall conditions. At time $\tau = 0$, the gas is assumed to be stationary and distributed uniformly throughout the flow field between $X = 0$ and $X = X_m$. Hence,

$$\left.\begin{aligned} \xi^o = \xi_i^o = \xi_e^o &= X \\ U(X,0) &= 0 \\ V_i^o = V_e^o &= 0 \\ EX(X,0) = EY(X,0) &= 0 \\ B(X,0) &= b_o \\ N(X,0) &= 1.0 \\ A(X,0) &= b_o(X - X_m) \end{aligned}\right\} \tag{27a}$$

At the left-hand wall, $X = 0$, an electric field is assumed to be applied in the y direction of magnitude

$$EY(0,\tau) = e_o(1 - e^{-\alpha\tau}) \tag{27b}$$

At the far boundary, $X = X_m$,

$$\left.\begin{aligned} EY(X_m,\tau) &= 0 \\ U(X_m,\tau) &= 0 \\ V(X_m,\tau) &= 0 \\ EX(X_m,\tau) &= 0 \\ A(X_m,\tau) &= 0 \end{aligned}\right\} \tag{27c}$$

Numerical treatment of the flow field is facilitated by the concentration of the uniform distribution of plasma into N_S discrete, coincident pairs of charge slabs, that is into N_S electrically neutral fluid elements, of thickness δ as illustrated schematically in sketch (c). The thickness of the slabs is then taken to be vanishingly small; $\delta \to 0$. Each fluid element contains an equal number of ions and electrons, and this number is the same for all of the elements (or sheets, since the thickness is zero). Hence, the amount of fluid per unit area or charge density on each sheet in dimensionless notation is X_m/N_S. The initial spacing of the sheets ($\tau = 0$) is taken to be

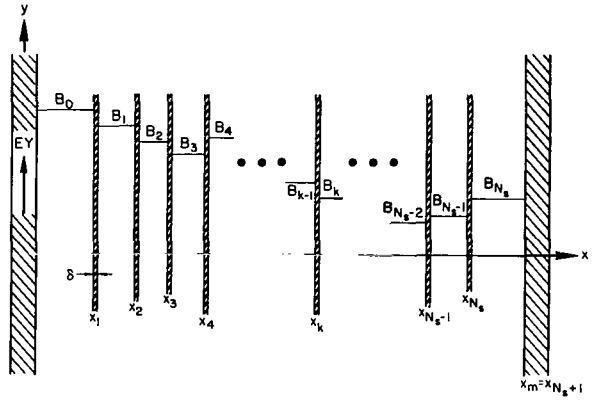

Sketch (c)

$$\xi_k^o = kX_m/(N_S + 1)$$

where $k = 1, 2, 3, \ldots, N_S$ so that the sheets are not located at the mass centers of the volume elements that they represent. Since the number of sheets will be of the order of 1000, $\xi_{N_S}^o = X_m N_S/(N_S + 1) \approx X_m$ and the small error incurred due to this initial displacement is ignored. It is also to be noted that a sheet is not located at the $X = X_m$ plane. The station X_{N_S+1} is the boundary at X_m and contains no plasma.

In the discussion that follows the phrases "charge slabs," "current sheets," and "particles," appropriately identified as to electron or ion, negative or positive, will be used interchangeably. Since charge neutrality is required everywhere, slabs or particles at a given location must be present in equal numbers.

Since all of the particles and therefore all of the electric currents are concentrated on sheets, the magnetic field (which is always tangential to the sheet) must change discontinuously across the surface. A given value of B is defined as that value of the magnetic field to the right of a given element; that is, B_k = magnetic field to the right of the kth sheet. Then the boundary condition on the kth sheet is

$$B_k - B_{k-1} = (V_e^k - V_i^k)\frac{X_m}{N_S} \tag{28a}$$

where X_m/N_S is the dimensionless number density of each species on the kth surface. Equation (28a) contains the assumption that the displacement current is negligible, because sheet velocity perpendicular to the ambient field is slow compared with the velocity of light. To this degree of approximation

the magnetic field remains unchanged in the reference frame moving with a sheet. (See, e.g., ref. 46, p. 330.) Also, equations (25) become

$$V_i^k + \frac{A_k}{R+1} = \frac{A_k^{o+}}{R+1} \tag{28b}$$

$$V_e^k - \frac{RA_k}{R+1} = -\frac{RA_k^{o-}}{R+1} \tag{28c}$$

since $V_i = V_e = 0$ initially. Hence,

$$B_k - B_{k-1} = \frac{X_m}{N_s}\left[\frac{R}{R+1}(A_k - A_k^{o-}) + \frac{1}{R+1}(A_k - A_k^{o+})\right] \tag{28d}$$

$$= \frac{X_m}{N_s(R+1)}\left[(R+1)A_k - (A_k^{o+} + R \cdot A_k^{o-})\right] \tag{28e}$$

A set of difference equations in matrix form can now be derived by the same technique used in the numerical codes developed for references 1 and 2. From equation (28a), the relationship between any three consecutive sheets can be found to be

$$-B_{k-1} + 2B_k - B_{k+1} = \frac{X_m}{N_s}\left[(V_e^k - V_i^k) - (V_e^{k+1} - V_i^{k+1})\right]$$

Equations (28b) and (28c) lead to the relations,

$$V_i^k - V_i^{k+1} = \frac{-1}{R+1}(A_k - A_{k+1} - A_k^{o+} + A_{k+1}^{o+})$$

$$V_e^k - V_e^{k+1} = \frac{R}{R+1}(A_k - A_{k+1} - A_k^{o-} + A_{k+1}^{o-})$$

The dimensionless expression for the magnetic vector potential, A_k, that is applicable to the stepwise changes to be anticipated in the flow field is from equation (17c)

$$A_k = A(X_k,\tau) = -\int_o^\tau EY(C,\tau')d\tau' + \int_o^{X_k} B(X',\tau)dX' - b_o X_m$$

Since the magnetic field is constant between sheets it can be rewritten as

$$A_k = A_k(\tau) = -\int_o^\tau EY(0,\tau')d\tau' + \sum_{I=1}^{k} (X_I - X_{I-1})B_{I-1} - b_o X_m$$

or, by equation (27b)

$$A_k = -\left[\tau + \frac{1}{\alpha}(e^{-\alpha\tau} - 1)\right]e_o + \sum_{I=1}^{k} (X_I - X_{I-1})B_{I-1} - b_o X_m \qquad (29a)$$

where $X_o = 0$ and $X_{N_s+1} = X_m$. If the integration is referred to X_m, then A_k can be expressed as

$$A_k = \sum_{I=k}^{N_s} (X_I - X_{I+1})B_I \qquad (29b)$$

and the following relations derived

$$A_k - A_{k+1} = -(X_{k+1} - X_k)B_k \qquad (30a)$$

$$A_k^{o+} - A_{k+1}^{o+} = -(X_{k+1}^{o+} - X_k^{o+})b_o \qquad (30b)$$

$$A_k^{o-} - A_{k+1}^{o-} = -\frac{X_m}{N_s + 1} b_o \qquad (30c)$$

In equation (30b) the indices k and $k + 1$ refer to the ion slab located at $X_k(\tau)$ and $X_{k+1}(\tau)$. As was illustrated in sketch (b), the initial positions of the kth and $(k + 1)$th ion slabs need not be the same as that of the electron slabs presently at X_k and X_{k+1}, respectively. Equation (30c) reflects the fact that sheet spacing is based on $N_s + 1$ locations. The difference equation for B_k can then be written in the form

$$-B_{k-1} + 2B_k - B_{k+1} = -\frac{X_m}{N_s}\left[(X_{k+1} - X_k)B_k - \frac{b_o}{R + 1}\left(\frac{RX_m}{N_s + 1} + X_{k+1}^{o+} - X_k^{o+}\right)\right]$$

or

$$B_k\left[2 + \frac{X_m}{N_s}(X_{k+1} - X_k)\right] = B_{k+1} + B_{k-1} + \frac{X_m b_o}{N_s(R + 1)}\left(\frac{RX_m}{N_s + 1} + X_{k+1}^{o+} - X_k^{o+}\right) \qquad (30d)$$

For reasonable numerical accuracy, a large number of fluid elements or sheets (about 1000) should be used in a computation. The matrix to be inverted is then sizable. Effort required to carry out the inversion is modest, however, because the matrix consists of only three terms that lie along a diagonal. A technique, used but not presented in references 1 and 2, that accomplishes the task requires that the foregoing difference equation for B_k be formed into the expressions

$$B_k = \mathcal{R}_k \cdot B_{k-1} + S_k \tag{31a}$$

where

$$\mathcal{R}_k = \frac{1}{2 + (X_m/N_s)(X_{k+1} - X_k) - \mathcal{R}_{k+1}} \tag{31b}$$

$$S_k = \mathcal{R}_k \left[S_{k+1} + \frac{X_m b_o}{N_s(R+1)} \left(\frac{RX_m}{N_s + 1} + X_{k+1}^{o+} - X_k^{o+} \right) \right] \tag{31c}$$

The quantities $\mathcal{R}_k$ and S_k are evaluated by starting at the plane $X = X_m$, whereas the quantity B_k is computed by means of conditions at the left-hand boundary, $X = 0$. Since the boundary at X_m is a plane of symmetry, the various quantities on both sides of that plane are mirror images of each other; in particular,

$$B_{N_s+1} = B_{N_s}$$

When this condition is inserted into equation (31a), it is seen to require that $\mathcal{R}_{N_s+1} = 1$ and $S_{N_s+1} = 0$ so that

$$\mathcal{R}_{N_s} = \frac{1}{1 + (X_m/N_s)(X_m - X_{N_s})} \tag{32a}$$

$$S_{N_s} = \mathcal{R}_{N_s} \frac{X_m b_o}{N_s(R+1)} \left(\frac{RX_m}{N_s + 1} + X_m - X_{N_s}^{o+} \right) \tag{32b}$$

since $X_{N_s+1} = X_m$. Once the values at the N_sth sheet are known, the remainder of the values of $\mathcal{R}_k$ and S_k are determined by the recursion relations (31b) and (31c).

At the left-hand boundary, the disturbance is generated by an electric field so that the value of the magnetic vector potential at $X = 0$ is given by equation (29a) as

$$A_o = A(0,\tau) = -e_o \left[\tau + \frac{1}{\alpha} \left(e^{-\alpha\tau} - 1 \right) \right] - X_m b_o \tag{33a}$$

From equation (30a)

$$A_1 - A_0 = X_1 B_0 \tag{33b}$$

where B_0 is the magnetic induction between the $X = 0$ plane and the first sheet which is located at $X = X_1$. This part of the flow field is often referred to as the vacuum or magnetic piston region because it contains no particles and only magnetic field. Equation (31a) provides the expression

$$B_1 = \mathcal{R}_1 \cdot B_0 + \mathcal{S}_1$$

where $\mathcal{R}_1$ and $\mathcal{S}_1$ are assumed known from the use of equations (31) and (32). When the foregoing relations are combined with equations (28), it is found that

$$B_1 - B_0 = \frac{X_m}{N_s}\left(A_1 - \frac{RA_1^{0-} + A_1^{0+}}{R+1}\right) \tag{33c}$$

Since A_0, $\mathcal{R}_1$, $\mathcal{S}_1$, A_1^{0-}, and A_1^{0+} have been computed at this stage of the analysis, the quantity B_0 can be found as

$$B_0 = \frac{-\left[\mathcal{S}_1 + \frac{X_m}{N_s}\left(A_0 - \frac{RA_1^{0-} + A_1^{0+}}{R+1}\right)\right]}{\left(\mathcal{R}_1 - 1 - \frac{X_1 X_m}{N_s}\right)} \tag{33d}$$

An equation of motion for the slabs of plasma is obtained from equation (24) as

$$\frac{\partial U_k}{\partial \tau} = \frac{\partial^2 X_k}{\partial \tau^2} = \frac{N_s}{2X_m}\left(B_{k-1}^2 - B_k^2\right) \tag{34}$$

Equations (31) through (34) constitute a closed system thereby making it possible to evaluate numerically the fluid motion and electromagnetic fields that occur when a given plasma is compressed quickly by a magnetic field. Typical cases that illustrate the various phenomena to be expected for a range of boundary conditions are present in figures 1 through 12. Pertinent characteristics to be noted will be pointed out and discussed in a later section.

WARM AMBIENT GAS: CODE II

The zero temperature assumed for the ambient gas ahead of the wave in the previous code is defined as the state wherein the gas particles are stationary and spaced uniformly within a magnetic field of constant strength. When the plasma in the undisturbed region has a finite temperature, the uniformity of the flow field is destroyed by any of the three sets of initial conditions that can be made finite and random rather than zero; these

quantities are: (1) velocities in the X direction; (2) velocities of the ions in the Y direction; and (3) velocities of the electrons in the Y direction. At a given instant any one of these three quantities can be thermalized while the others are uniform; but the more plausible situation is one wherein all are acting simultaneously. Furthermore, the initial sheet spacing can be made random thereby simulating a more probable initial state.

Code II, as developed by Kilb (ref. 21), introduces the foregoing temperature effects into the ambient gas at time $\tau = 0$ by specifying that the particles have random X velocities at locations that are placed randomly about a uniform distribution. Differences (or lack of correlation) between the Y velocities of the two species constitute a thermalization of the electric current. A consequence of this arbitrary current distribution is a randomization of the electric and magnetic fields. Supplementing the initial conditions that can be imposed on the particles, the effect of an electron pressure gradient is incorporated by relaxing the restriction that ions and electrons remain always paired. If instead only the guiding center of an electron moves on a sheet of plasma, then the temperature of the electrons is manifested by the random motion of the electrons with respect to the guiding centers, superimposed on the initial random motion of their guiding centers. Since the parameter R_f has been assumed to be infinite for this case, the X locations and velocities of the ions and guiding centers of the electrons are the same for each pair. So, once again, as for Case I, a sheet of plasma consists of an equal number of ions and electron guiding centers; each sheet is identical in composition with all of the rest and the number density of each species is X_m/N_s.

Modifications to the equations used in Code I in order to account for the thermalized nature of the ambient plasma are explained and justified in reference 21. Only the barest essentials of that work will be presented here so that four new parameters for the thermal effects can be defined.

A measure of the temperature of the gas is obtained by comparing its pressure with the pressure of the ambient magnetic induction B_∞. For the electrons, such a ratio is defined as,

$$\beta_e = \beta_g + \beta_{eg} = \frac{p_e}{p_{B_\infty}} = \frac{p_g + p_{eg}}{p_{B_\infty}} \tag{35}$$

where

$$p_e = \frac{1}{2} n_o m_e \left[\left\langle u_g^2 \right\rangle + \left\langle v_g^2 \right\rangle \right]_{t=o} + p_{eg} = n_o k T_e$$

$$p_{B_\infty} = \frac{B_\infty^2}{2\mu}$$

and

p_g initial pressure due to motion of electron guiding centers

p_{eg} pressure due to electron motion about guiding center

T_e temperature of electrons

$\langle\ \rangle$ mean value based on hybrid cyclotron period

Similarly, for the ions

$$\beta_i = \frac{p_{io}}{p_{B_\infty}} \tag{36}$$

where

p_{io} initial pressure due to motion of ions, $\frac{1}{2} n_o m_i \left[\left\langle u_i^2 \right\rangle + \left\langle v_i^2 \right\rangle \right]_{t=o} = n_o k T_{io}$

T_{io} initial temperature of ions

Since the ions and electron guiding centers must have the same X locations and velocities at all times as a consequence of the assumption that $R_f = \infty$,

$$\left\langle u_g^2 \right\rangle = \left\langle u_i^2 \right\rangle = \left\langle u^2 \right\rangle \tag{37}$$

In the dimensionless notation introduced previously (eqs. (10) and (11)), the necessary additional parameters that include the averages of the several flow variables in the ambient plasma are defined as,

$$X_{vav} = \frac{\sqrt{\left\langle u^2 \right\rangle_{t=o}}}{U^*} = \text{rms velocity in X direction} \tag{38a}$$

$$Y_{vi} = \frac{\sqrt{\left\langle v_i^2 \right\rangle_{t=o}}}{V^*} = \text{rms Y velocity of ions} \tag{38b}$$

$$Y_{vg} = \frac{\sqrt{\left\langle v_g^2 \right\rangle_{t=o}}}{V^*} = \text{rms Y velocity of electron guiding centers} \tag{38c}$$

$$\beta_i = \frac{R}{b_o^2 (R+1)} \left[X_{vav}^2 + \frac{(R+1)^2}{R} Y_{vi}^2 \right] \tag{38d}$$

$$\beta_e = \frac{1}{b_o^2 (R+1)} \left[X_{vav}^2 + \frac{(R+1)^2}{R} Y_{vg}^2 \right] + \beta_{eg} \tag{38e}$$

where

$$\langle u \rangle = \langle u_g \rangle = \langle v_i \rangle = \langle v_g \rangle = 0$$

The four parameters that are used as input quantities to the computer code are: X_{vav}, Y_{vi}, Y_{vg}, and β_{eg} and they must be of such a size that

$$1 > (\beta_i + \beta_e) \tag{39}$$

Specific values of X, U, V_i, and V_g at $\tau = 0$ for each plasma slab are read into the computer from a series of random numbers chosen such that each distribution is Gaussian about the zero mean where $\langle \Delta X_k \rangle = X_m/(N_s + 1)$. The sum over the sheet velocities and the total momentum are then nearly zero. A different set of random numbers may be chosen for the specific number that make up the average quantities X_{vav}, Y_{vi}, and Y_{vg} or any combination of them could use the same set. When two quantities use the same set and sequence of input numbers, they are said to be correlated and the correlation coefficient is unity. Since the random numbers were read into the computer on cards, ten numbers per card, identical decks represent correlated random variables. If, however, one of the decks is shuffled, the correlation coefficient of the new set of numbers and the original set is not necessarily zero because the numbers on each card were not shuffled. However, the contribution to the joint distribution by the two sets of random numbers is assumed negligible because $N_s = 500$ or larger. Therefore the term uncorrelated is employed here to mean only that, of two identical decks of cards, one deck has been shuffled. Possible variations of the input are then quite numerous because the several sets of numbers employed in a given run can each be correlated or uncorrelated with the other random variables or certain quantities of the plasma can be assumed not to be thermalized. The ambient magnetic induction is presented in figure 13 for six separate combinations of initial data with $\beta_{eg} = 0.01$ to illustrate some of the possible variations and the structure of the ambient magnetic field that they produce. Random electric currents in the Y direction, J_k, (lack of correlation of Y velocities of ions, V_i^k, and electrons, V_e^k) are noted to produce long wavelength disturbances in addition to a ragged character of the magnetic field. Introducing a thermal character into the X velocities, $\dot{X}_k$, of the slabs causes only a short wavelength or ragged appearance to the magnetic field after a short time ($\tau = 1$). From a physical point of view the initial random spacing of the plasma sheets has no effect on the magnetic field but the manner in which the computer code was used resulted in a slight variation in the induction. The second graph in figure 13 illustrates the short blips that result when the random spacing of sheets allows adjacent sheets to overlap. Relative to the much more marked, physical effects brought about by $\dot{X}_k$ and J_k, the influence of random ΔX_k can be ignored (cf. graphs 4 and 5 in fig. 13).

The effect of several of these different types of input on the structure of the compressed layer is illustrated in figures 14 through 17. Pertinent details of these results will be discussed in the next section.

The difference equations to be used in the electronic computer code were developed in reference 21. Several assumptions were made regarding the thermal behavior of the particles. First, the magnetic moment of the electron is an adiabatic invariant of the motion and the electrons act like a fluid with pressure. Second, the pressure of the electrons is assumed to be less than the magnetic pressure, so that, $\beta_e < 1$. Then the approximation was made that the electrons are on the average fixed relative to the local magnetic field lines so that

$$\frac{n_e}{B} \approx \frac{n_o}{B_\infty} \tag{40}$$

The pressure resulting from electron motion that is statistically independent of the motion of the ions or guiding centers can then be written as,

$$p_{eg} = p_{eo} \frac{B^2}{B_\infty^2} = \beta_{eg} \frac{B^2}{2\mu} \tag{41}$$

where β_{eg} is a constant. In the analysis, the guiding centers of the electrons are followed rather than the electrons themselves. Motion of the various slabs then can still be treated by means of the momentum equations used in Code I (i.e., eqs. (24) and (25)) provided V_e is replaced by V_g and a modification is made to the transverse electron current, j_{ye}. In order to account for the motion of the electron about the guiding center which is manifested as the pressure, p_{eg}, a contribution by the gradient of that pressure must be added to the drift current, $-n_o e v_g$; that is,

$$\begin{aligned} j_{ye} &= -n_o e v_g + \frac{1}{B} \frac{\partial p_{eg}}{\partial x} \\ &= -n_o e v_g + \frac{\beta_{eg}}{\mu} \frac{\partial B}{\partial x} \end{aligned} \tag{42}$$

Maxwell's equation for the magnetic induction then becomes in dimensionless notation,

$$(1 + \beta_{eg}) \left.\frac{\partial B}{\partial \xi}\right|_\tau = V_g - V_i \tag{43}$$

and the acceleration of a given slab of plasma is

$$\frac{\partial^2 X_k}{\partial \tau^2} = \frac{(1 + \beta_{eg})}{2} \frac{N_s}{X_m} \left(B_{k-1}^2 - B_k^2 \right) \tag{44}$$

(cf., eqs. (26b) and (34)). These equations can now be used to generate both the matrix and the inversion relations used in the computations.

DISCUSSION OF RESULTS

Graphical presentation of the large amount of numerical data obtained with the two computer codes makes it possible to observe and follow the development of the compressed layers of plasma for the various types of collisionless compression waves. An attempt was made to arrange each graph so that the data would be largely self-explanatory and the structure of the disturbances evident. Cases chosen for presentation were those which were felt to demonstrate best the mode of development and propagation typical for a given category of parameters. The results presented next may be summarized according to the listing below.

Ambient plasma	Solutions presented	Figure number
Cold	Structure vs. Alfvén Mach number: disturbance field parallel to b_o	1 - 6
Cold	Structure vs. Alfvén Mach number: disturbance field antiparallel to b_o	7,8
Cold	Structure vs. mass ratio	9
Cold	Structure for colliding waves	10,11
Cold	Reversal of electric field during compression of plasma	12
Warm	Effect of initial conditions on structure	13
Warm	Structure vs. Alfvén Mach number and β: disturbance field parallel to b_o	14 - 17

A detailed summary of the parameters and conditions appears in a table at the end of the paper.

The purpose of this section is to call to the reader's attention a few salient features of the various solutions. Its content is designed to supplement that of references 1, 2, and 21, and an attempt is made to repeat as little as possible.

The bulk of the figures presented in this paper are plots of magnetic field versus distance at uniformly spaced time intervals. In general, the earliest record shown in the upper right-hand corner of the figures is that at $\tau = 1$. The $\tau = 0$ result is not shown because it is trivial when the ambient gas is cold and is very much like the $\tau = 1$ record when the ambient plasma is warm. The portion of the magnetic field profile that is uniform and near $X = 0$ is the magnetic piston or vacuum region that contains no plasma. This region is separated from the compressed plasma layer by a narrow transition zone that is indicated in sketch (d) as the contact region. In the

figures containing plots of the type illustrated in the sketch (except for fig. 9) typical graphs have the trailing edge of the contact zone labelled. Only a part of the magnetic field profile in the undisturbed region out ahead of the wave is shown because the graphs for the cold cases are amputated when the magnetic field returns to within about 0.01 percent of its ambient value. All of the magnetic record between $X = 0$ and X_m is presented for the warm code because there is activity in the entire flow field when the ambient plasma has temperature.

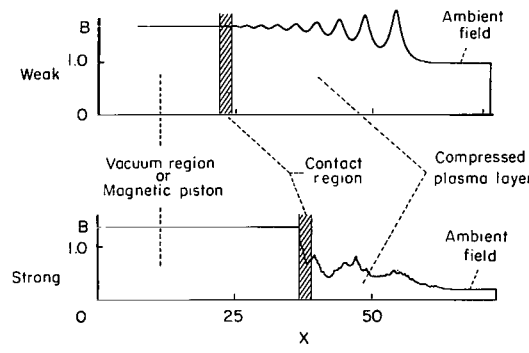

Sketch (d)

Before the computations were put into production, a series of short runs were made to determine a suitable mesh size for ξ and τ that would produce results essentially independent of the number of points used in the calculations.[1] Naturally, the largest permissible mesh size is used in order to reduce the computer time and hence cost of the data. It was found that the weak waves and the gross features of the strong waves converge quickly to the fine mesh result. However, the minute details of the strong wave solutions appear always to depend on mesh size. Therefore, the reader should use caution when attempting to apply or interpret any of the very fine structure presented in the graphs because some of it may be due to the use of a finite number of discrete slabs of fluid. A portion of the raggedness of the line graphs also arises because the mechanical plotter draws a straight line between the points. The mesh size used throughout the calculations was, with only a few exceptions, $\Delta\xi = 0.2$ and $\Delta\tau = 0.2$. See table I for complete details.

In order to retain a constant scale factor for the figures, the disturbance field e_o was taken as 1.0 and the ambient field b_o was changed. A measure of the strength of the disturbance is given by the ratio e_o/b_o. The time rate of application of the disturbance field, α, in equation (27b) was chosen as 0.12 except in the cases noted. Structure of the waves is noticeably influenced by this parameter if the cases compared are for large and small values of α. A large value of α will cause a random character to set in sooner when the Alfvén Mach number of the wave system is near 2. When $M_A < 2$, the amplitude of the wavelets increases with α but the gross nature of the structure of the compressed layer does not change. The most obvious feature in the flow field is that the magnetic piston region increases to a limited extent with α because the input disturbance becomes larger; that is

$$(B_{piston}) \cdot (X_{piston}) \leq e_o \left[\tau - \frac{1}{\alpha} (1 - e^{-\alpha\tau}) \right]$$

[1]Relationship of the numerical solutions such as those presented here to the "exact" solutions of these equations are discussed in references 1, 2, 35, and 36.

Hence, the magnetic field originally generated by the electrical disturbance becomes a part of the compressed layer (see also eq. (25) of ref. 1); that is, it forms the contact surface between the piston and the compressed plasma. The width of this transition region or contact surface is approximately $3\lambda/\lambda$ as illustrated in sketch (d). One unit of λ corresponds to the skin depth of a zero frequency electromagnetic disturbance,

$$\frac{c}{\left[\frac{ne^2(m_i + m_e)}{\epsilon m_i m_e}\right]^{1/2}}$$

and to the hybrid Larmor radius when the particles move with the Alfvén velocity.

Cold Ambient Plasma

Basic results.- The first sequence of solutions, presented in figures 1 through 6, demonstrates how the nature of the compressed layer changes with the strength of the disturbance (i.e., e_o/b_o or M_A) for an initially cold plasma ($T_{eo} = T_{io} = \beta_e = \beta_i = 0$). Situations represented in figures 1, 2, and 3 for weak or subcritical disturbances ($M_A < 2$) have the property that the slabs of plasma retain their original order and do not interchange positions throughout the duration of the event. As a result, the magnetic field in the wave structure is a smoothly undulating function of distance. As the disturbance intensity increases toward the condition that produces an Alfvén Mach number of 2, the crests of the individual waves become sharper until at $M_A \approx 2$ they are cusped or razor sharp. As this condition is approached from below, a slab of plasma will occasionally move out of its original order deserting the company of its former companions to move on a rather unusual excursion all its own. Such an occurrence causes the small blip on the last four or five magnetic field records shown on figure 3 for $M_A = 1.94$ and in the middle of figure 4(a) for $M_A = 2.17$. These results suggest that any disorder observed in a magnetic field record is attributable to the meandering motion of a slab or slabs of plasma. In figure 11(c) is shown the time-distance history of every tenth sheet that was used in the calculation, that is, k = 1, 11, 21, ... Motion of the wayward slab of plasma, as it seeks a new set of neighbors, is indicated in the middle of the figure by the approximately sinusoidal curve with the largest amplitude while the rest of the sheets that are shown stay in formation. (At this point the reader should ignore all data shown in fig. 11(c) for $\tau > 80$.) Such disregard for orderly motion by a single sheet appears to induce other slabs of plasma to go on similar junkets when $M_A > 2$ thereby leading to an end result wherein the entire flow field becomes chaotic as shown in figure 4(b) and in the lower part of 4(a). When $M_A < 2$ ($M_A = 1.94$, see fig. 3), excursions of individual sheets do not seem to be enough to produce chaos in the entire flow field; the wayward slab or slabs appear to find a new set of companions and content themselves by a regular undulating motion in their new location in the sheet order.

As the strength of the disturbance e_o/b_o is increased further, as in figures 5 and 6, the Alfvén Mach number exceeds two by a substantial amount and the original ion sheet arrangement is destroyed immediately. It is to be recalled that the assumption was made that the electrons stay in the strict formation set down at $\tau = 0$, so that only the ion slabs mix with distant neighbors. Out of the disorder in the sheet arrangement, a semblance of order is noted in the magnetic field profiles. Both figures 5 and 6 exhibit situations where the amplitude of a given pulse within the compressed layer builds up to a certain amount and then, at or near its crest, divides into two or more pulses. It also appears that as time progresses and the compressed layer attains some thickness, waves of a sort propagate back and forth between the front of the compressed layer and the magnetic piston. (The reader is asked to observe the figure horizontally at about eye level in order to best detect wave patterns and movement. It is to be noted that the diagonal format used for the plots emphasizes the rearward moving waves.) This bit of organization in an otherwise chaotic situation can be associated with the fact that a number of slabs (figs. 5(e) and 5(f)) associate themselves temporarily as a group even though other fluid elements may pass through or leave the group.

These orderly and disorderly characteristics in the magnetic field and time-distance records for the plasma slabs also appear in the velocity components. (See figs. 2(c) and 5(g).) Shown as points are the velocity components possessed by the sheets at several instants of time for both a weak ($M_A = 1.54$) and a strong ($M_A = 5.80$) disturbance. Note that the points near the origin represent sheets near the front and ahead of the wave. Since U^* is not equal to V^*, the y velocity had to be rescaled for these figures in order to have the direction properly oriented. The orderly character exhibited for the weak wave is lacking in the strong wave, thereby suggesting a thermalization of the compressed plasma as pointed out in reference 2. It should be noted here that wavelets in the subcritical cases originate with a small amplitude at the piston-plasma interface and propagate forward with their spacing and amplitude increasing with time. At large time, the spacing and amplitude become constant so as to form a continuous wave train like that considered by Davis, Lüst, and Schlüter in reference 6. In the supercritical cases, $M_A > 2$, waves seem to appear almost anywhere in the flow field. Properties of the wave structure for the transcritical (M_A slightly greater than 2) disturbances appear to be even more individualistic. Rate of application of the disturbance (i.e., the magnitude of α) also influences the structure of the wave front and the breakdown of order.

For each case presented, the characteristic times, the particle orbit periods, are different because they depend on b_o. Based on the ambient magnetic field, B_∞, the following periods are useful in analyzing wave patterns:

$$\tau_{ch} = \frac{2\pi}{b_o}, \qquad \tau_{ci} = \sqrt{R}\,\tau_{ch}, \qquad \tau_{ce} = \frac{1}{\sqrt{R}}\,\tau_{ch}$$

When examining the figures, especially figures 5 and 6, it is recommended that these times be borne in mind since the peak splitting in the strong wave solutions occurs at approximately one hybrid period.

Supplemental results.- Figures 7 through 12 present further results obtained with Code I that demonstrate the effect on the structure of the compressed layer brought about by reversed ambient magnetic field, b_o (figs. 7 and 8); mass ratio, R (fig. 9); impact of wave with centerplane, X_m (figs. 10 and 11); electric field reversal during compression (fig. 12). Although the number of cases presented for each is small, these solutions do indicate the general way in which the flow field is modified when the boundary conditions are changed in one of the foregoing ways.

Reversal of the ambient magnetic field for a weak (fig. 7) and a strong (fig. 8) disturbance leads to what may be called a thickening of the contact region between the magnetic piston and compressed layer. For a weak wave this region is characterized by a randomness or disorganization of the particles and of the magnetic field (fig. 7). No change appears in the organization and smoothness of the waves in the compressed layer when compared with the corresponding alined field case shown in figure 2.

Since the general structure of the flow field is already irregular for the strong wave case, a reversal of the ambient magnetic field simply inverts (without greatly altering) the magnetic field profile (fig. 8) as compared with the corresponding alined field case shown in figure 5. In both the weak and strong disturbance situations, the sheet order in the broadened contact region seems to roll or orbit about one another; see figure 7(c) and references 1 and 2.

It was shown in reference 1 that the weak wave solutions are independent of mass ratio, R. See equations (28), (30d), and (31) with $A_k^{o+} = A_k^{o-}$ and $(X_{k+1}^{o+} - X_k^{o+}) = X_m/(N_s + 1)$. Hence, it is necessary to consider only the supercritical cases here. When the disturbance is strong, the wave structure was found in reference 2 to depend on mass ratio by the approximate relation

$$\frac{\tau_1}{\tau_2} = \frac{X_1}{X_2} = \sqrt{\frac{R_1}{R_2}}$$

that is, to achieve a similar profile for the magnetic field at a given time, the spacing in time between graphs is adjusted so that $\delta\tau_1 = \sqrt{R_1/R_2}\,\delta\tau_2$. A comparison of the graphical results presented in figure 5 ($R = 25$, $M_A = 5.80$) with that in figure 9 for $R = 4$ and 100 demonstrates that this rule is very good qualitatively but is not exact (e.g., for $R_1 = 4$ and $R_2 = 25$, $\delta\tau = 0.4$). The magnetic profiles can be made to compare almost exactly on a quantitative basis, however, if the time of comparison is displaced a given amount for each case. A rule for the time shift to be applied was not found.

It has been supposed that a body of plasma in outer space could collide with another (ref. 42), for example, during magnetic solar storms. Under these conditions, it is possible that two collisionless shock waves would meet

and interact to establish some new type of phenomena. In other words, does the intersection of two collisionless compression waves give rise to any wave structure not observed for a single compression wave moving into a cold undisturbed plasma? An answer to such a question can be had from Code I for the case of two identical waves moving in the opposite direction and meeting at the $X = X_m$ station. This possibility exists because the midplane may be thought of as a perfect conductor that reflects any incident wave without loss. Reflection of a wave can be interpreted as the intersection of two identical waves moving in opposite directions at that point. For this reason, several solutions were carried out for subcritical disturbances ($M_A < 2$, see figs. 10 and 11) and one for a supercritical ($M_A > 2$) disturbance. Figure 10 illustrates the reflection (or interaction) of a wave system so weak that its reflection is still subcritical. An increase in the strength of the disturbance leads to a flow field wherein the compressed layer of the incident wave is weak, but a portion of the reflected field is randomized or of the supercritical type. Local intensification of the magnetic field in the region where the reflection is effective occurs for all wave intensities $M_A < 2$ and > 2. A change in flow-field order does not occur at all when the incident wave is strong. For this reason, a solution is not presented. Only for weak disturbances whose strength is approaching the critical is a change observed in the flow-field structure. Figure 11(c) exhibits a particle trajectory that departs markedly from the paths of adjacent elements before the weak wave ($M_A = 1.94$) impacts on the center plane. (See also fig. 3. The peak of the leading pulse shown there starts to drop and a small pip appears ahead of the wave as if to indicate that this foremost wave is about to split or divide.)

Nuclear fusion research devices sometimes use a positive magnetic pulse to initiate the compression of a plasma and then apply a reversed magnetic field to compress and heat the plasma further. Results from an attempt to simulate this process with Code I is shown in figure 12. Attention is first directed to the diagram in figure 12(a) that illustrates the type of disturbance studied. A second set of waves is generated by the change on the sign of the disturbance, e_o, in addition to the one usually present and the direction of motion of the contact surface changes twice. It is to be noted in the three parts of figure 12 that the first wave train generated proceeds almost independently of the events taking place at the initiating plane, $X = 0$. A slight spreading of the separate pulses appears to be taking place. This, once again, demonstrates the high degree of stability of the pulses found for the subcritical cases. Reversal of the electric field at $X = 0$ initiates a second wave train that appears to be moving faster and thereby overtaking the first. Time-distance records of selected sheets display the reversal of the sheet velocities and displacement induced at about $\tau = 20$ by the changing of the disturbance.

Warm Ambient Plasma

Numerical data presented graphically in figures 1 through 12 were obtained with a code that assumed the gas initially ahead of the compression wave had no temperature and therefore all particles were stationary and uniformly spaced. The more usual condition to be expected is for a fully ionized

gas to have some random motion and therefore temperature. Such motion may be very small in comparison with the directed motion of the entire mass so that a zero temperature approximation is a very good one. A computer code for a gas with initial temperature, as developed by Kilb in reference 21, is used here to study the effect of temperature in the ambient gas on the structure of the compressed layer of gas. These results, presented in figures 13 through 17, illustrate how the magnetic field in the compressed layer is modified by temperature from the cold case.

Since temperature manifests itself in several different ways, figure 13 was prepared in order to illustrate the initial ($\tau = 1$) magnetic field perturbations brought about in the ambient gas by assuming that the slabs of plasma have random (1) X-velocities, $\dot{X}_k$, (2) ion velocities, V_i^k, and (3) electron guiding center velocities, V_g^k. The sheet spacing is randomized also to simulate a more realistic initial state. Item (1) is seen to impart a short wavelength or jagged character to the ambient magnetic induction. Items (2) and (3) combine to give an electric current, J_k, when V_i^k and V_g^k are uncorrelated, that produces both a jagged and long wavelength character in the ambient field. Random sheet locations cause a very slight but detectable change in the magnetic field that, as mentioned previously, is due only to the manner in which the computer code was used. Any one or combination of the three items above could be used as input to simulate the temperature of the ambient plasma. In the calculations, some variations in the initial data were assumed to determine if there was a substantial effect on the wave structure. As can be seen from the figures presented here, no strongly evident change occurs when one or more temperature properties are taken as negligible in the ambient gas. In one case considered, the ion and electron guiding center temperatures were assumed to be nearly equal, that is, $\beta_i \approx \beta_g$ (fig. 14) but in all other cases the root mean squares of the random velocities were assumed to be equal, that is, $\beta_i = R\beta_g$ (figs. 13, 15, 16, and 17).

Results shown in figures 14 and 15 for a weak disturbance indicate that even a small temperature in the ambient gas brings about the destruction of the very orderly character of the subcritical solutions for the cold gas (cf. figs. 1, 2, and 3). A slow return to the smooth wave solution is evident for the leading pulses, but it appears that the thermal energy must be decreased to a very small β in order to bring about a completely smooth profile for the magnetic field in the compressed layer.

When $\beta = 0$, the magnetic profile in the compressed layer is smooth if the initial sheet spacing is not uniform provided that the sheets are renumbered before the calculation is commenced. The small fluctuations that appear in the second graph of figure 13 are due to an initially random sheet spacing without renumbering. This allows sheet crossing into the weak wave solutions. Although this nonphysical effect is small (cf. graphs 4 and 5 in fig. 13) it tends to exaggerate the thermal character of the compressed layer when β is very small and the disturbance is weak, as can be seen in figure 15.

Figures 1, 2, and 3 suggest that the magnetic field is everywhere continuous and no surface current exists at the contact surface. Such is not the case since a discontinuity, not resolved by the scale of the plot, does occur at the vacuum-plasma interface. In figures 14 and 15, however, the jump in

the magnetic field at the interface is evident. A somewhat larger surface current than that for the corresponding cold plasma separates the vacuum region from the compressed layer and a kinetic pressure must exist ($\beta_s \neq 0$). The existence of a jump in the magnetic induction for weak disturbances in cold plasma is in accord with the continuum theory as can be seen in sketch (e) in the next subsection, although for $M_A = 1.16$, $b_v - b_s \approx 0$. It should also be noted in figures 14 and 15 that there are waves in the ambient gas, some of which propagate and others which appear to be pulsations that do not move.

In figures 16 and 17, it appears that only the fine structure of the strong disturbance solutions is changed to any extent by the finite temperature of the ambient gas. The seemingly smaller magnitude of the undulations in the ambient gas is due to the scale of the magnetic field that was used. For example, if the vertical scales of B are adjusted so that the free-stream magnetic fields are equal, the random fluctuations also become equal. Temperature effects are relatively less important for a strong disturbance wave than for a weak one. Hence, the overall effect on the structure of the compressed layer of the strong wave would be expected to be smaller, as observed in figures 16 and 17. The supercritical waves are affected by temperature in that the formation of a pulse is delayed slightly and its maximum amplitude and sharpness are reduced. The time-distance diagrams illustrate the movement of selected slabs of plasma before and during their interaction with the compression wave. Slab motion prior to the passage of the disturbance is associated entirely with the selection of random numbers for the quantities: ΔX_k, $\dot{X}_k$, $V_i^k - V_e^k$ at $\tau = 0$.

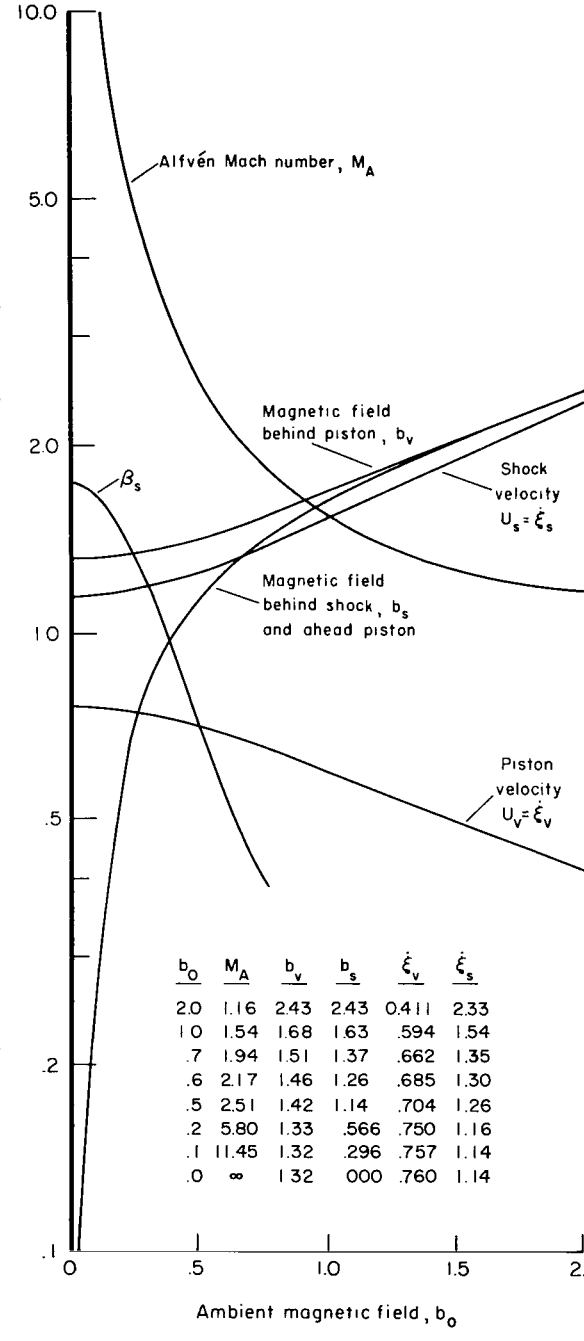

b_0	M_A	b_v	b_s	$\dot{\xi}_v$	$\dot{\xi}_s$
2.0	1.16	2.43	2.43	0.411	2.33
1.0	1.54	1.68	1.63	.594	1.54
.7	1.94	1.51	1.37	.662	1.35
.6	2.17	1.46	1.26	.685	1.30
.5	2.51	1.42	1.14	.704	1.26
.2	5.80	1.33	.566	.750	1.16
.1	11.45	1.32	.296	.757	1.14
.0	∞	1.32	000	.760	1.14

Sketch (e)

Predictions of Rankine-Hugoniot Theory

Certain time-averaged behavior of the foregoing machine solutions can be related to the corresponding results

obtained from "snowplow" theory. In the latter situations, the shock front and the piston front can be taken as infinitely thin transition regions separating the flow field into the following three regions: vacuum, shocked plasma, and unshocked plasma. The Rankine-Hugoniot jump conditions are then applied across the two transition zones. Predicted values of the magnetic field in vacuum and shocked plasma regions and the piston and shock velocities calculated by Auer, Hurwitz, and Kilb (see table I of ref. 2) are reproduced here in tabular and graphical form in sketch (e). The sketch shows M_A, b_V, b_S, U_V, and U_S plotted as functions of the ambient magnetic field and employs only the data provided in the table. The equations from which these curves were obtained are set forth in reference 2. The quantity, $\beta_S = p_S/(B^{*2}/2\mu) = b_V^2 - b_S^2$, is also shown and it is to be noted that the maximum theoretical pressure in the shocked plasma is roughly $1.7E_O\sqrt{n_O(m_i + m_e)/4\mu}$.

From figures 1 through 6 the value of the magnetic field on either side of the contact zone that separates the vacuum region from the compressed plasma as well as the piston and shock velocities, when averaged over a hybrid cyclotron period, can be compared with the predictions of Rankine-Hugoniot theory for a magnetic plasma obeying an equation of state with ratio of specific heats, $\gamma = 2$. The quantity, b_V, the vacuum magnetic field based on continuum theory, is indicated by a dashed line in the insert in figure 1, 2(a), 3, 4(a), 5(a), and 6(a) and also on the last graph of figure 1, 2(a), 3, 4(b), 5(d), and 6(d). The graphs in the inserts depict the temporal behavior of the magnetic and electric field in the piston region. It is to be noted that for the two cases, $M_A = 5.80$ and 11.45, the curve in the insert labelled $B_O(\tau)$ can be seen to oscillate about the predicted value with approximately the hybrid cyclotron frequency before settling down to within a percent of b_V. The quantity, b_S, the magnetic field in the shocked plasma based on continuum theory, is indicated on the last graph of figures 1, 2(a), 3, 4(b), 5(d), and 6(d), also by a dashed line. It can be seen that a space average is required before a comparison can be made. If the latest available graph is used, namely, solutions at $\tau = 70$, 70, 140, 260, and 277, respectively, the time variation of a space average may be assumed, for purposes of discussion, to be negligible. This is true at least for $B_O(\tau)$ as can be seen by inspection of the figure inserts. A quantitative comparison of b_S with a space average, such as

$$\frac{\sum_{k=L}^{M} B_k \, \Delta X_k}{\sum_{k=L}^{M} \Delta X_k}$$

is then possible provided the integers L and M, M > L, are chosen to eliminate the wave set and the contact zone. The contact region is about 3 units in width so its limits are well defined but the demarcation between wave sets and wakes for strong disturbance solutions is somewhat arbitrary. Because of this arbitrariness, only a visual comparison is presented.

Estimates of the average piston and disturbance front speed can be obtained from the figures mentioned above as well as from the time-distance plots (figs. 2(b), 7(b), and 7(c)) and compared with the corresponding value given here in sketch (e). To facilitate quantitative and visual comparison, the shock and piston velocities are shown on the latter three figures as dashed lines with slopes corresponding to U_V and U_S.

The relationship between the predicted shock and piston velocities, U_S and U_V, respectively, and the characteristic velocities, U_A and U_D, that is, the Alfvén velocity and the electric drift velocity, is illustrated in sketch (f). It summarizes for all six cases just presented, the four velocities that are pertinent to this analysis using the snowplow velocity, U^*, as a reference and the expression $U_A = b_o U^* = b_o$. From this it follows that $U_D = 1/b_o$. From the figures in the sketch U^* is omitted but would appear as a straight line with 45^o slope. The region between the lines indicating the piston and the disturbance front velocity is shaded. This sketch also illustrates the range of parameters used in the analysis, bringing out graphically a number of features. For example, the double streaming condition, namely, $U_S = 2U_A$, occurs when $U_p = U_A$ (see the $M_A = 1.94$ insert). Also, in the limit of very weak disturbances the inserts illustrate the trend of the shock velocity to that of the Alfvén velocity and the electric drift velocity to the piston velocity.

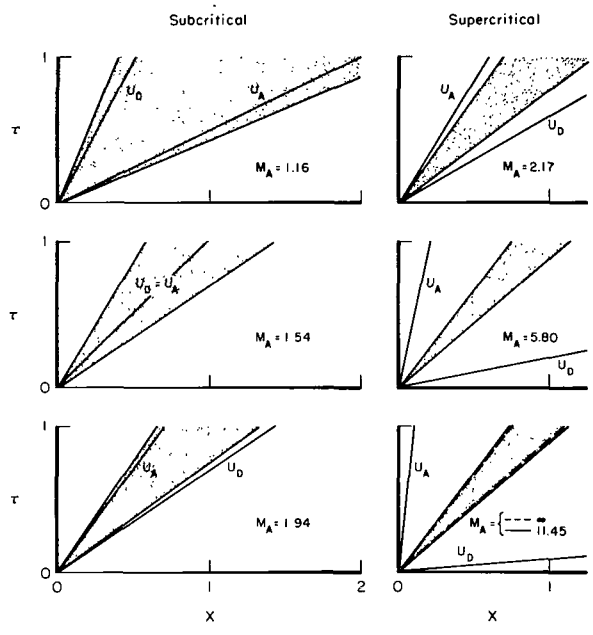

Sketch (f)

The predictions obtained from the Rankine-Hugoniot theory that has been applied to the "snowplow" model in reference 2 and summarized in sketch (e) can be extended to the situation in which the ambient plasma is tepid. In reference 21 it is shown that the numerical data reproduced in sketch (e) can be used when the plasma has an initial temperature that is characterized by the parameters, β_e and β_i (eqs. (35) and (36)). If the quantities, b_o and b_s, are replaced by $b_o(1 + \beta_e + \beta_i)^{1/2}$ and $b_s(1 + \beta_e + \beta_i)^{1/2}$, respectively, the remainder of the tabulated data in the sketch is unchanged. As an example of the modification brought about by the inclusion of temperature effects, the jump in the magnetic induction across the contact surface is calculated for $M_A = 1.54$. The jump is given by

$$b_v - b_s = 1.68 - 1.63 = 0.05$$

for cold, ambient plasma. For the same Alfvén Mach number and $\beta_e = \beta_i = 0.01$, the jump is given by

$$b_v - b_s(1 + \beta_e + \beta_i)^{-1/2} \approx 1.68 - 1.63\left(1 - \frac{\beta_e + \beta_i}{2}\right) = 0.07$$

The predicted increase in the surface current at the piston is one of the conspicuous differences between the numerical results for cold and tepid ambient plasma with $M_A = 1.54$ that have been presented (cf. figs. 2(a), 14(a), and 15).

CONCLUDING REMARKS

Presentation of data in the graphical form used in this paper makes it possible to observe certain wave systems and the evolution of the magnetic structure in the compressed layers of plasma. From the number of cases considered, it is possible to identify certain properties of the flow field with its boundary conditions. For compression waves with subcritical strength ($M_A < 2$) moving into cold plasma, the waves originate at the magnetic piston with vanishingly small amplitude and move forward with increasing amplitude and spacing. As time progresses, the compressed layer of plasma thickens to where its foremost part forms a long train of equally spaced smooth waves all of the same shape. All sheets of plasma remain in their original formation or order throughout the duration of the event. It appears that a small initial temperature of the ambient gas can destroy the smooth magnetic profiles and the highly organized slab motion and increase the jump in the magnetic field at the contact surface.

When the Alfvén Mach number of the wave front approaches 2, a slab or slabs of ions move out of order on wild excursions causing jaggedness in the magnetic profile. Such random wandering becomes more frequent as M_A increases and eventually brings about the rapid and complete destruction of orderliness in the compressed layer when M_A is substantially above 2. If the ambient plasma is warm, the radomization or thermalization of the compressed gas occurs at lower values of M_A, but the over-all features of the flow field are not altered appreciably. When disorder is significant, there is such a wide range of fluid motions that the detailed flow features of each situation appear to be individualistic with only the gross features being common to the entire group of solutions for $M_A > 2$. Disorder in the sheet arrangement is closely tied to the roughness in the magnetic field profile.

Ease of definition or sharpness of the compressed layer at its boundaries is a requirement for the experimenter interested in measuring the location and thickness of the compressed layer. It is therefore to be noted that the front of the subcritical waves would be quite easy to detect but the location of the contact region or the magnetic piston is obscure. When the disturbance is intense enough that $M_A > 2$, the magnetic piston is prominent but the wave front tends to blend with the ambient field - especially when the undisturbed gas has an initial temperature.

Calculations carried out for the graphs presented here usually assume the mass ratio, R, to be 25. When a wave propagates with a speed for which the Alfvén Mach numbers is less than 2, and the ambient plasma is cold, the result is independent of R and hence applicable to any situation in which the other parameters apply. In the supercritical, cold plasma cases and in all of the warm plasma cases, the solutions are found to depend on the mass ratio according to the approximate rule given by Auer, Hurwitz, and Kilb, that is, $\tau_1/\tau_2 = X_1/X_2 = (R_1/R_2)^{1/2}$. Qualitative properties of the flow field are carried over very well, and a number of quantitative detailed features are also represented if a small time shift is applied in addition to the foregoing rule.

Finally, it is to be noted that the physical situations that led to the analysis and calculations presented here vary with three space dimensions and time, whereas the solutions were carried out for a flow field that is a function of one space dimension and time. If these results are used to study a two- or three-dimensional configuration, only certain features found for the compressed layer in one-dimension can be applied to segments of the two- and three-dimensional waves.

Ames Research Center
National Aeronautics and Space Administration
Moffett Field, Calif., Aug. 31, 1964

APPENDIX

RÉSUMÉ OF THE LITERATURE RELATED TO PRESENT WORK

Theoretical consideration of magnetic compression waves in rarefied plasmas appears to have started with the work of Adlam and Allen (refs. 3 and 4). They analyzed the structure of a disturbance probably best described as a solitary wave propagating in a direction perpendicular to the ambient magnetic field. It is assumed there that the original thermal energy of a particle is negligible in comparison with the energy it acquires in the wave; that is, the ambient gas is effectively at zero temperature or cold. Also, the particles may move in an x and y direction but are not permitted to interchange positions or permute their order. Since even a small charge separation results in a large electric field, the number densities of the electrons and protons are taken to be everywhere equal. The electric field in the direction of wave motion is determined as that required to force a given pair of electrons and ions to have the same x velocity. Such an assumption is equivalent to the statement that the plasma frequency is much much greater than the ion or electron cyclotron frequency. Electrostatic oscillations are assumed thereby to play an insignificant role compared with motions resulting from the magnetic field. Subsequent investigations of the structure of the wave and of the compressed layer (refs. 5 through 17) treat the nature of these compression waves and their application to certain physical situations. Generalization of these results to a plasma that has a temperature before it enters the wave is described in references 18 through 23. The structure of an electrostatic shock ($B = 0$) is studied in reference 24. Changes brought about by electrostatic oscillations on an initially cold plasma embedded in a magnetic field are studied in reference 25. Recently, the second author of this paper extended in reference 26 the material of references 1 and 2 to include charge separation by treating the motion of electrons and ions as independent particles rather than as pairs. References 27 through 30 consider the wave characteristics when the ambient magnetic field is either parallel to or canted at an arbitrary angle to the direction of propagation.

The majority of the aforementioned papers employ differential equations that are solved analytically or numerically for a mathematically continuous plasma. Solution by direct numerical integration of the basic differential equations for a discrete model of a plasma in a magnetic field was first carried out by Auer, Hurwitz, and Kilb in references 1 and 2 wherein they examined the structure of the entire compression region in detail. Lagrangian coordinates were employed to follow the motion of groups of particles from which the local electric and magnetic fields were determined. Agreement with the previous analytical results was found to be good for waves that move at Alfvén Mach numbers between 1 and 2. For higher wave speeds, a new type of structure for the compressed layer not previously predicted was discovered and is reported in reference 2. It consists of a randomlike distribution of the flow quantities suggesting a temperature increase or thermalization of the originally cold and well ordered ions.

Questions arise as to the convergence and accuracy of such numerical solutions as compared with so-called exact results because the governing differential equations are replaced by difference equations and because the continuum plasma is replaced by discrete elements. Insight is obtained for the reliability of such a method by referring to studies of collisionless plasmas under several different situations (refs. 31 through 36) wherein the technique is similar and the computer studies of the discrete models employed recover the exact results. Although these results are not directly applicable to the present investigation, they tend to bring about a feeling of confidence that the numerical results presented here do approximate quite closely the solution of the differential equations and therefore do represent the flow field considered.

REFERENCES

1. Auer, P. L., Hurwitz, H., Jr., and Kilb, R. W.: Low Mach Number Magnetic Compression Waves in a Collision-Free Plasma. The Physics of Fluids, vol. 4, no. 9, Sept. 1961, pp. 1105-1121.

2. Auer, P. L., Hurwitz, H., Jr., and Kilb, R. W.: Large-Amplitude Magnetic Compression of a Collision-Free Plasma. II. Development of a Thermalized Plasma. The Physics of Fluids, vol. 5, no. 3, March 1962, pp. 298-316.

3. Adlam, J. H., and Allen, J. E.: The Structure of Strong Collision-Free Hydromagnetic Waves. Phil. Mag., 8th ser., vol. 3, no. 29, May 1958, pp. 448-455.

4. Adlam, J. H., and Allen, J. E.: Hydromagnetic Disturbance of Large Amplitude in a Plasma. Proc. Second United Nations International Conference on the Peaceful Uses of Atomic Energy, vol. 31, Theo. and Exp. Aspects of Controlled Nuclear Fusion, Geneva, 1-13 Sept. 1958, pp. 221-224.

5. Gardner, C. S., et al.: Hydromagnetic Shock Waves in High-Temperature Plasmas. Proc. Second United Nations International Conference on the Peaceful Uses of Atomic Energy, vol. 31, Theo. and Exp. Aspects of Controlled Nuclear Fusion, Geneva, 1-13 Sept. 1958, pp. 230-237.

6. Davis, L., Lüst, R., and Schlüter, A.: The Structure of Hydromagnetic Shock Waves. I. Nonlinear Hydromagnetic Waves in a Cold Plasma. Zeitschrift für Naturforschung, v. 13a, 1958, pp. 916-936.

7. Adlam, J. H., and Pyle, I. C.: Collision Free Compression of a Plasma. Proc. Fourth International Conference on Ionization Phenomena in Gases, vol. II, part IVC., The Azimuthal Pinch, Uppsala, Sweden, 17-21 Aug. 1959, pp. 1077-1081.

8. Sagdeev, R. Z.: "Shock" Waves in Rarefied Plasma. Proc. Fourth International Conference on Ionization Phenomena in Gases, vol. II, part IVD., Shock-Waves, Uppsala, Sweden, 17-21 Aug. 1959, pp. 1081-1085.

9. Kantrowitz, A., et al.: Collision Free Magnetohydrodynamic Shock Wave. Proc. Fourth International Conference on Ionization Phenomena in Gases, vol. II, part IVD, Uppsala, Sweden, 17-21 Aug. 1959, pp. 1086-1091.

10. Dungey, J. W.: Strong Hydromagnetic Disturbances in a Collision-Free Plasma. Phil. Mag., 8th ser., vol. 4, no. 41, May 1959, pp. 585-593.

11. Blank, A. A., and Grad, H.: Steady One-Dimensional Fluid-Magnetic Collisionless Shock Theory. Part IV-D. International Astronomical Union and International Union of Theoretical and Applied Mechanics. Proc. 4th Symposium on Cosmical Gas Dynamics. Aerodynamic Phenomena in Stellar Atmospheres I. A. U. Symposium No. 12, Aug. 18-30, 1960, Varenna, Italy, Supplemento del Nuovo Cimento, vol. XXII, n. 1, 1961 Serie X, pp. 459-467.

12. Davis, L., Chairman: Discussion. Part IV-D. International Astronomical Union and International Union of Theoretical and Applied Mechanics. Proc. 4th Symposium on Cosmical Gas Dynamics. Aerodynamic Phenomena in Stellar Atmospheres I. A. U. Symposium No. 12, Aug. 18-30, 1960, Varenna, Italy, Supplemento del Nuovo Cimento, vol. XXII, n. 1, 1961 Serie X, pp. 468-486.

13. Gardner, C. S., and Morikawa, G. K.: Similarity in the Asymptotic Behavior of Collision-Free Hydromagnetic Waves and Water Waves. NYO-9082, New York University, May 1, 1960.

14. Morawetz, C. S.: Magnetohydrodynamic Shock Structure Without Collisions. The Physics of Fluids, vol. 4, no. 8, Aug. 1961, pp. 988-1006.

15. Morawetz, C. S.: Modification for Magnetohydrodynamic Shock Structure Without Collisions. The Physics of Fluids, vol. 5, no. 11, Nov. 1962, pp. 1447-1450.

16. Loladze, Ts. D., and Tsintsadze, N. L.: Nonlinear Vibrations of a Two-Component Plasma in a Magnetic Field. Soviet Physics - Technical Physics, vol. 6, no. 11, May 1962, pp. 944-946.

17. Sagdeev, R. Z.: The Fine Structure of a Shock-Wave Front Propagated Across a Magnetic Field in a Rarefied Plasma. Soviet Physics - Technical Physics, vol. 6, no. 10, April 1962, pp. 867-871.

18. Hain, K., Lüst, R., and Schlüter, A.: Hydromagnetic Waves of Finite Amplitude in a Plasma with Isotropic and Nonisotropic Pressure Perpendicular to a Magnetic Field. Reviews of Modern Physics, vol. 32, no. 4, Oct. 1960, pp. 967-972.

19. Auer, P. L., and Nation, J. A.: Magneto-Compressional Disturbance in a Tepid Plasma. Il Nuovo Cimento, vol. XXII, n. 3, Nov. 1, 1961, pp. 533-547.

20. Baños, A., Jr., and Vernon, R.: Large Amplitude Waves in a Collision-Free Plasma. I. - Single Pulses with Isotropic Pressure. Il Nuovo Cimento, vol. XV, n. 2, 1960, pp. 269-287.

21. Kilb, R. W.: Large Amplitude Magnetic Compression of a Collision-Free Plasma. III. Plasma Magnetic Shock Waves with Initial Temperatures. GE Res. Lab. Rep. No. 62-RL-(3169E), Nov. 1962.

22. Morton, K. W.: Large-Amplitude Compression Waves in an Adiabatic Two-Fluid Model of a Collision-Free Plasma. Jour. Fluid Mech., vol. 14, pt. 3, Nov. 1962, pp. 369-384.

23. Moiseev, S. S., and Sagdeev, R. Z.: Collisionless Shock Waves in a Plasma in a Weak Magnetic Field. Jour. Nuclear Energy, vol. 5, pt. C, pp. 43-47.

24. Colgate, S. A.: Collisionless Plasma Shock. The Physics of Fluids, vol. 2, no. 5, Sept.-Oct. 1959, pp. 485-493.

25. Wolf, F. A.: The Effect of Charge Separation on Nonlinear Waves in a Collision-Free Plasma. Univ. of Calif. UCRL-6700, June 1962.

26. Rossow, V. J.: Magnetic Compression of Collision-Free Plasmas With Charge Separation. The Physics of Fluids, vol.

27. Parker, E. N.: A Quasi-Linear Model of Plasma Shock Structure in a Longitudinal Magnetic Field. Jour. Nucl. Energy, vol. 2, pt. C: Plasma Physics, 1961, pp. 146-153.

28. Tverskoi, B. A.: Propagation of One-Dimensional Self-Similar Plasma Waves Along a Magnetic Field. Soviet Physics JETP, vol. 15, no. 3, Sept. 1962, pp. 581-584.

29. Saffman, P. G.: Propagation of a Solitary Wave Along a Magnetic Field in a Cold Collision-Free Plasma. Jour. Fluid Mech., vol. 11, 1961, pp. 16-20.

30. Saffman, P. G.: On Hydromagnetic Waves of Finite Amplitude in a Cold Plasma. Jour. Fluid Mech., vol. 11, 1961, pp. 552-566.

31. Dawson, J. M.: Nonlinear Electron Oscillations in a Cold Plasma. Physical Review, vol. 113, no. 2, Jan. 15, 1959, pp. 383-387.

32. Dawson, J. M.: The Breaking of Large Amplitude Plasma Oscillations. Plasma Physics Laboratory Rep. MATT-31, Princeton University, Feb. 1960.

33. Buneman, O.: Maintenance of Equilibrium by Instabilities. J. Nucl. Energy, pt. C: Plasma Physics, 1961, vol. 2, no. 1-4, pp. 119-134.

34. Dawson, J. M.: One-Dimensional Plasma Model. The Physics of Fluids, vol. 5, no. 4, April 1962, pp. 445-459.

35. Eldridge, O. C., and Feix, M.: One-Dimensional Plasma Model at Thermodynamic Equilibrium. The Physics of Fluids, vol. 5, no. 9, Sept. 1962, pp. 1076-1080.

36. Eldridge, O. C., and Feix, M.: Numerical Experiments with a Plasma Model. The Physics of Fluids, vol. 6, no. 3, March 1963, pp. 398-406.

37. Spreiter, J. R., and Jones, W. P.: On the Effect of a Weak Interplanetary Magnetic Field on the Interaction Between the Solar Wind and the Geomagnetic Field. Jour. Geophys. Res., vol. 68, no. 12, June 1963, pp. 3555-3564.

38. Hines, C. O.: The Magnetopause: A New Frontier in Space. Science, vol. 141, no. 3576, July 1963, pp. 130-136.

39. Axford, W. I.: The Interaction Between the Solar Wind and the Earth's Magnetosphere. Jour. Geophys. Res., vol. 67, no. 10, 1962, pp. 3791-3796.

40. Kellogg, P. J.: Flow of Plasma Around the Earth. Jour. Geophys. Res., vol. 67, no. 10, Sept. 1962, pp. 3805-3811.

41. Dessler, A. J.: Further Comments on Stability of Interface Between Solar Wind and Geomagnetic Field. Jour. Geophys. Res., vol. 67, no. 12, Nov. 1962, pp. 4892-4894.

42. Kahn, F. D.: Collision of Two Highly Ionized Clouds of Gas. Reviews of Modern Physics, vol. 30, no. 3, July 1958, pp. 1069-1072.

43. Parker, E. N., and Tidman, D. A.: Radio Emission from Plasma Shocks. The Physics of Fluids, vol. 3, no. 3, May-June 1960, pp. 369-372.

44. Tidman, D. A.: Radio Emission by Electrons in the Fine-Structure Electric Fields of Shock Waves. The Physics of Fluids, vol. 5, no. 9, Sept. 1962, pp. 1104-1112.

45. Colgate, S. A., and Wright, R. E.: Collapse - The Shock Heating of a Plasma. Proc. Second United Nations International Conference on the Peaceful Uses of Atomic Energy, vol. 32, Controlled Fusion Devices, Geneva, Sept. 1-13, 1958, pp. 145-149.

46. Panofsky, W. K. H., and Phillips, Melba: Classical Electricity and Magnetism. Second ed., Addison-Wesley, 1962, p. 330.

TABLE I.- SUMMARY OF PARAMETERS AND CONDITIONS FOR SOLUTIONS PRESENTED

	Disturbance field (α = 0.12)	Equivalent Alfvén Mach number	Mass ratio	Flow field size	Initial plasma state	Current sheet initial conditions		
Figure	e_o/b_o	M_A	R	X_m/N_s	β_e/β_i	Spacing, ΔX_k	Velocity, $\dot{X}_k$	Current, J_k
1	1.0/2.0	1.16	25	300/1500	0/0	Uniform	0	0
2	1.0/1.0	1.54	25	300/1500	0/0	Uniform	0	0
3	1.0/0.7	1.94	25	300/1500	0/0	Uniform	0	0
4	1.0/0.6	2.17	25	300/1500	0/0	Uniform	0	0
5	1.0/0.2	5.80	25	300/1500	0/0	Uniform	0	0
6	1.0/0.1	11.45	25	300/1500	0/0	Uniform	0	0
7	1.0/-1.0	1.54	25	300/1500	0/0	Uniform	0	0
8	1.0/-0.2	5.80	25	300/1500	0/0	Uniform	0	0
9a,b	1.0/0.2	5.80	4	300/1500	0/0	Uniform	0	0
9c,d	1.0/0.2	5.80	100	300/1500	0/0	Uniform	0	0
10	1.0/1.0	1.54	25	50/250	0/0	Uniform	0	0
11	1.0/0.7	1.94	25	100/500	0/0	Uniform	0	0
12	+&-1.0/1.0	1.54	25	200/1000	0/0	Uniform	0	0
13	1.0/0.908	1.54	25	200/1000	0.02/0.2	- See figure -		
14	1.0/0.988	1.54	25	200/1000	0.02/0.01	Random	Random	Random
15	1.0/0.999	1.54	25	200/1000	0.0002/0.0025	Random	Random	Random
16	1.0/0.181	5.80	25	200/1000	0.02/0.2	Random	Random	Random
17	1.0/0.181	5.80	25	200/1000	0.02/0.2	Random	Random	0

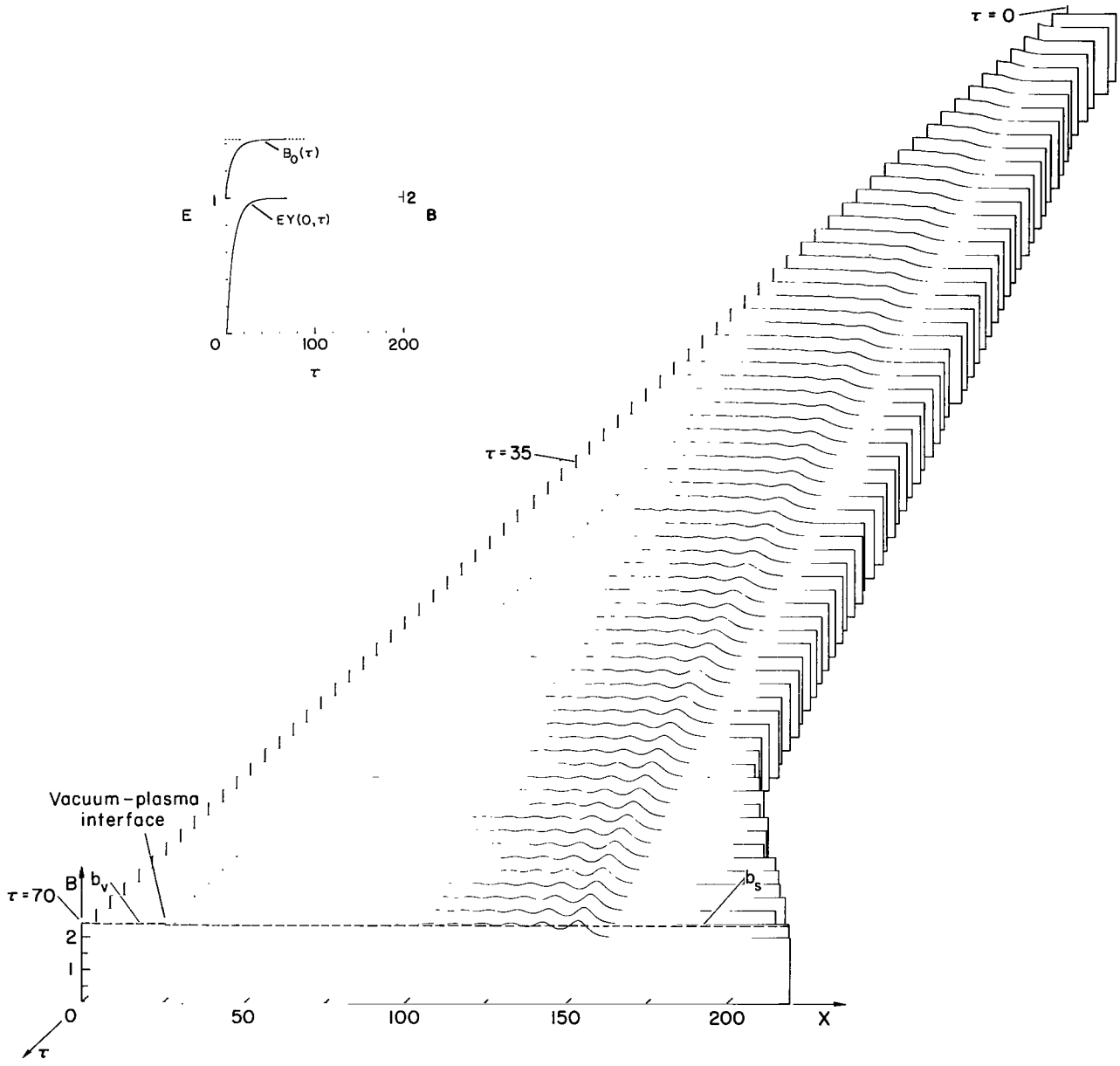

Figure 1.- Development of magnetic induction with time for a weak disturbance: $e_o = 1.0$, $b_o = 2.0$ ($M_A = 1.16$), $R = 25$.

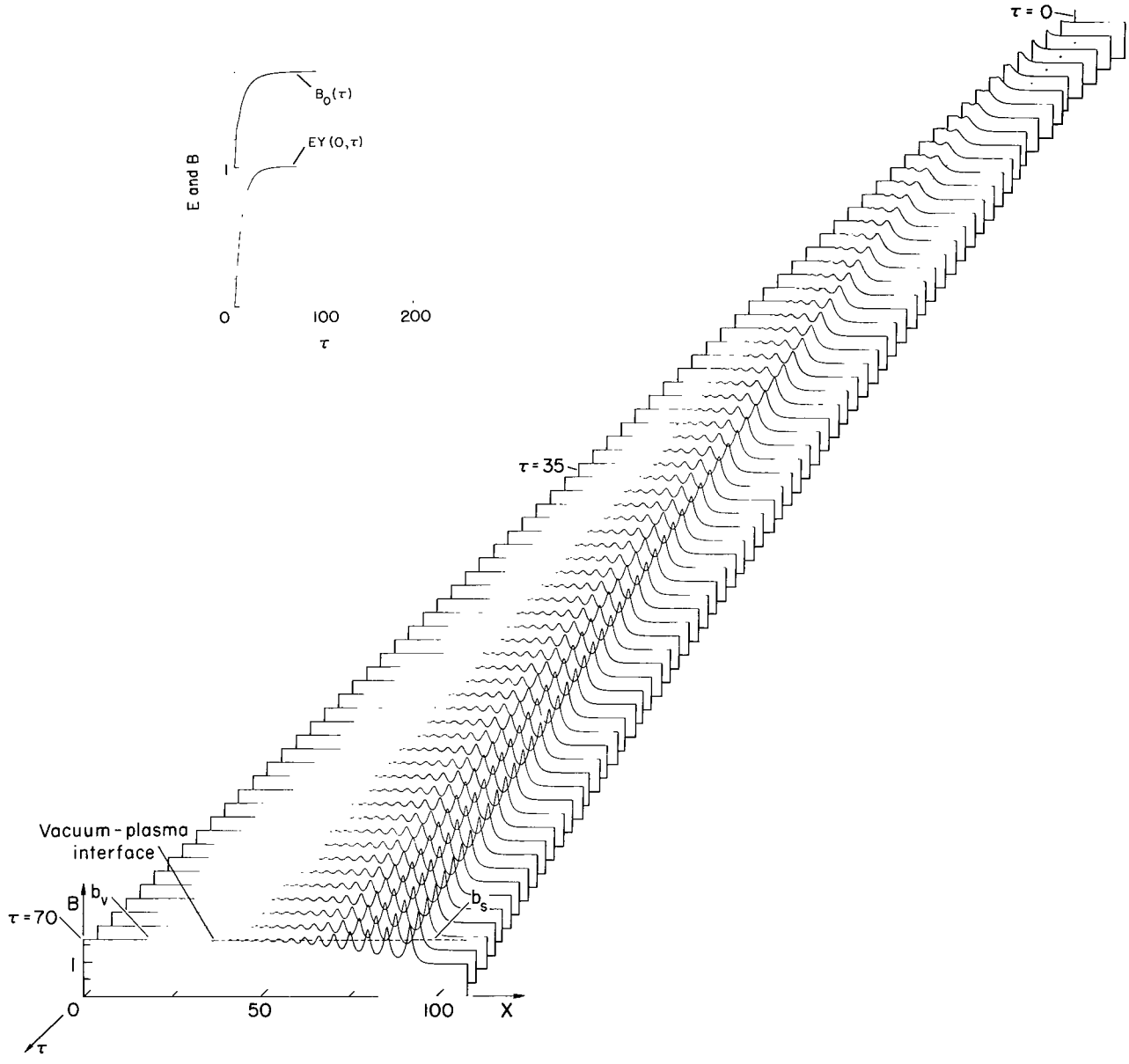

(a) Magnetic induction.

Figure 2.- Development of flow field with time for a weak disturbance: $e_o = 1.0$, $b_o = 1.0$ ($M_A = 1.54$), R = 25.

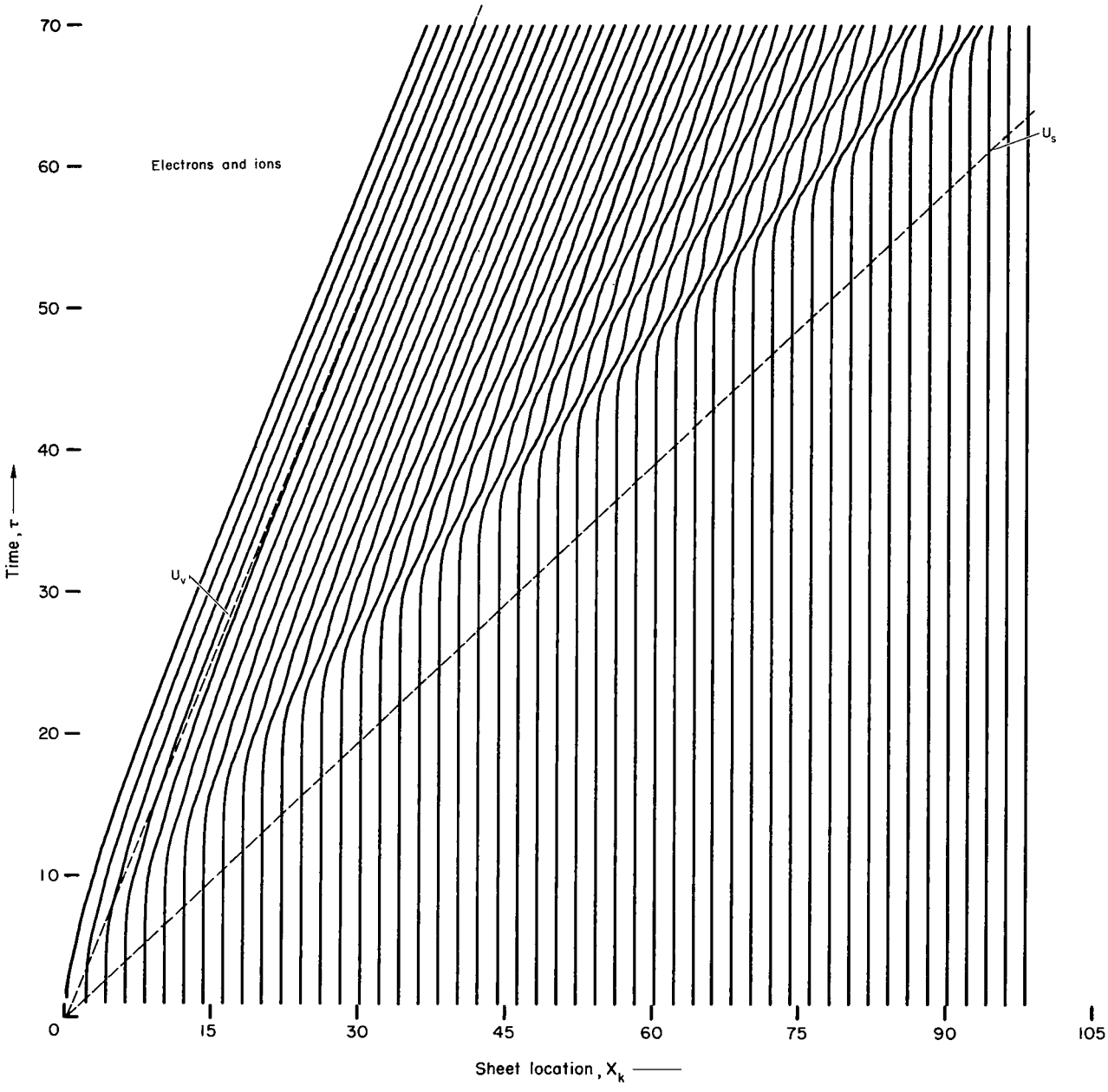

(b) Time-distance records of every tenth sheet, X_K vs. τ; k = 1, 11, 21, . . .

Figure 2.- Continued.

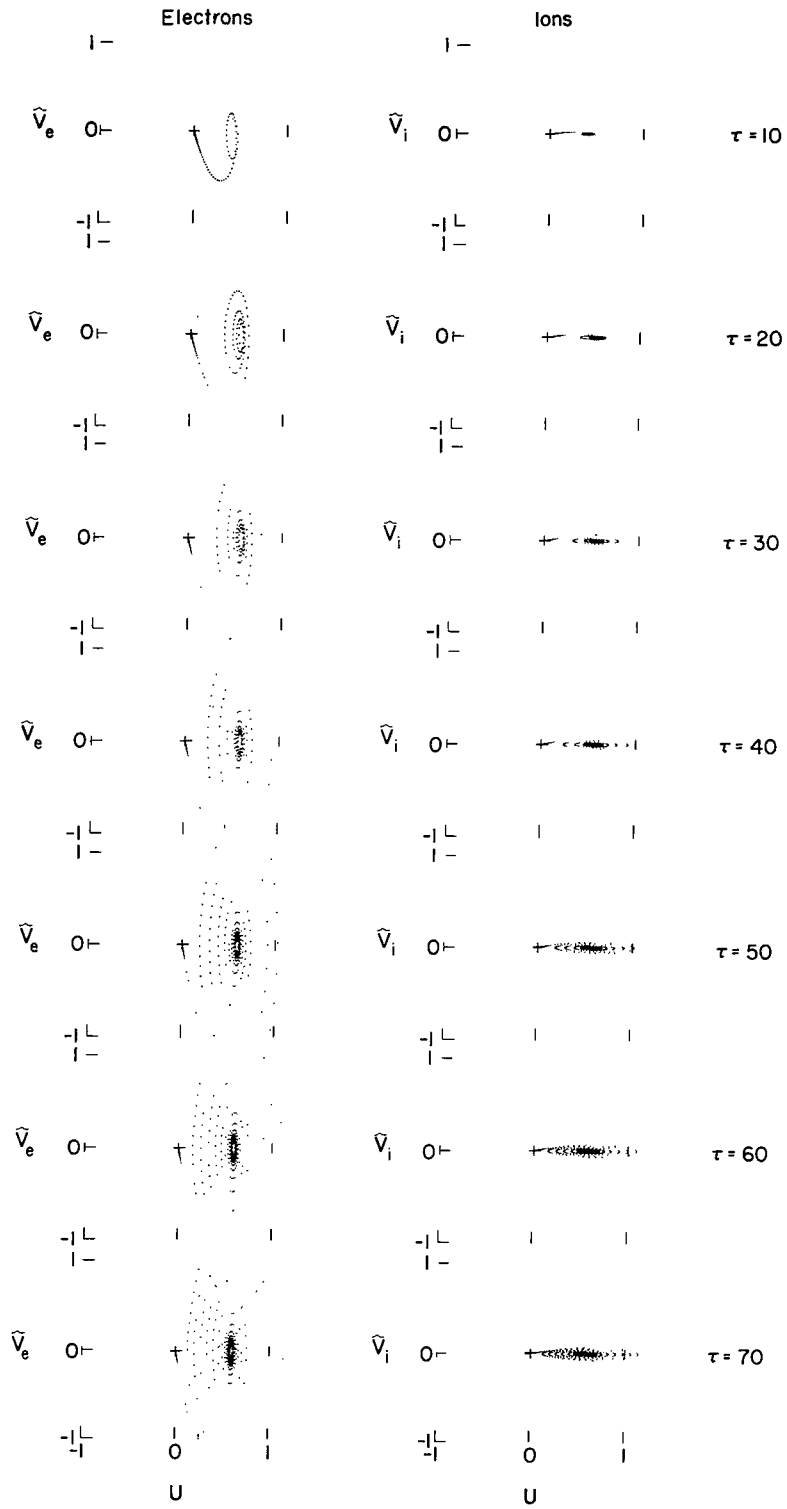

(c) Distribution in velocity space for all sheets, $\tilde{V} = VV^*/U^*$.

Figure 2.- Concluded.

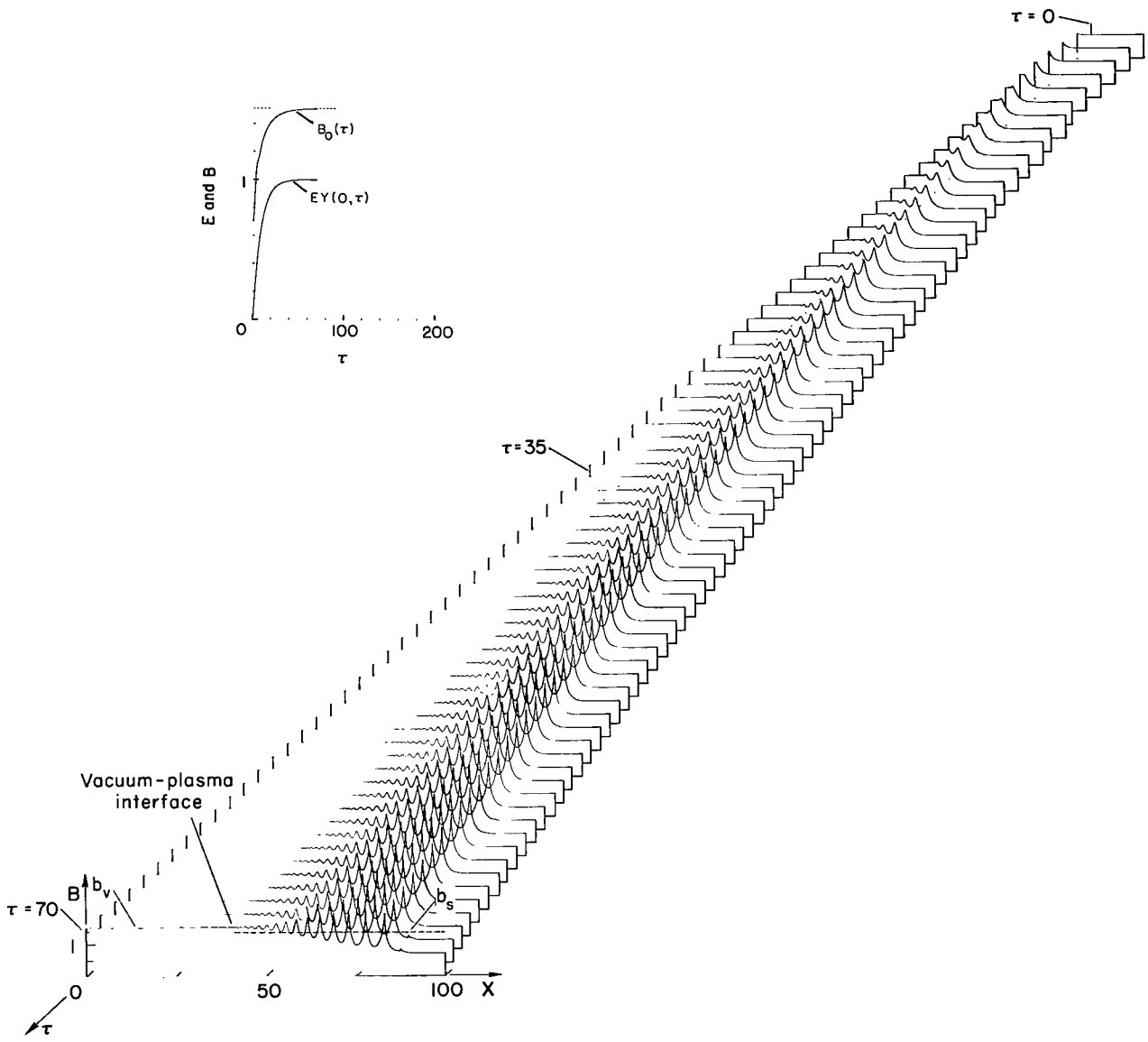

Figure 3.- Development of magnetic induction with time for a weak disturbance: $e_o = 1.0$, $b_o = 0.7$ ($M_A = 1.94$), R = 25.

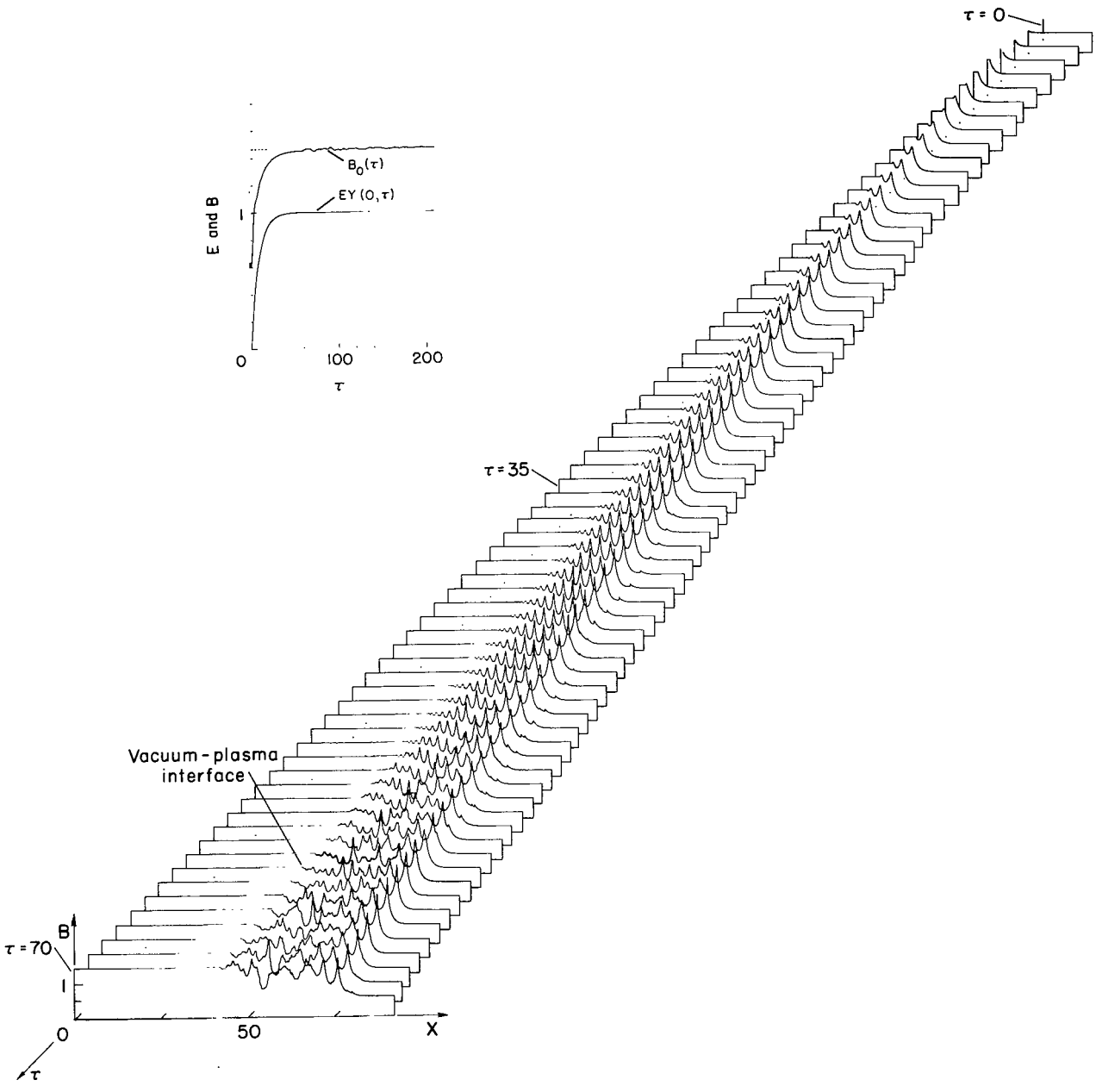

(a) τ = 0 - 70

Figure 4.- Development of magnetic induction with time for transitional disturbance: e_o = 1.0, b_o = 0.6 (M_A = 2.17), R = 25.

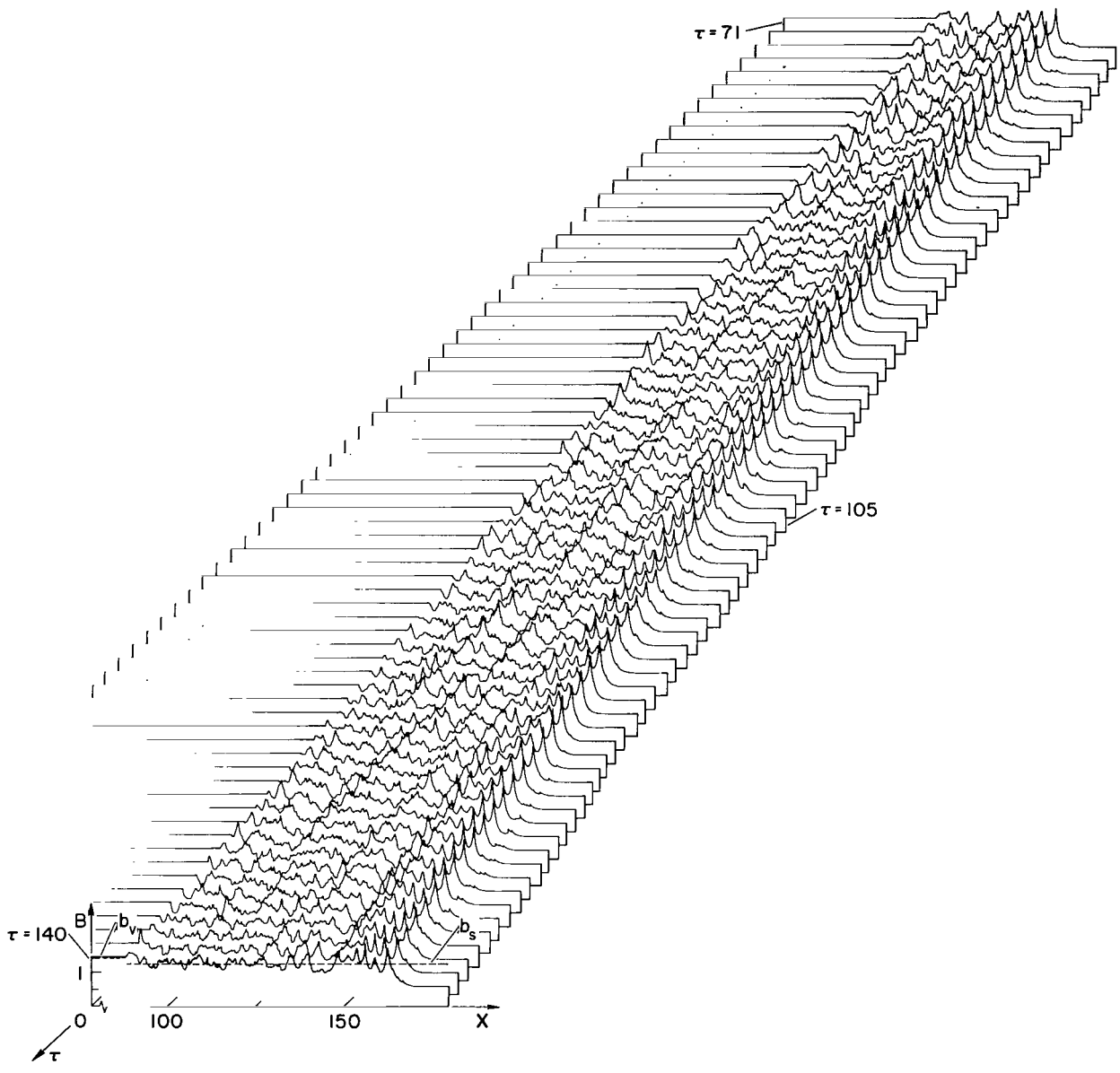

(b) τ = 71 - 140

Figure 4.- Concluded.

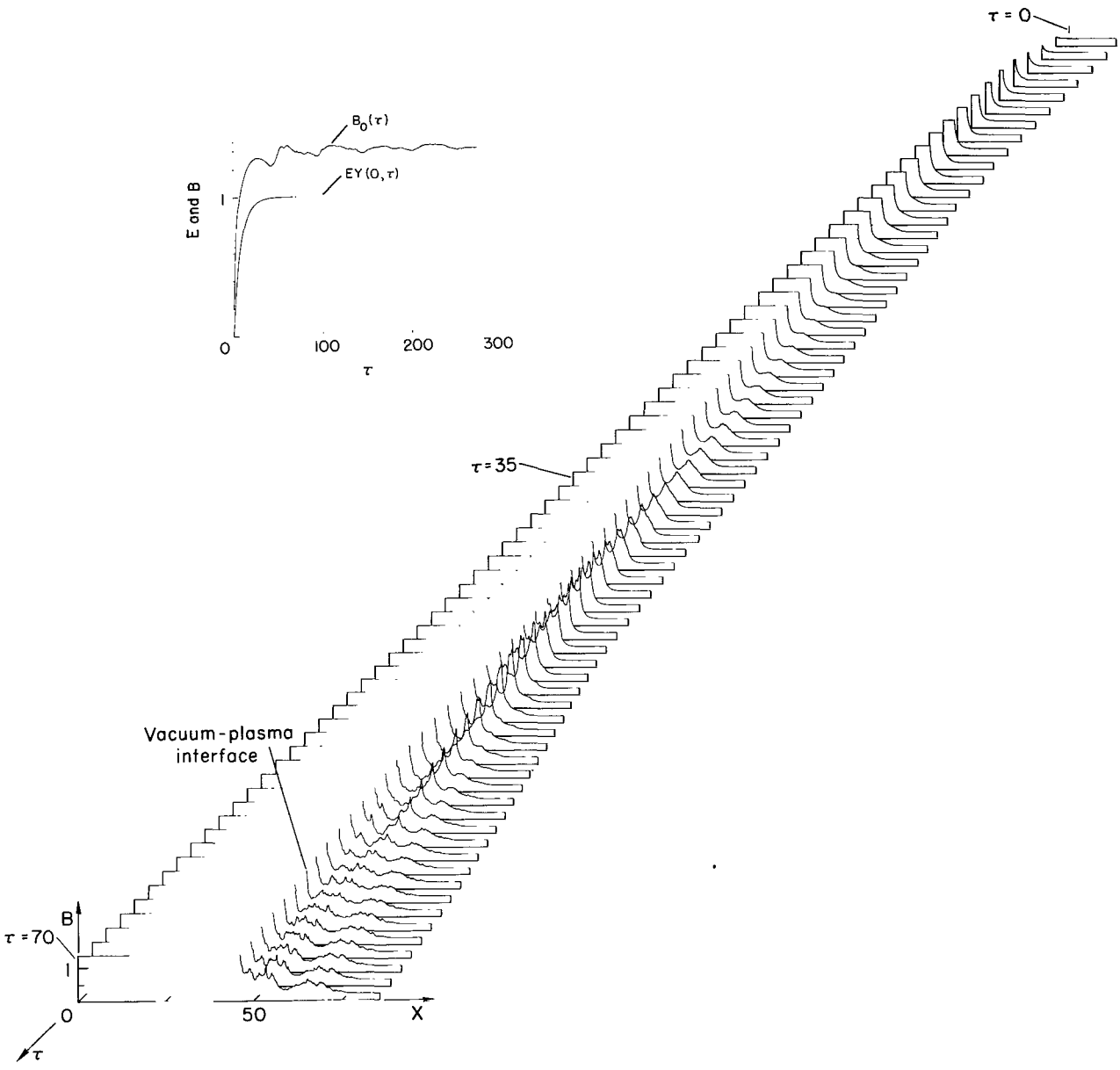

(a) Magnetic induction, τ = 0 - 70.

Figure 5.- Development of flow field with time for a strong disturbance: e_o = 1.0, b_o = 0.2 (M_A = 5.80), R = 25.

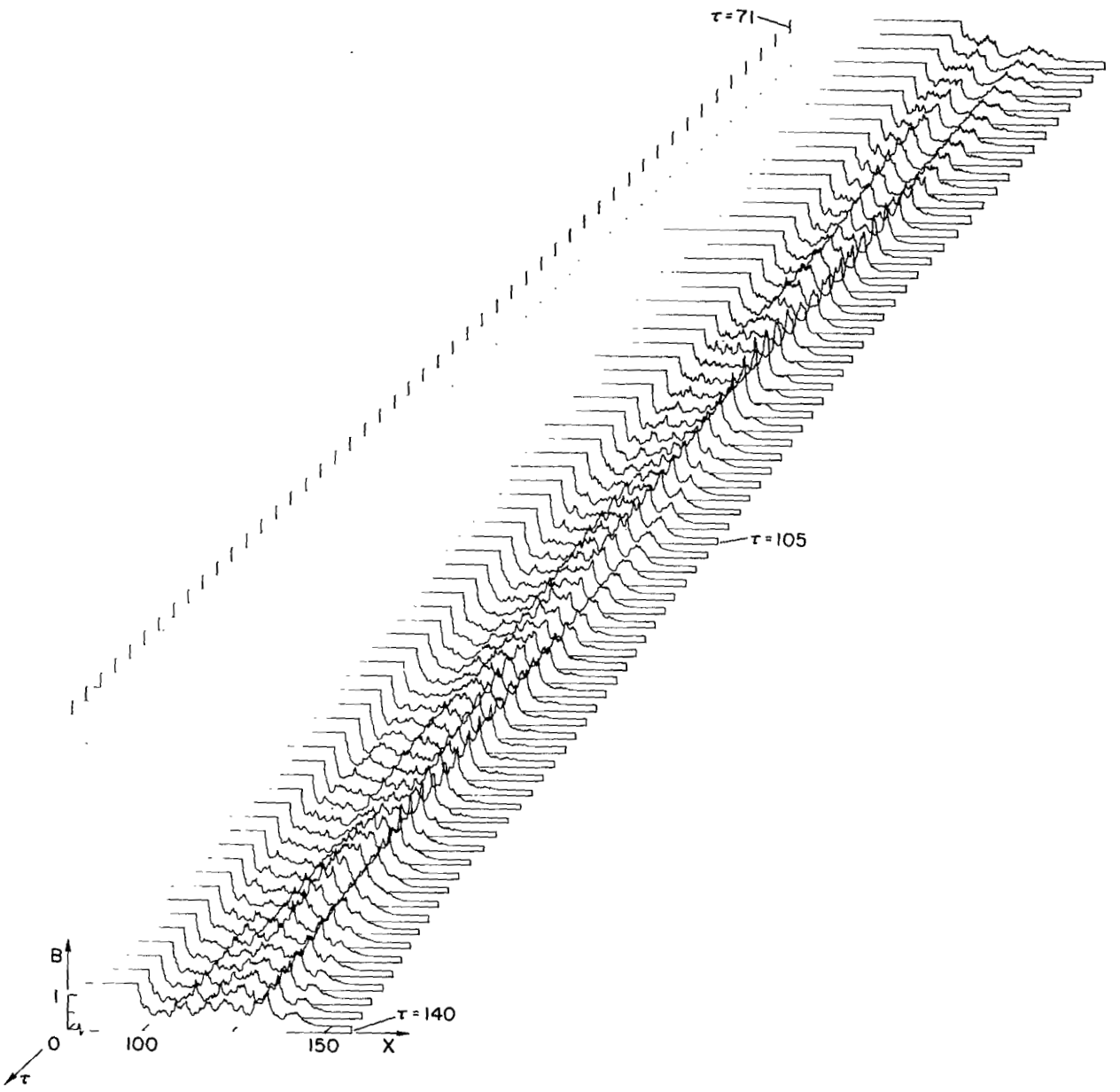

(b) Magnetic induction, τ = 71 - 140.

Figure 5.- Continued.

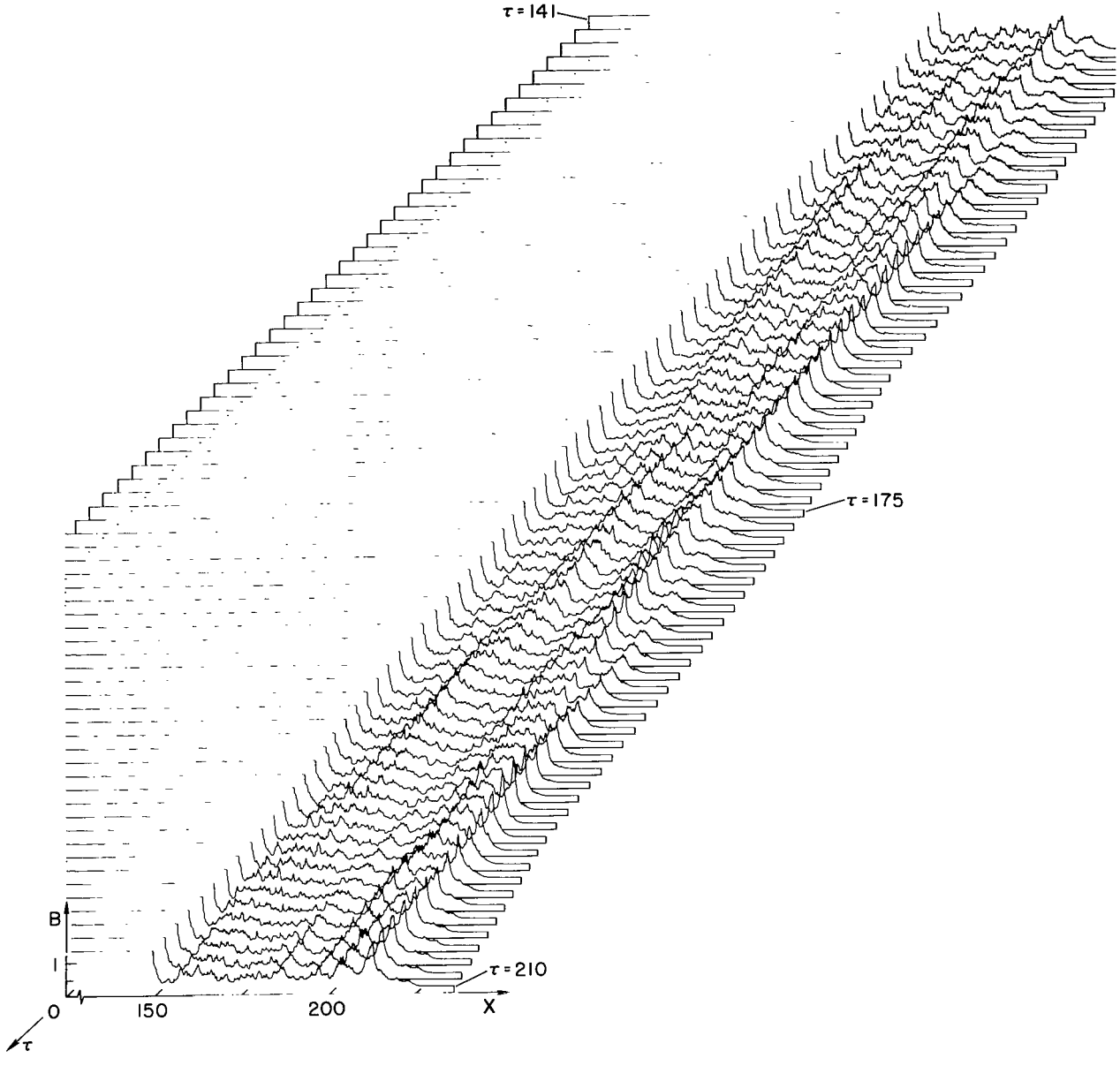

(c) Magnetic induction, τ = 141 - 210.

Figure 5.- Continued.

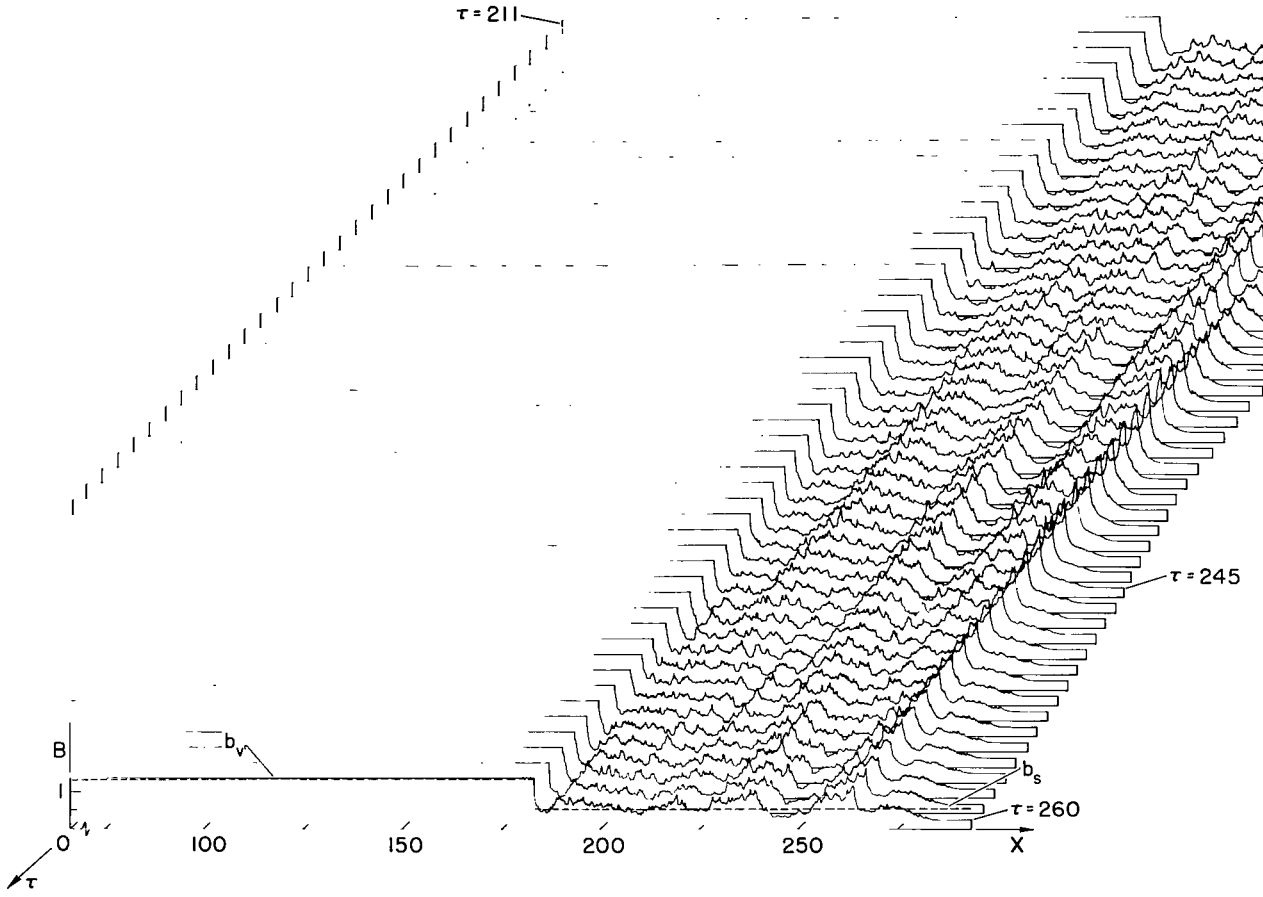

(d) Magnetic induction, τ = 211 - 260.

Figure 5.- Continued.

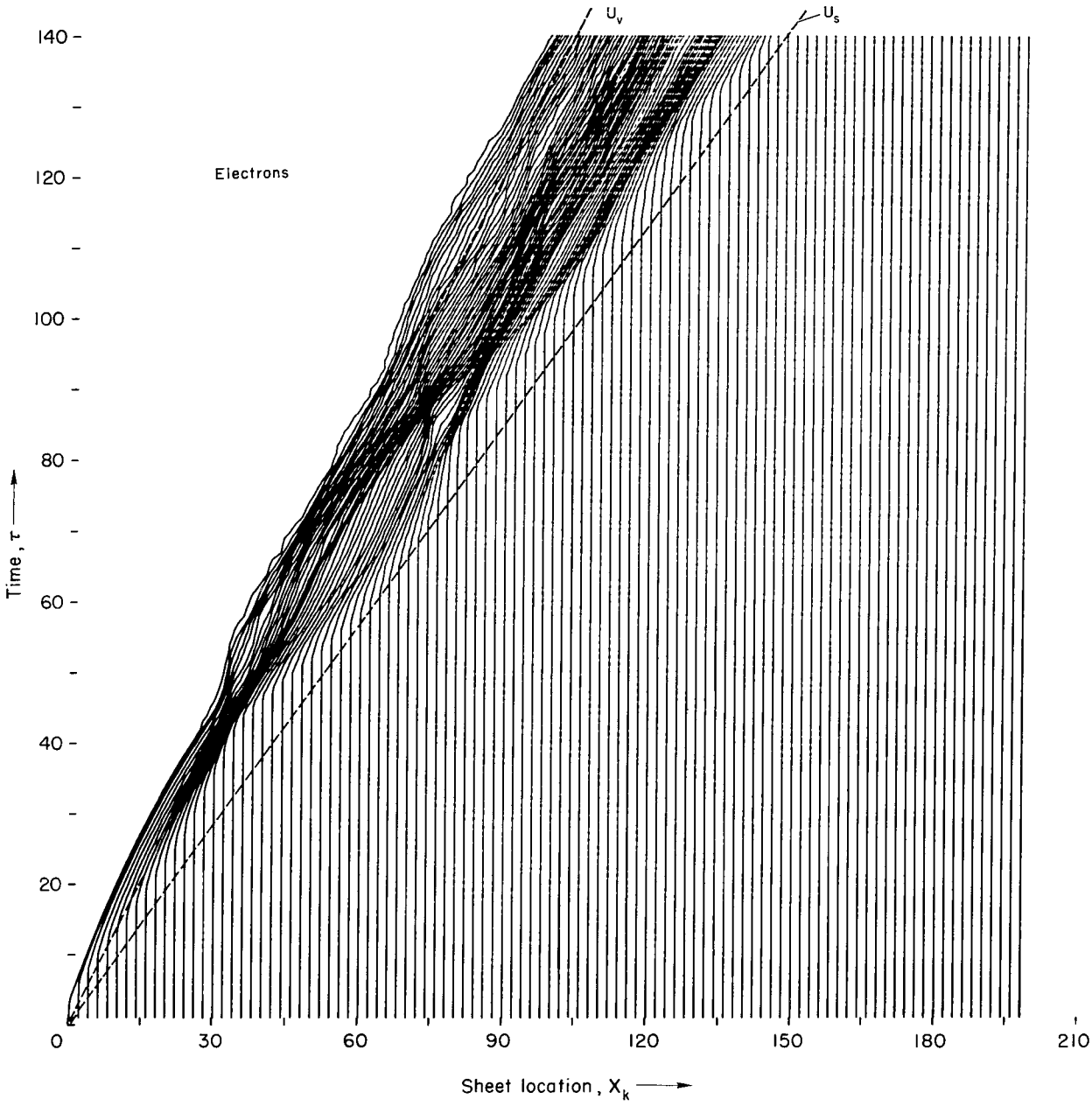

(e) Time-distance records of every tenth electron sheet; k = 1, 11, 21, . . .

Figure 5.- Continued.

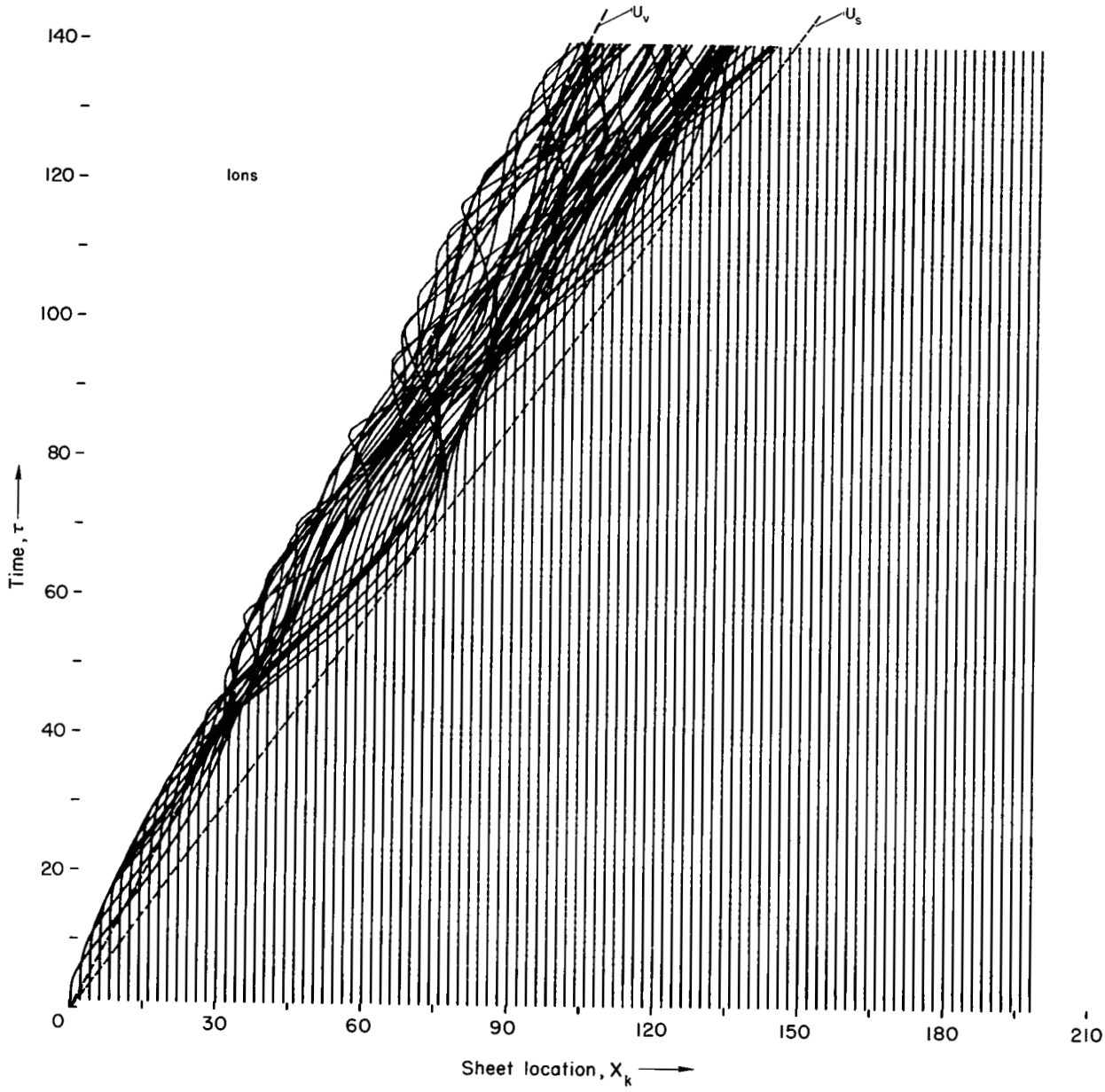

(f) Time-distance records of every tenth ion sheet; k = 1, 11, 21, . . .

Figure 5.- Continued.

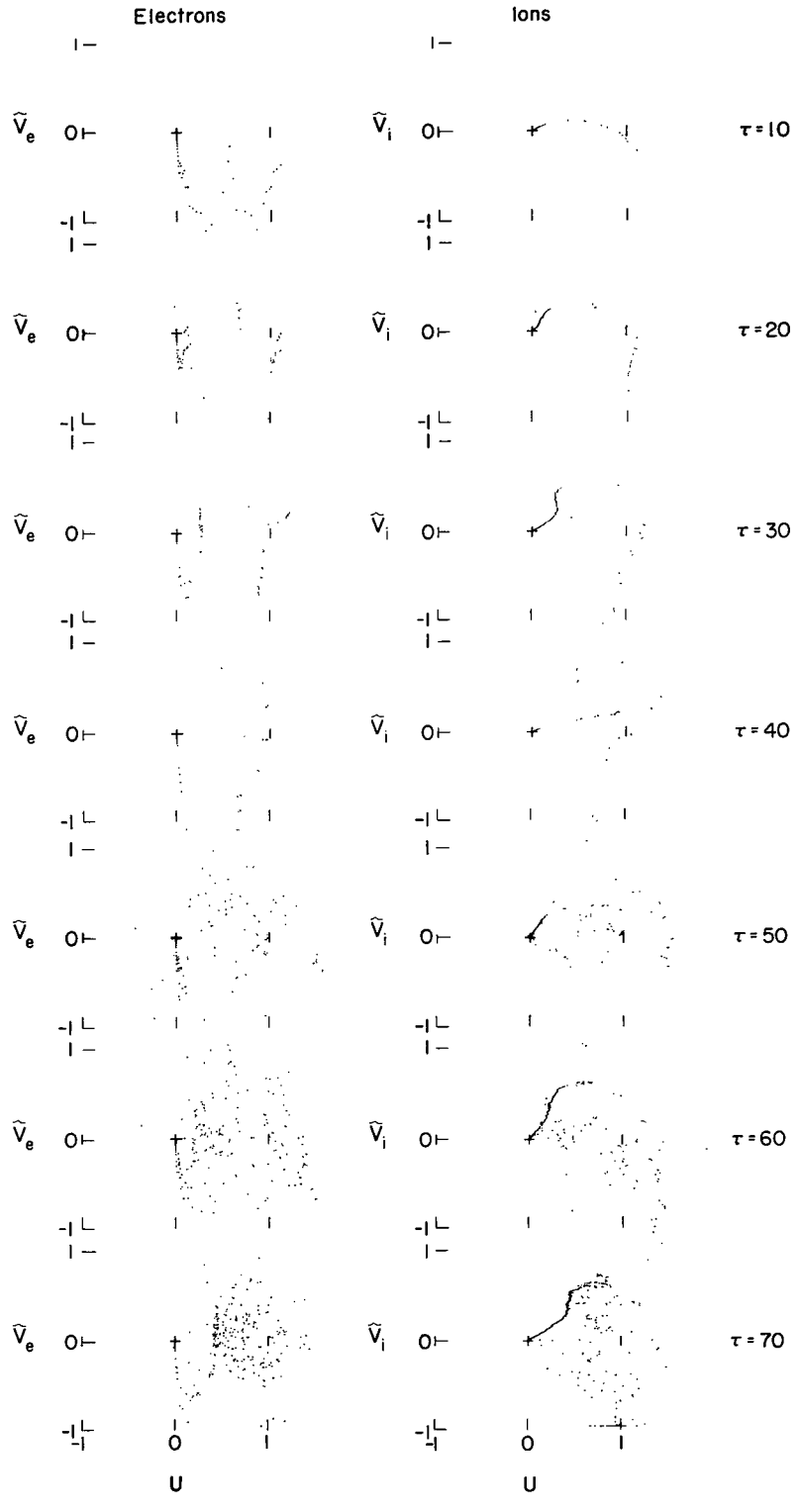

(g) Distribution in velocity space for all sheets, $\tilde{V} = VV^*/U^*$.

Figure 5.- Concluded.

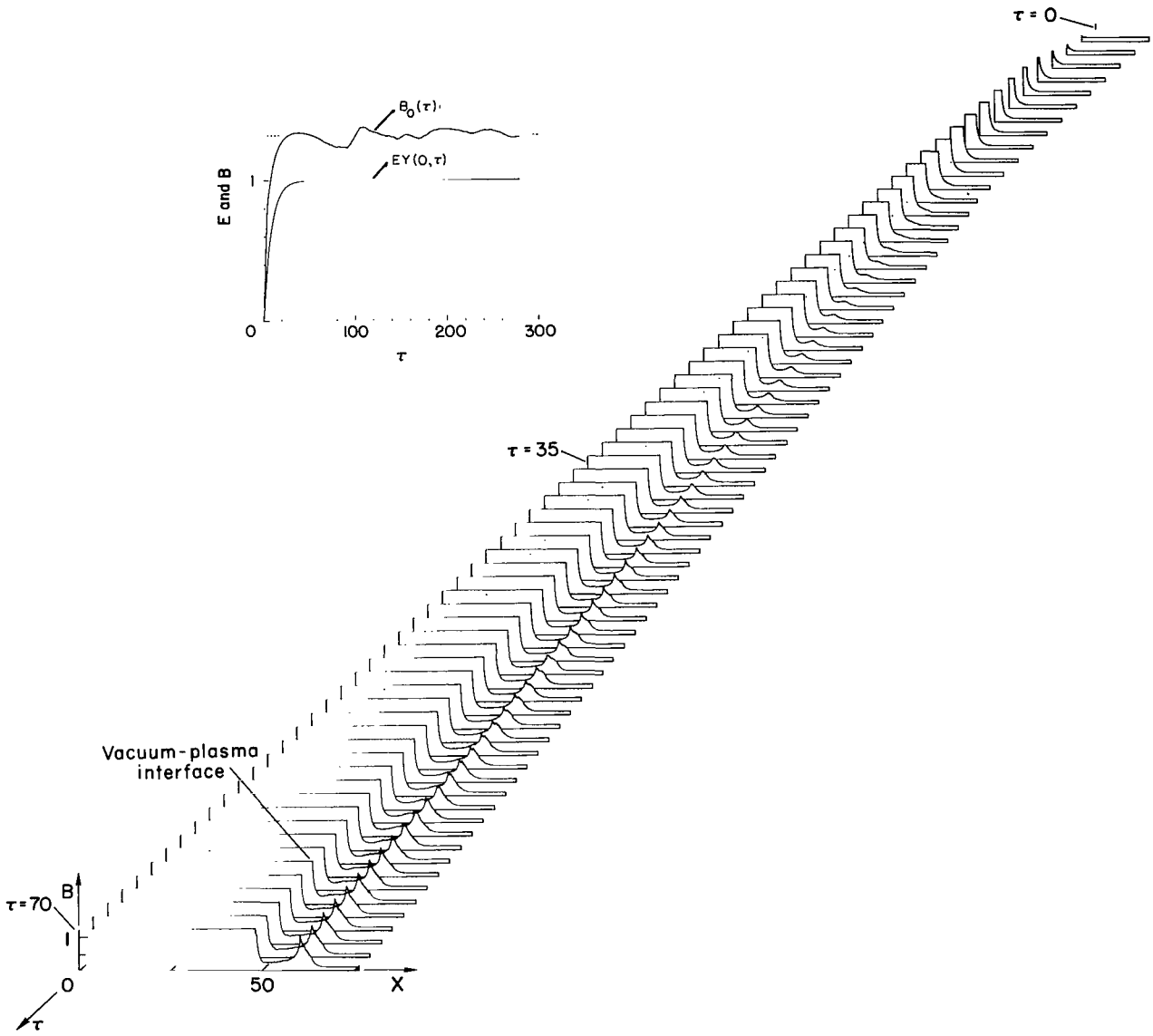

(a) τ = 0 - 70

Figure 6.- Development of magnetic induction with time for strong disturbance: e_o = 1.0, b_o = 0.1 (M_A = 11.45), R = 25.

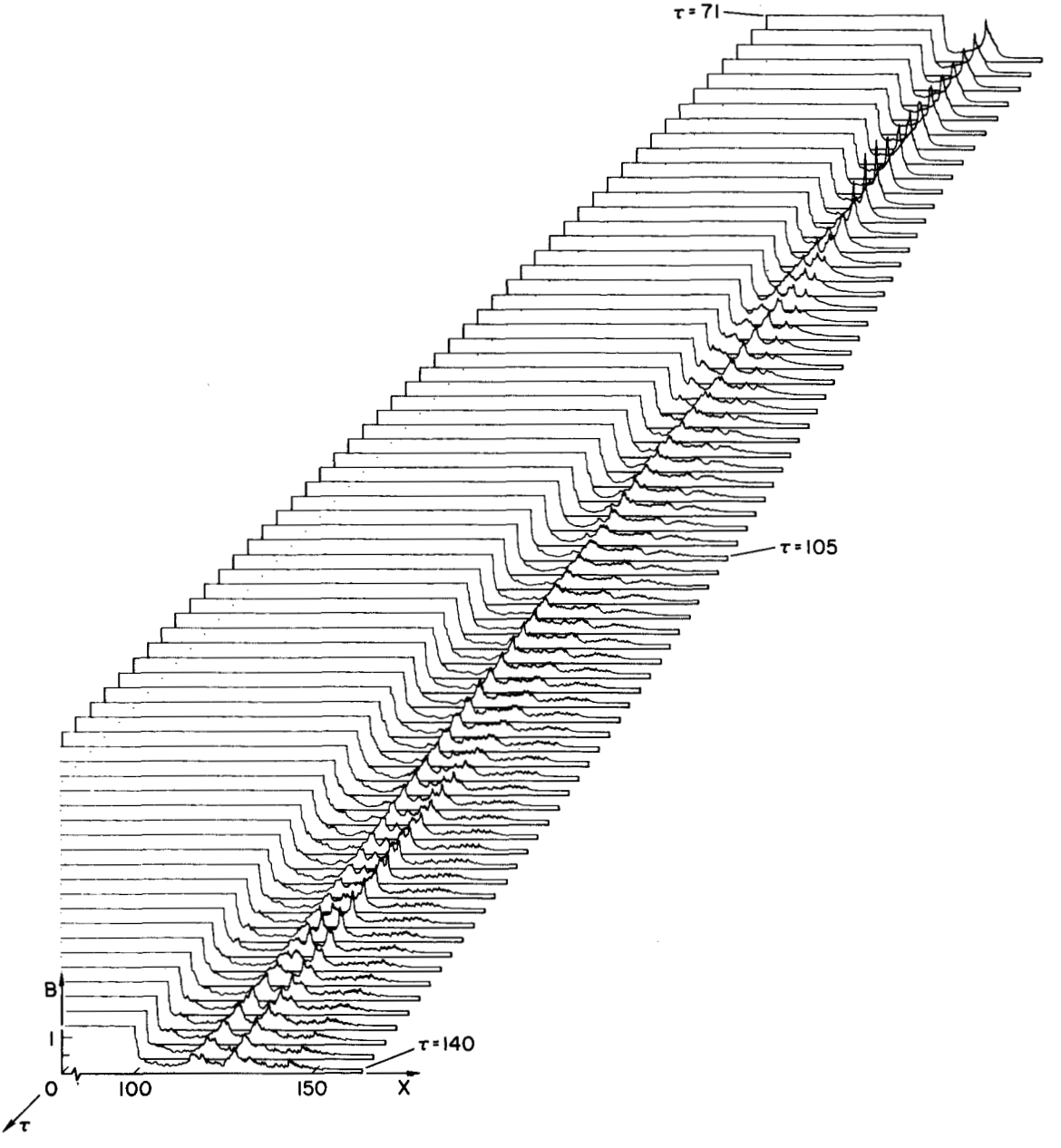

(b) τ = 71 - 140

Figure 6.- Continued.

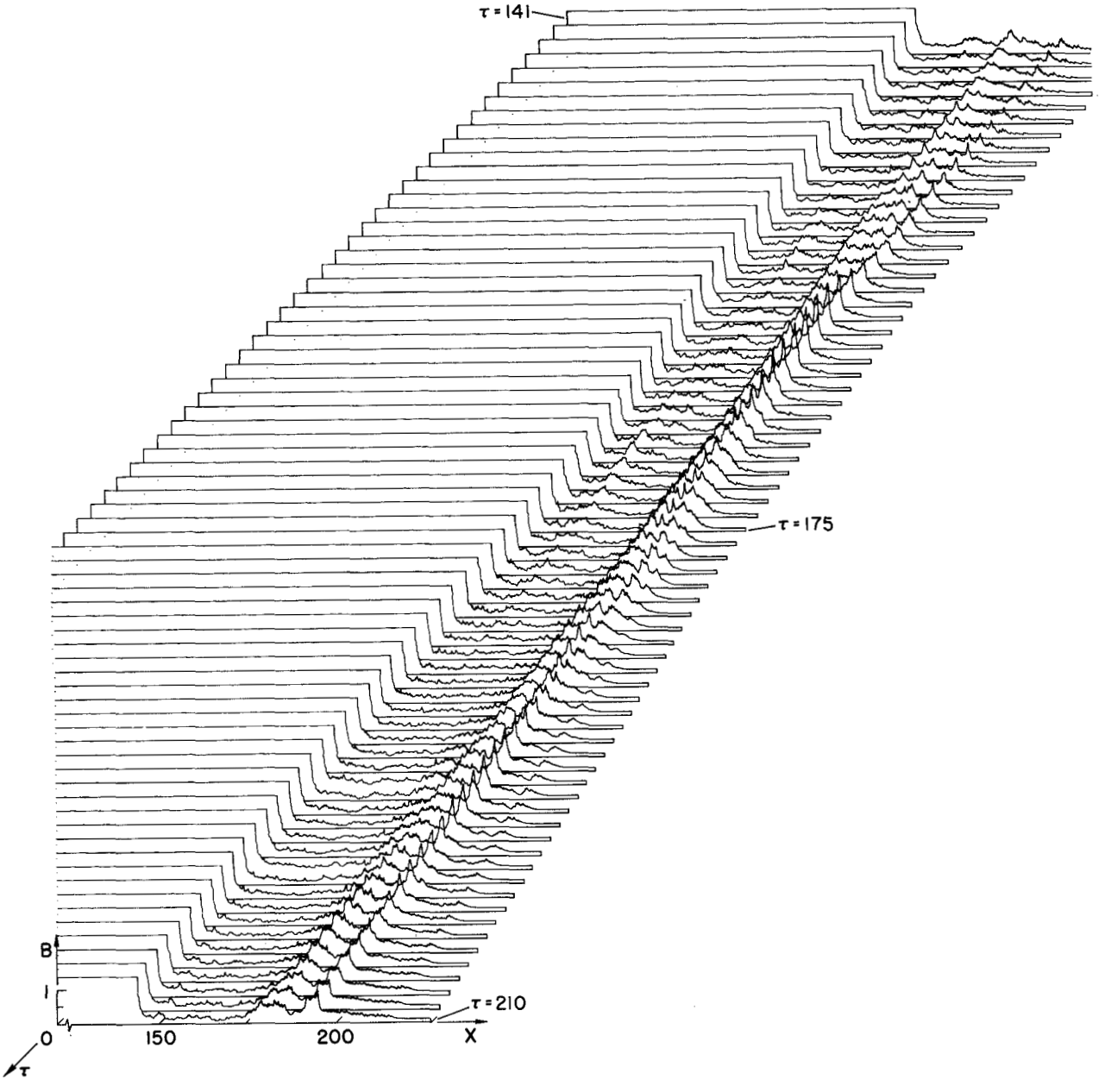

(c) τ = 141 - 210

Figure 6.- Continued.

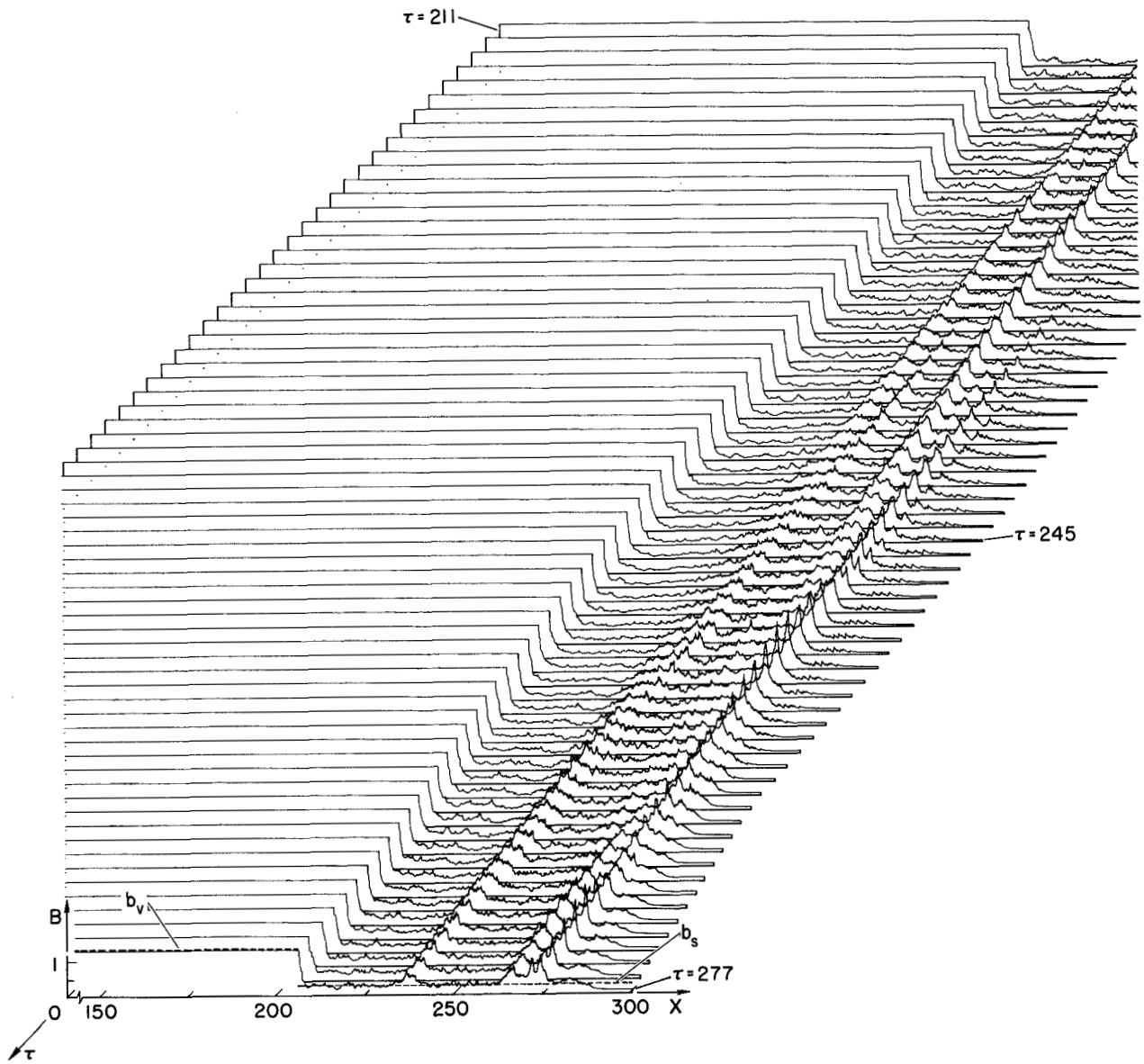

(d) τ = 211 - 277

Figure 6.- Concluded.

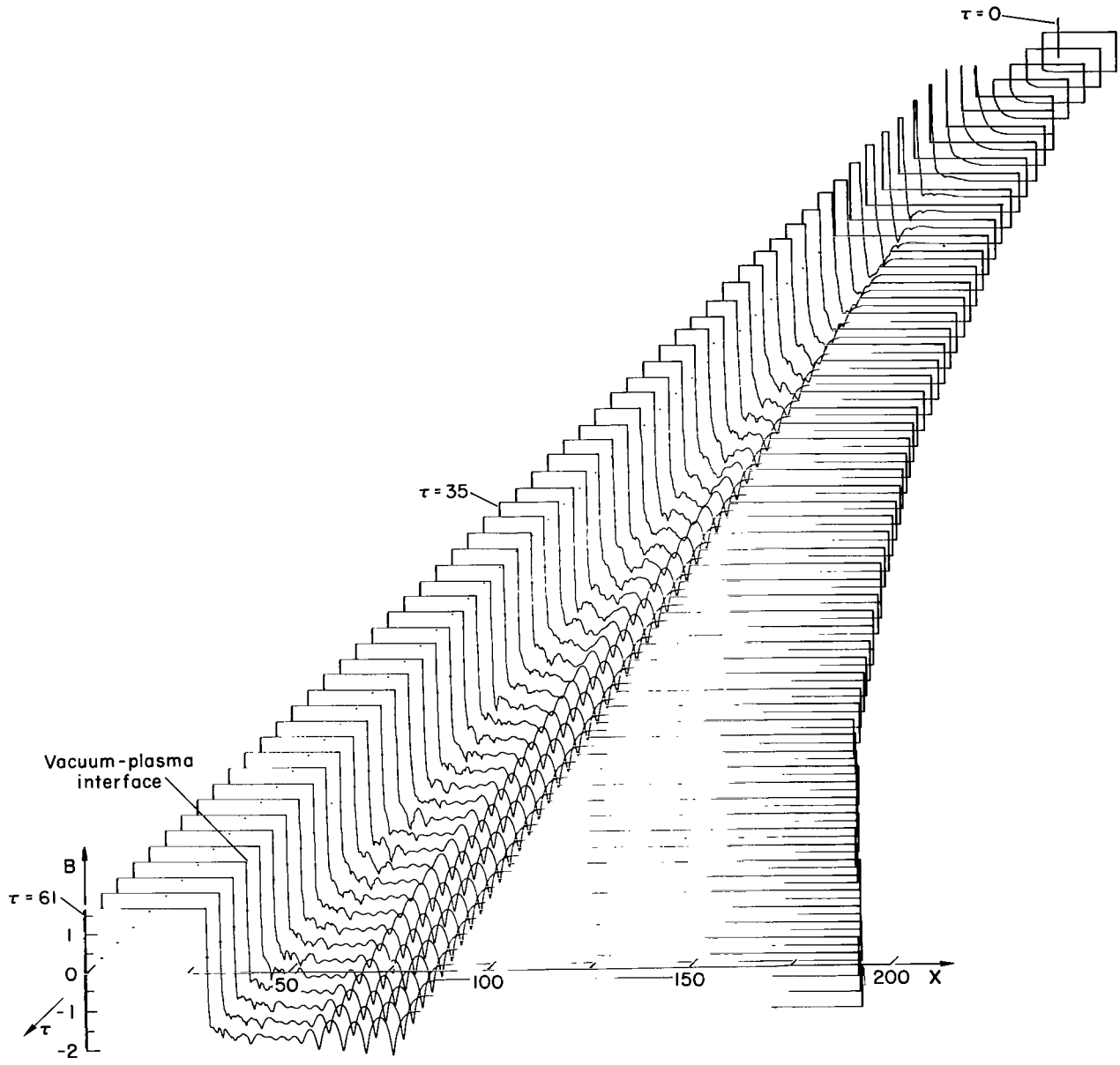

(a) Magnetic induction.

Figure 7.- Growth of the flow field with time for a weak disturbance moving into an oppositely directed ambient magnetic field: $e_o = 1.0$, $b_o = -1.0$ ($M_A = 1.54$), $R = 25$.

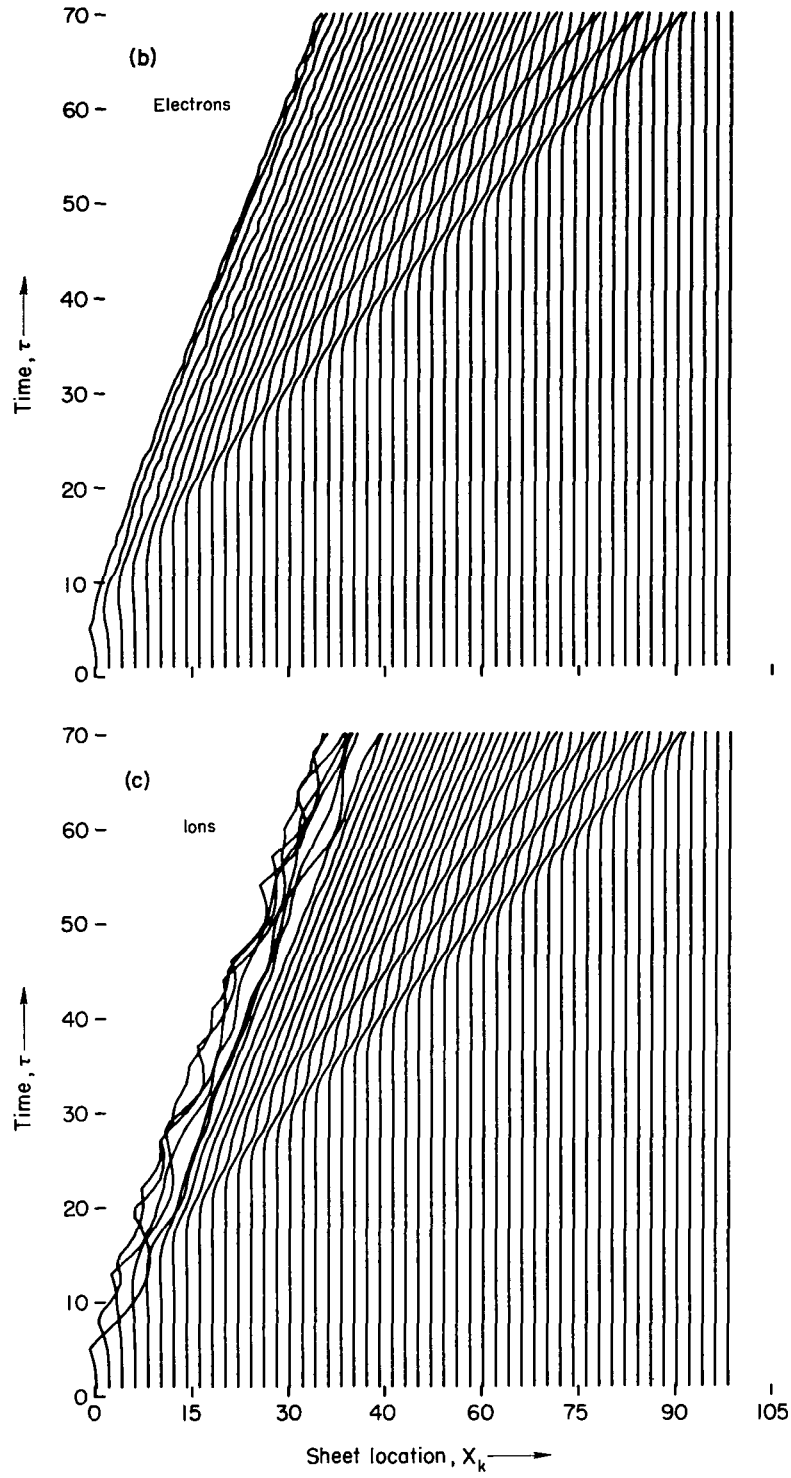

(b) Time-distance records of every tenth electron sheet; k = 1, 11, 21, . . .
(c) Time-distance records of every tenth ion sheet; k = 1, 11, 21, . . .

Figure 7.- Concluded.

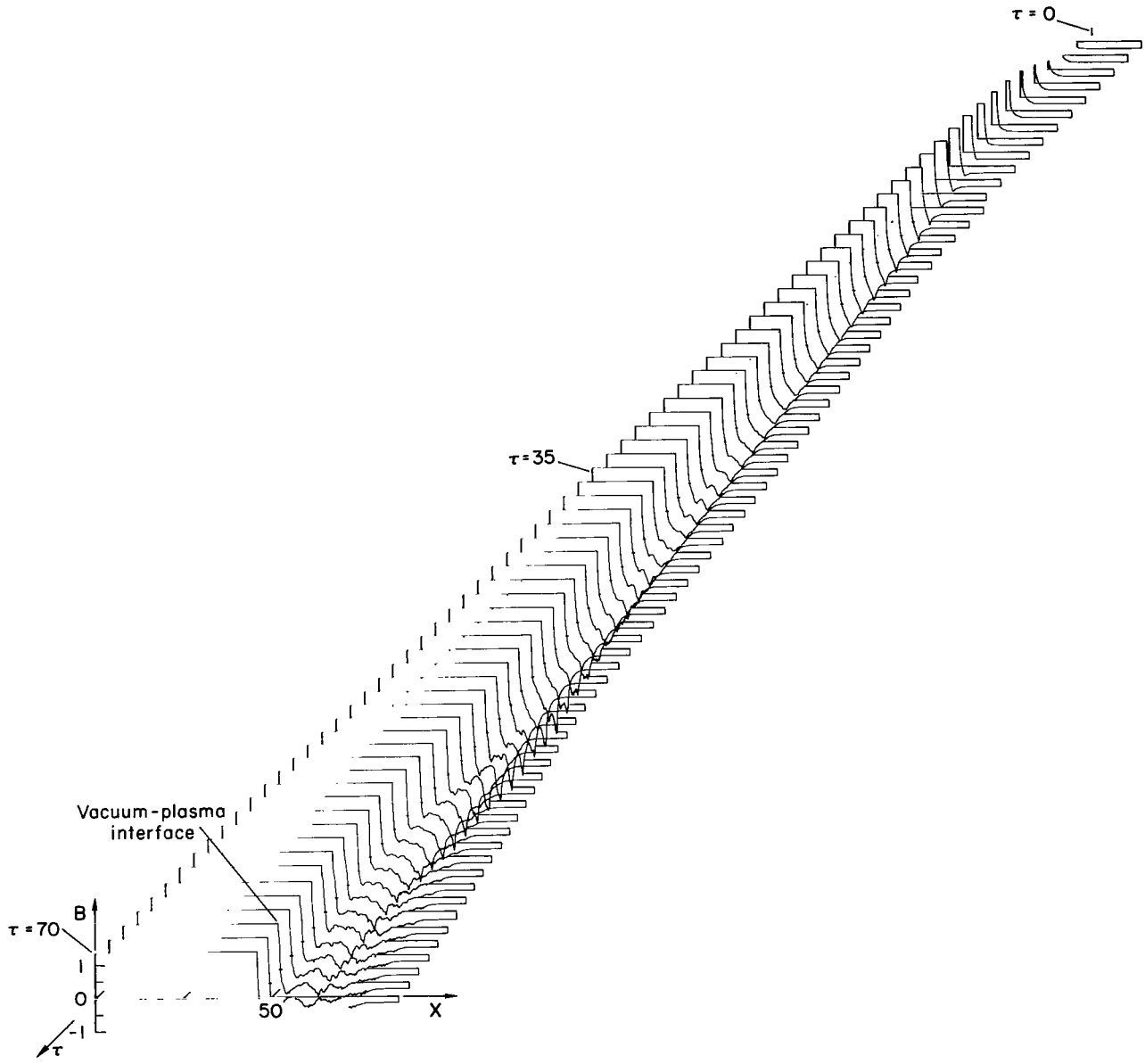

Figure 8.- Development of the magnetic induction with time for a strong disturbance moving into an oppositely directed ambient magnetic field: $e_o = 1.0$, $b_o = -0.2$ ($M_A = 5.80$), R = 25.

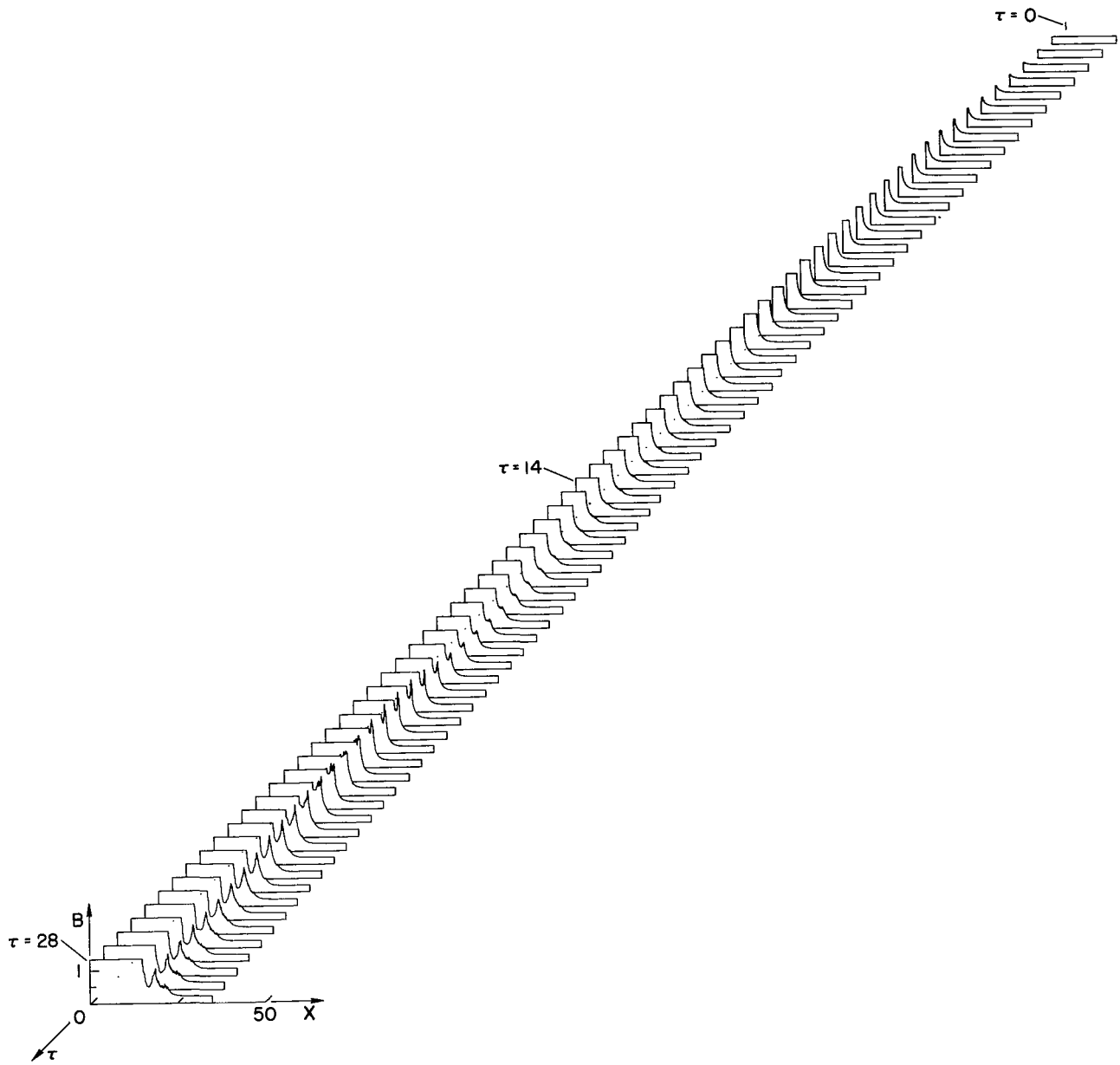

(a) R = 4, $\Delta\tau$ plot = 0.4.

Figure 9.- Development of the magnetic induction with time for a strong disturbance for several different mass ratios and time intervals between graphs: e_o = 1.0, b_o = 0.2 (M_A = 5.80).

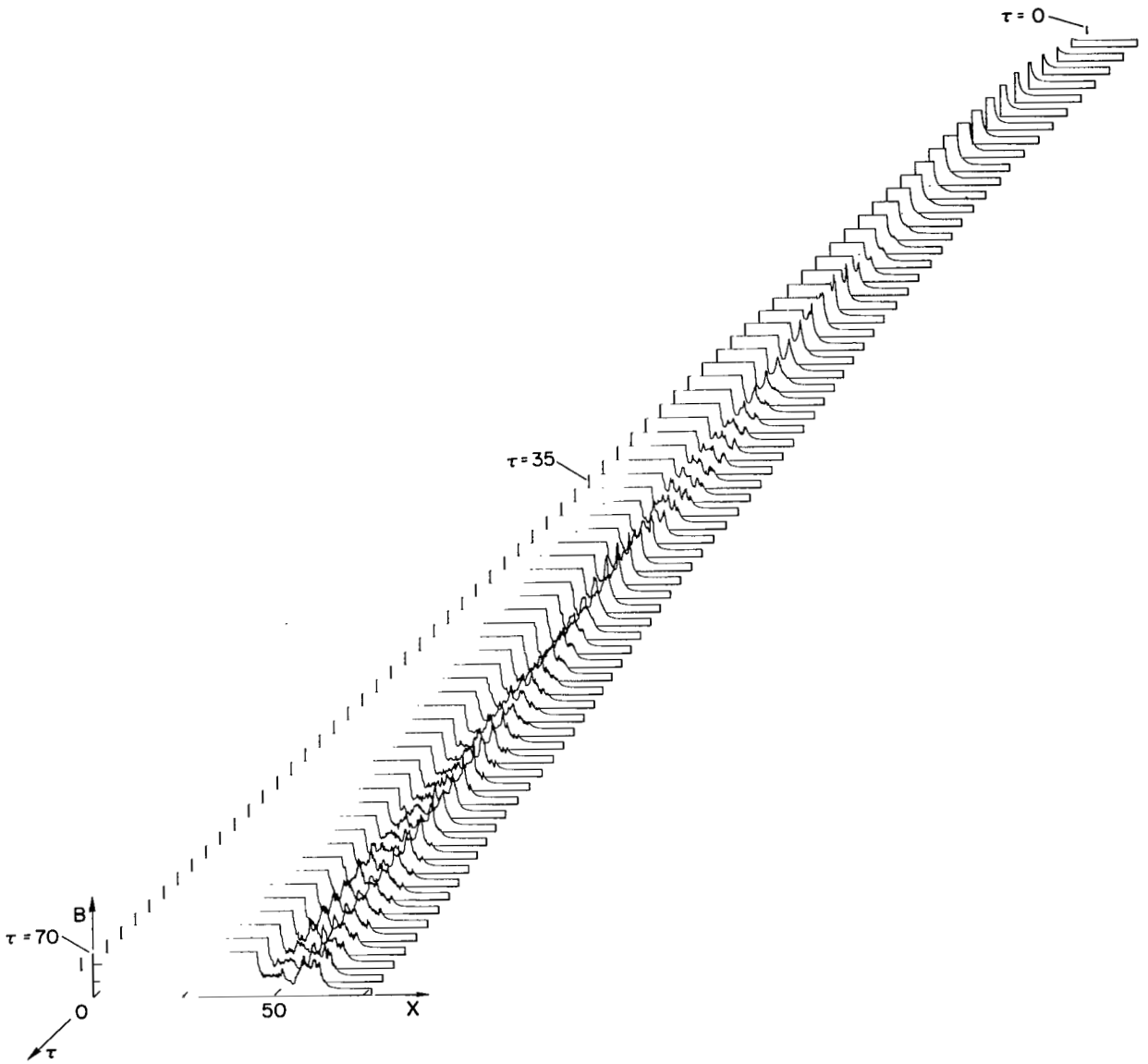

(b) R = 4, $\Delta\tau$ plot = 1.0.

Figure 9.- Continued.

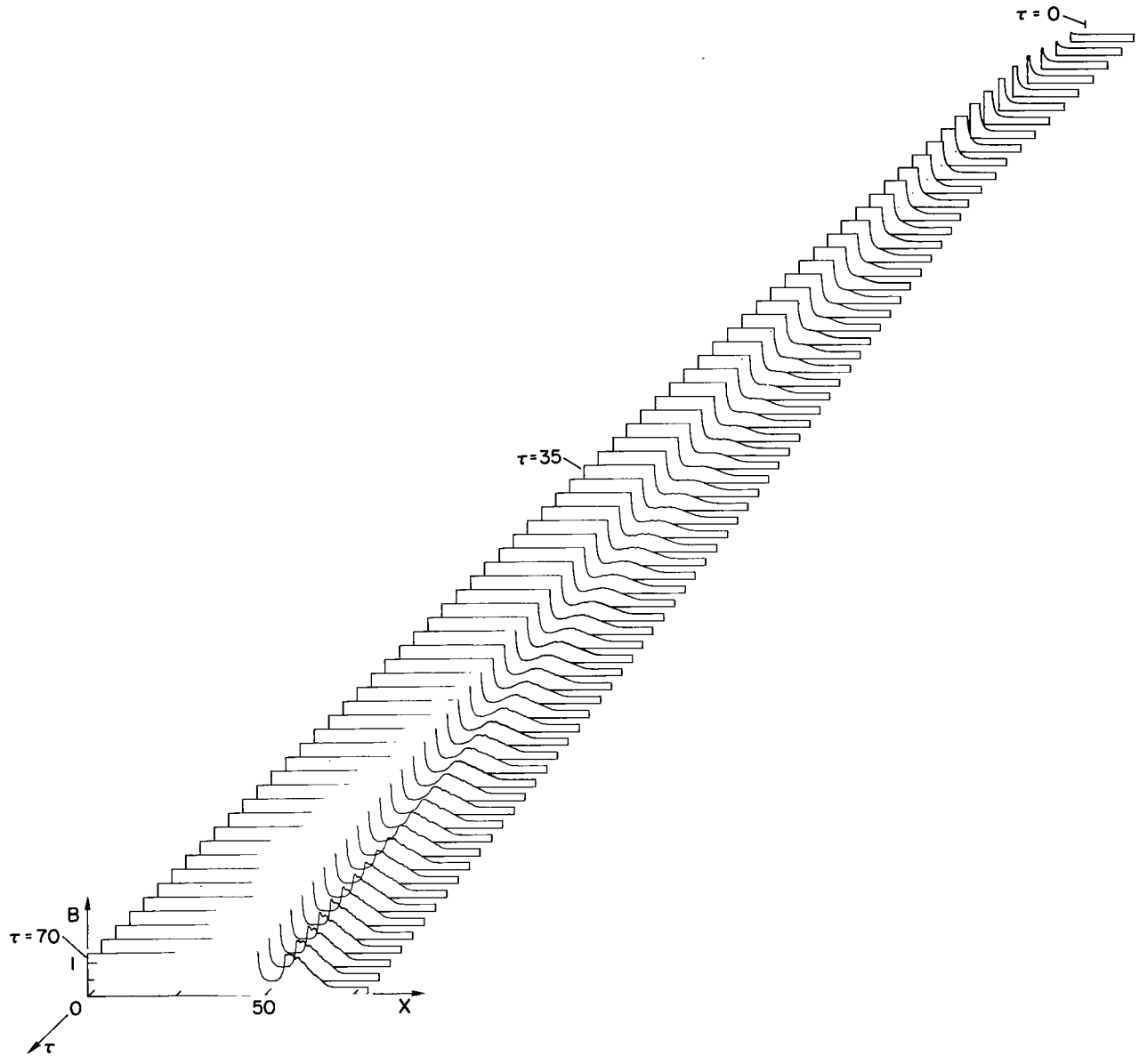

(c) R = 100, $\Delta\tau$ plot = 1.0.

Figure 9.- Continued.

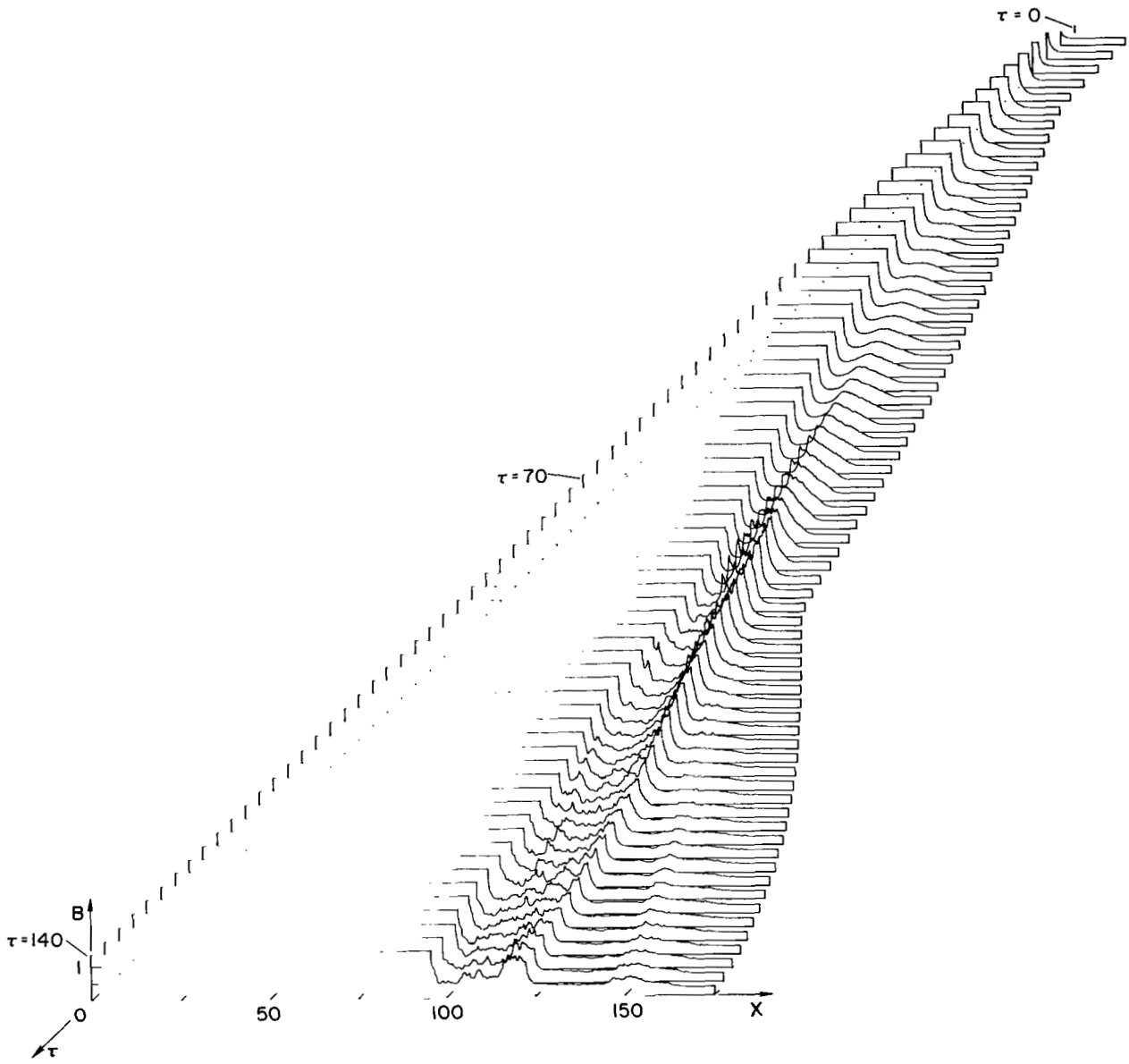

(d) R = 100, $\Delta\tau$ plot = 2.0.

Figure 9.- Concluded.

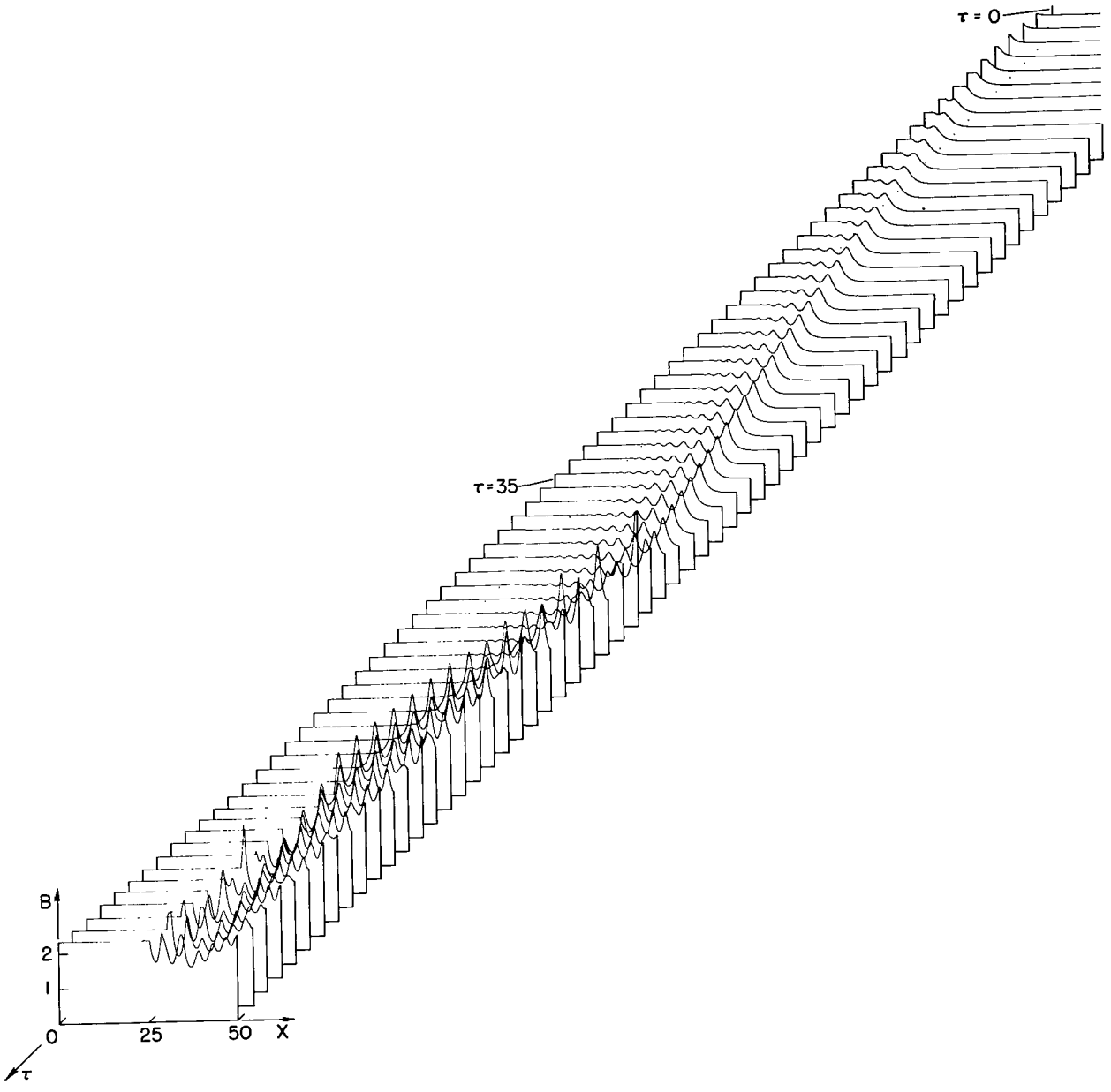

Figure 10.- Magnetic induction distribution during impact of a subcritical weak disturbance with centerplane: $e_o = 1.0$, $b_o = 1.0$ ($M_A = 1.54$), $R = 25$, $X_m = 50$.

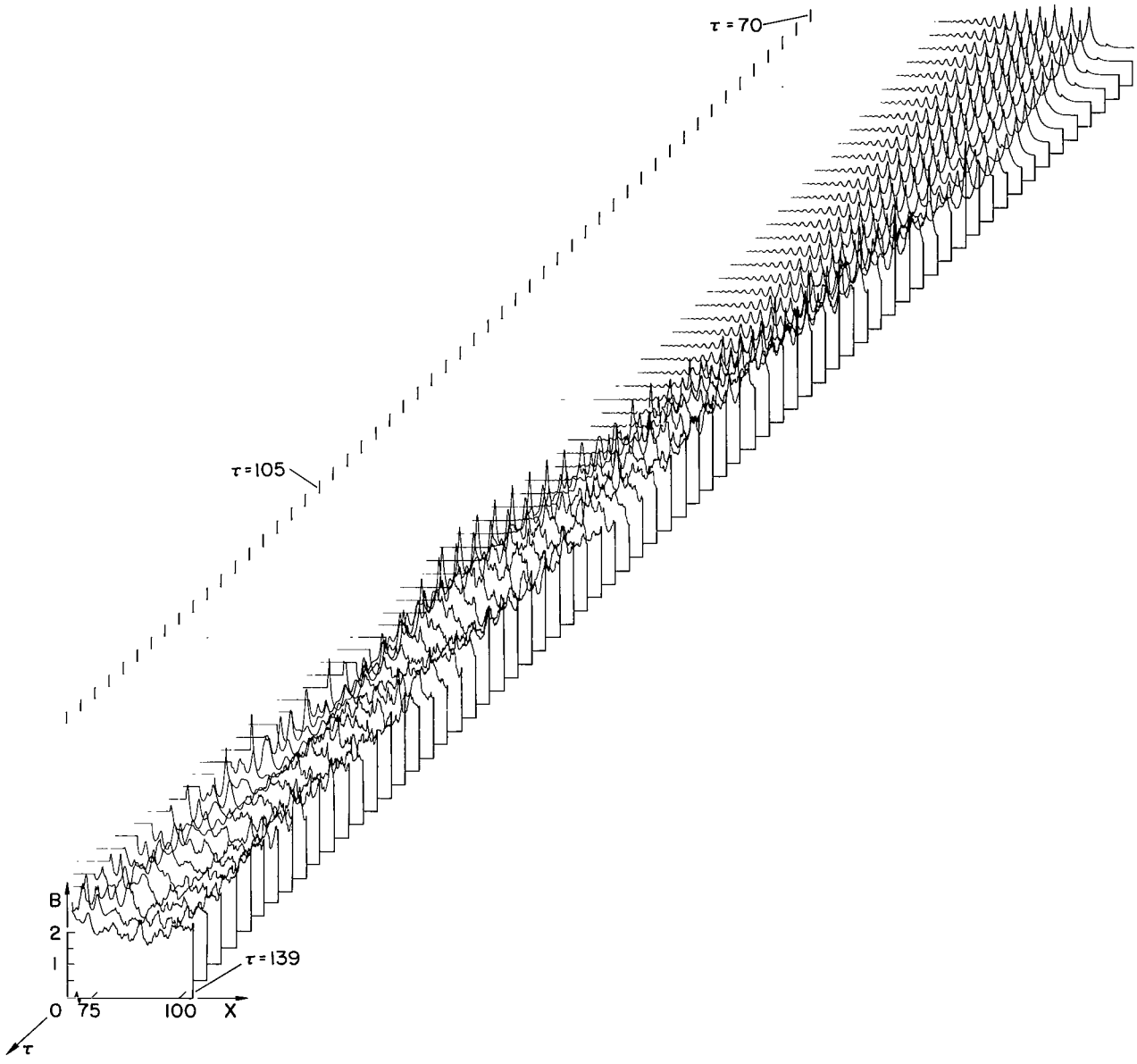

(a) Magnetic induction.

Figure 11.- Impact of a weak disturbance with centerplane: $e_o = 1.0$, $b_o = 0.7$ ($M_A = 1.94$), $R = 25$, $X_m = 100$.

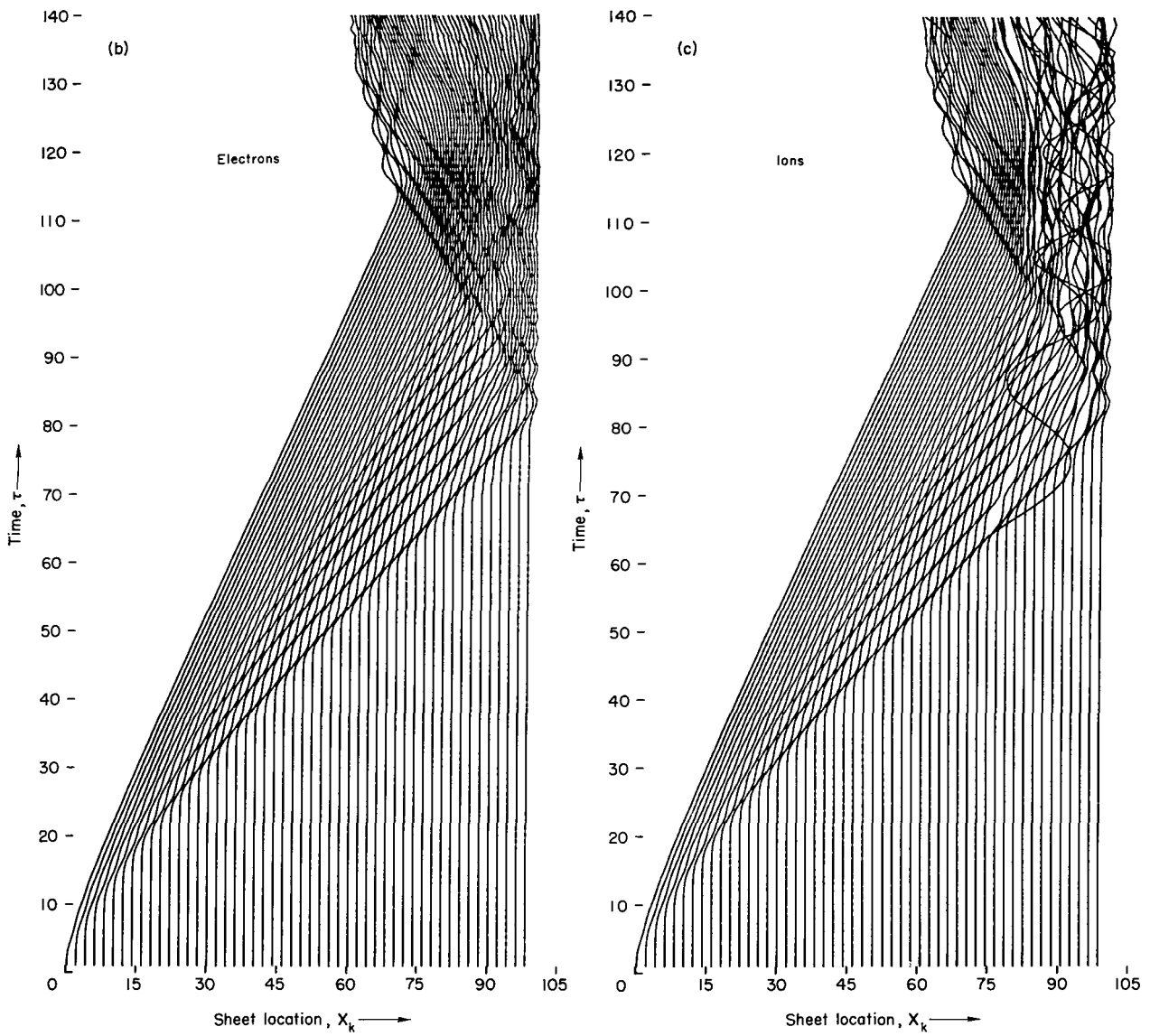

(b) Time-distance records of every tenth electron sheet; k = 1, 11, 21, . . .
(c) Time-distance records of every tenth ion sheet; k = 1, 11, 21, . . .

Figure 11.- Concluded.

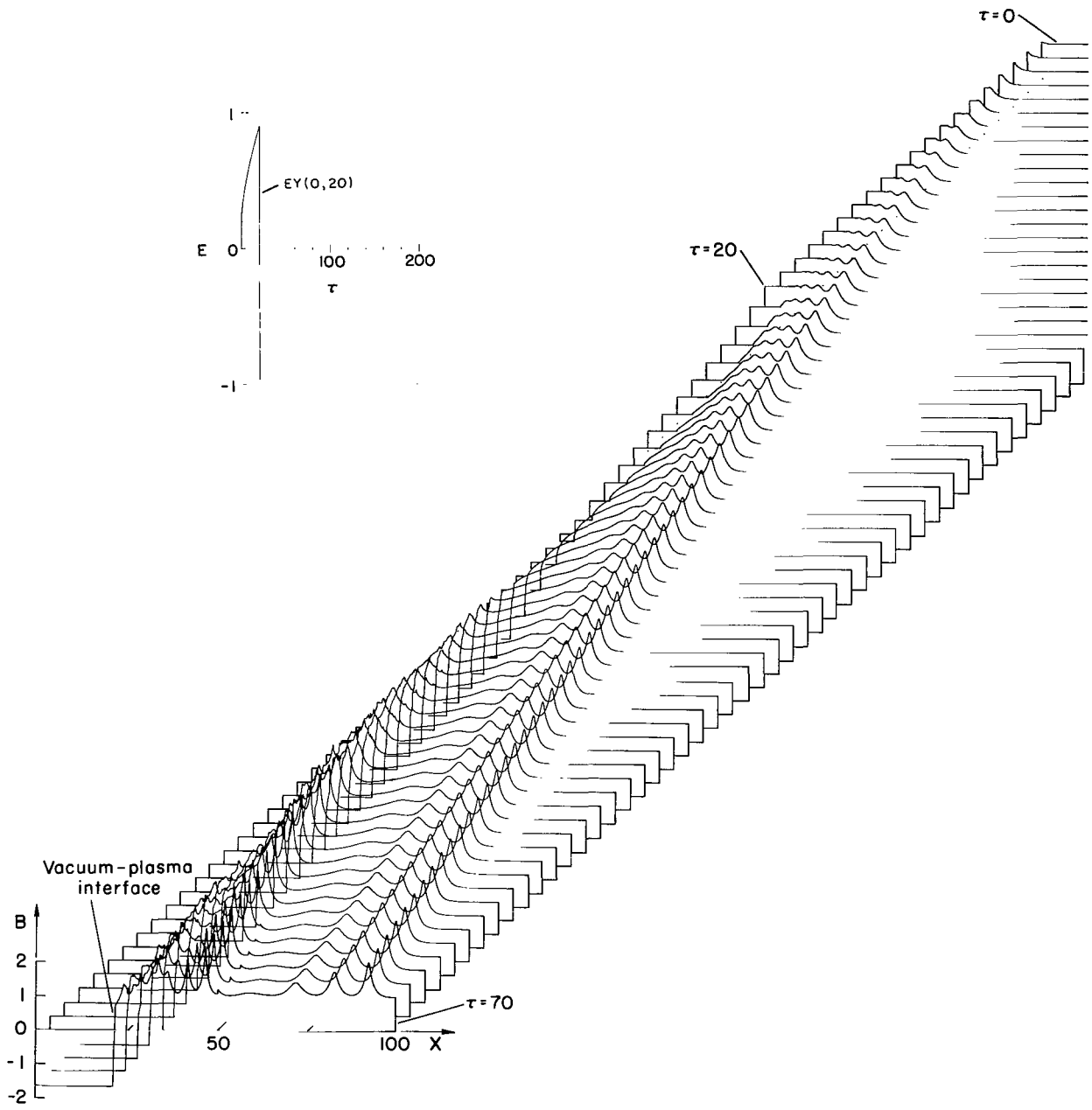

(a) Magnetic induction.

Figure 12.- Flow field that results from reversal of impressed electric field during compression of plasma: $e_o = 1.0$ for $\tau < 20$, $EY(o,\tau) = -1.0$ for $\tau \geq 20$, $b_o = 1.0$ ($M_A = 1.54$), $R = 25$.

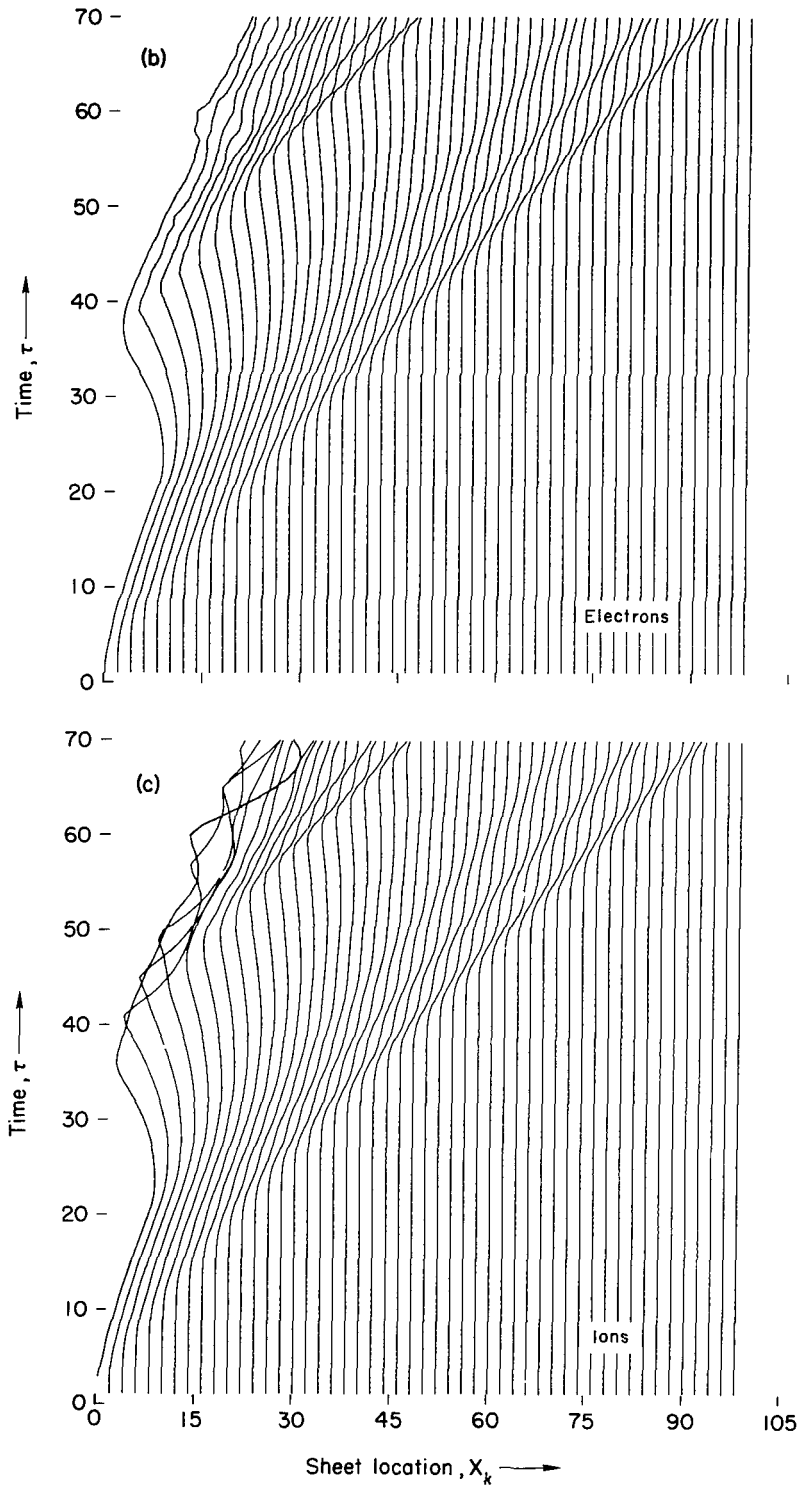

(b) Time-distance records of every tenth electron sheet; k = 1, 11, 21, . . .
(c) Time-distance records of every tenth ion sheet; k = 1, 11, 21, . . .

Figure 12.- Concluded.

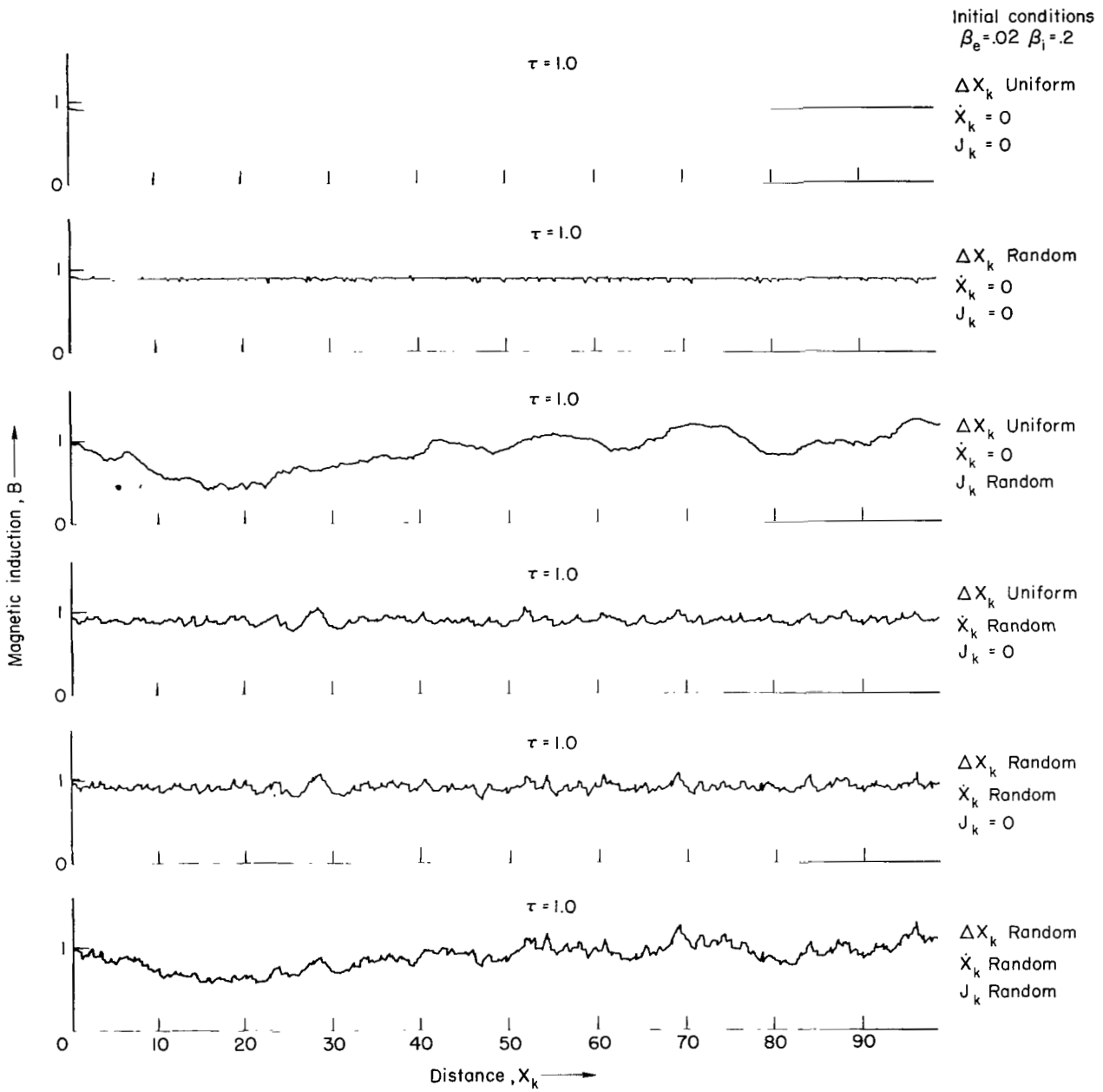

Figure 13.- Effect on initial ambient magnetic induction distribution brought about by various ways in which temperature manifests itself: e_o = 1.0, b_o = 0.908 ($b_o\sqrt{1 + \beta_e + \beta_i} = 1$; M_A = 1.54), R = 25, β_g = 0.008, β_{eg} = 0.01, β_i = 0.2, τ = 1.0.

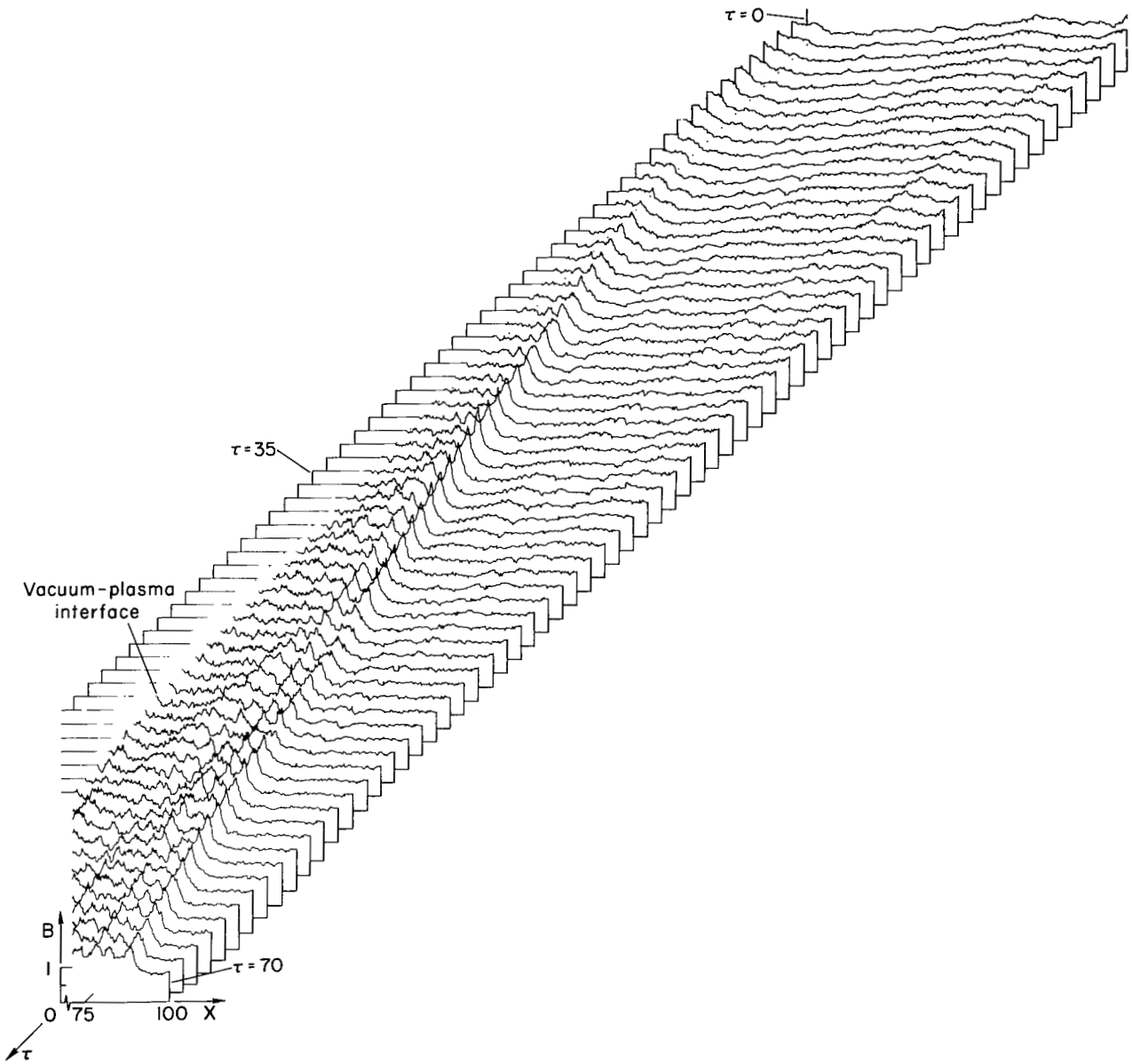

(a) Magnetic induction.

Figure 14.- Development of flow field with time for a weak disturbance moving into a warm plasma: $e_o = 1.0$, $b_o = 0.988$ ($b_o\sqrt{1 + \beta_e + \beta_i} = 1$; $M_A = 1.54$), $R = 25$, $\beta_g = 0.01$, $\beta_{eg} = 0.01$, $\beta_i = 0.01$, ΔX_k random, $\dot{X}_k$ random, J_k random.

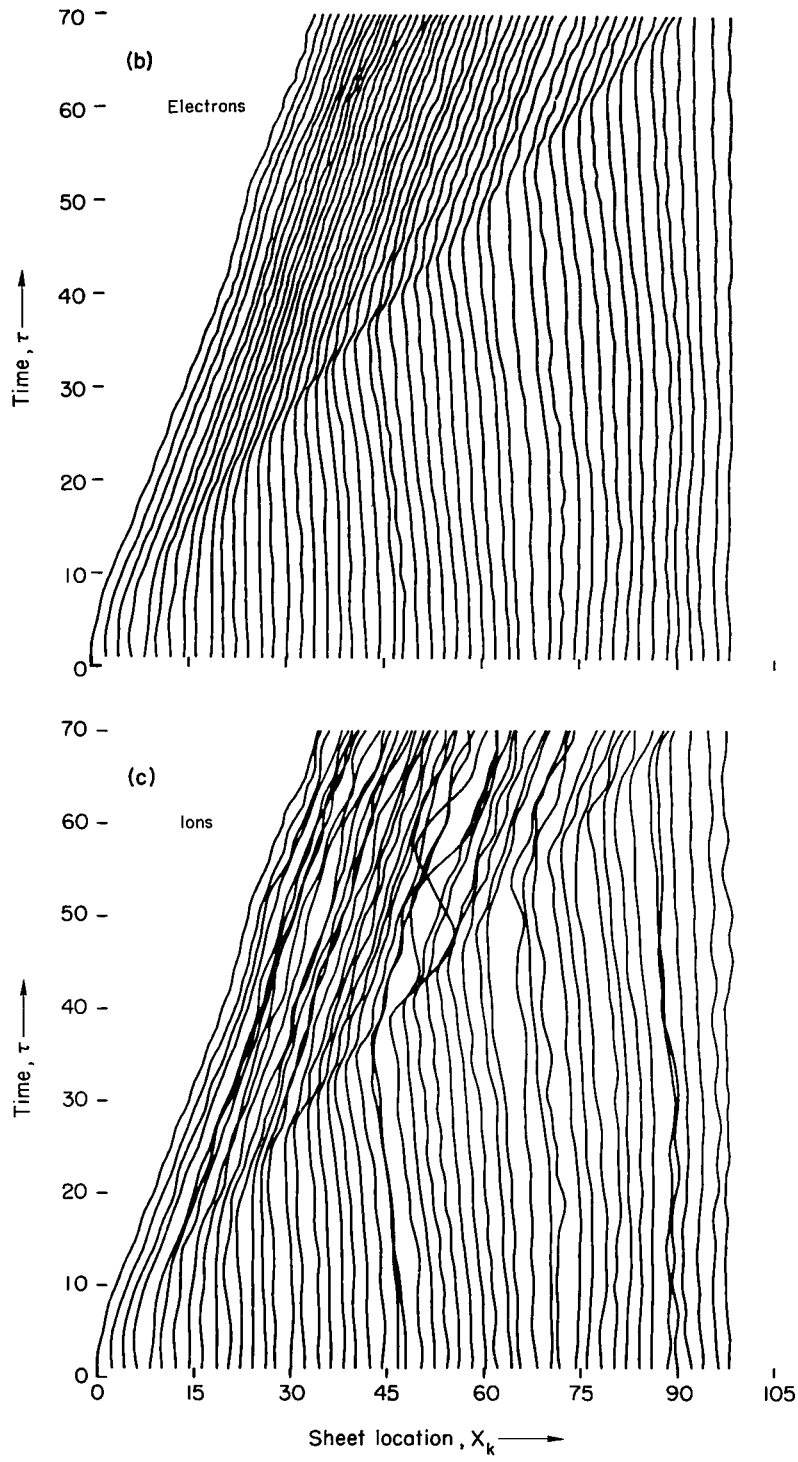

(b) Time-distance records of every tenth electron sheet; k = 1, 11, 21, . . .
(c) Time-distance records of every tenth ion sheet; k = 1, 11, 21, . . .

Figure 14.- Concluded.

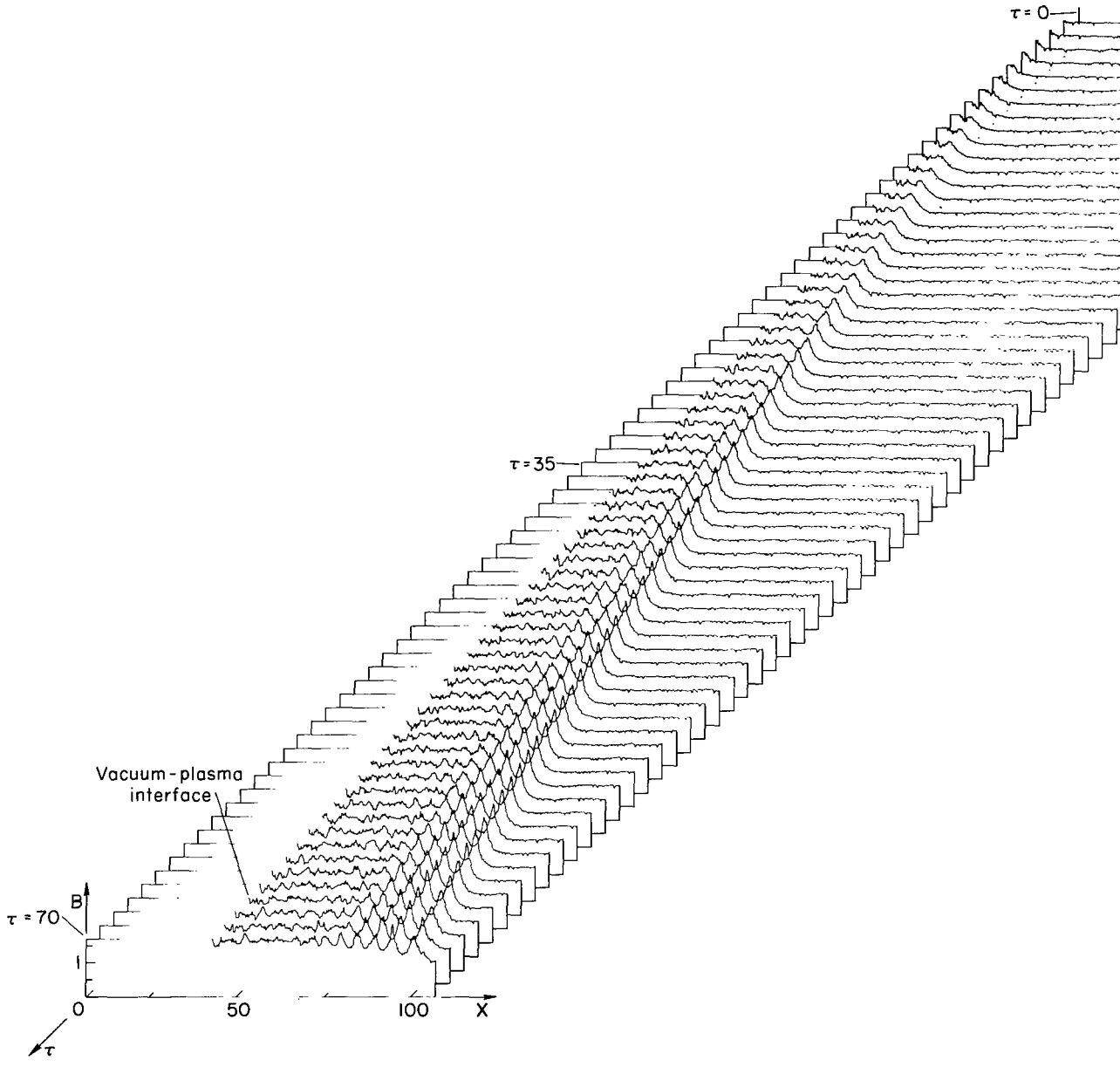

Figure 15.- Development of magnetic induction with time for weak disturbance moving into warm plasma: $e_o = 1.0$, $b_o = 0.999$ ($b_o\sqrt{1 + \beta_e + \beta_i} = 1$; $M_A = 1.54$), R = 25, $\beta_g = 0.0001$, $\beta_{eg} = 0.0001$, $\beta_i = 0.0025$, ΔX_k random, $\dot{X}_k$ random, J_k random.

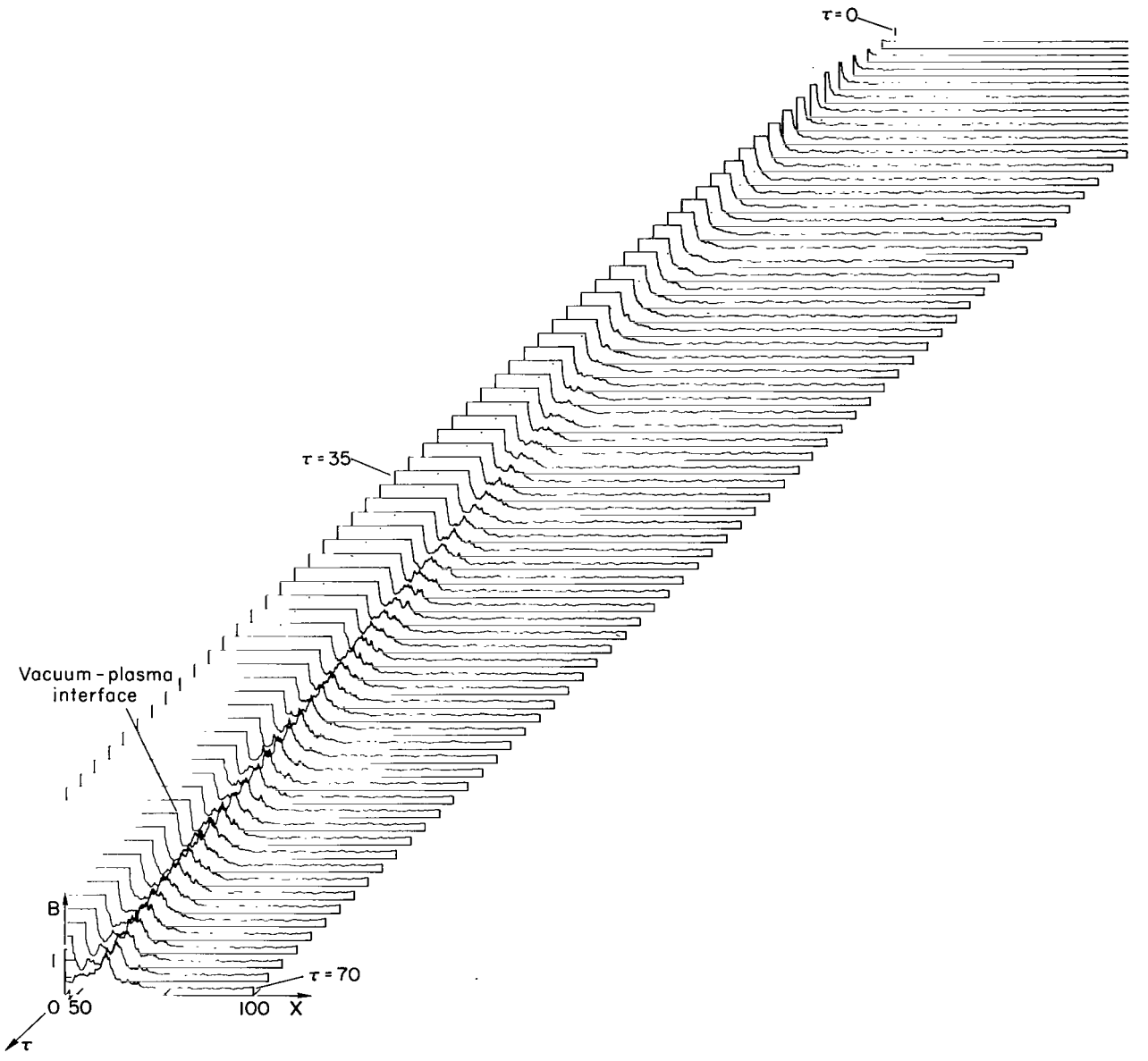

(a) Magnetic induction.

Figure 16.- Development of flow field with time for a strong disturbance moving into a warm plasma: $e_o = 1.0$, $b_o = 0.181$ ($b_o\sqrt{1 + \beta_e + 3_i} = 0.2$; $M_A = 5.80$), $R = 25$, $\beta_g = 0.008$, $\beta_{eg} = 0.01$, $\beta_i = 0.2$, ΔX_k random, $\dot{X}_k$ random, J_k random.

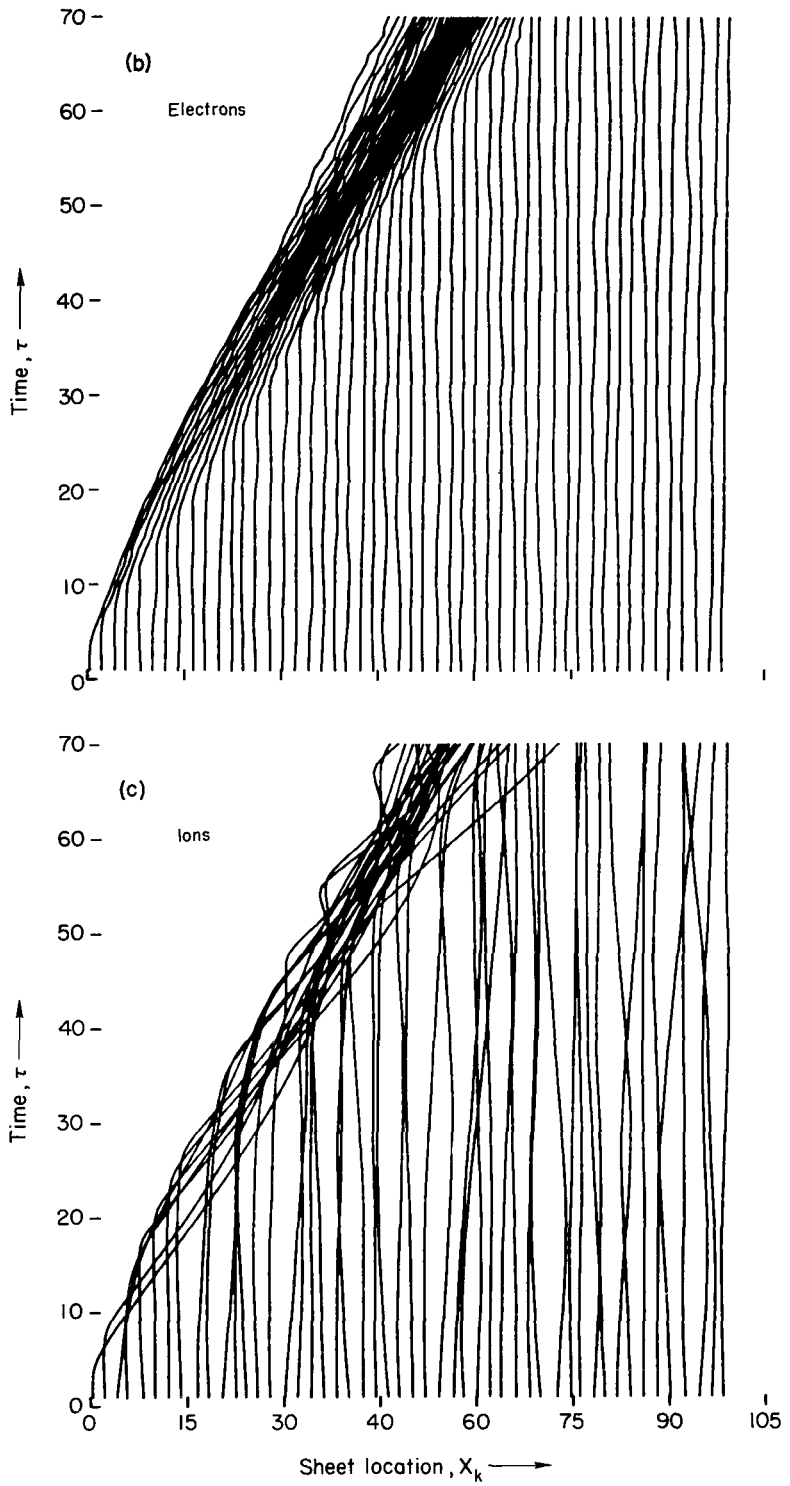

(b) Time-distance records of every tenth electron sheet; k = 1, 11, 21, . . .
(c) Time-distance records of every tenth ion sheet; k = 1, 11, 21, . . .

Figure 16.- Concluded.

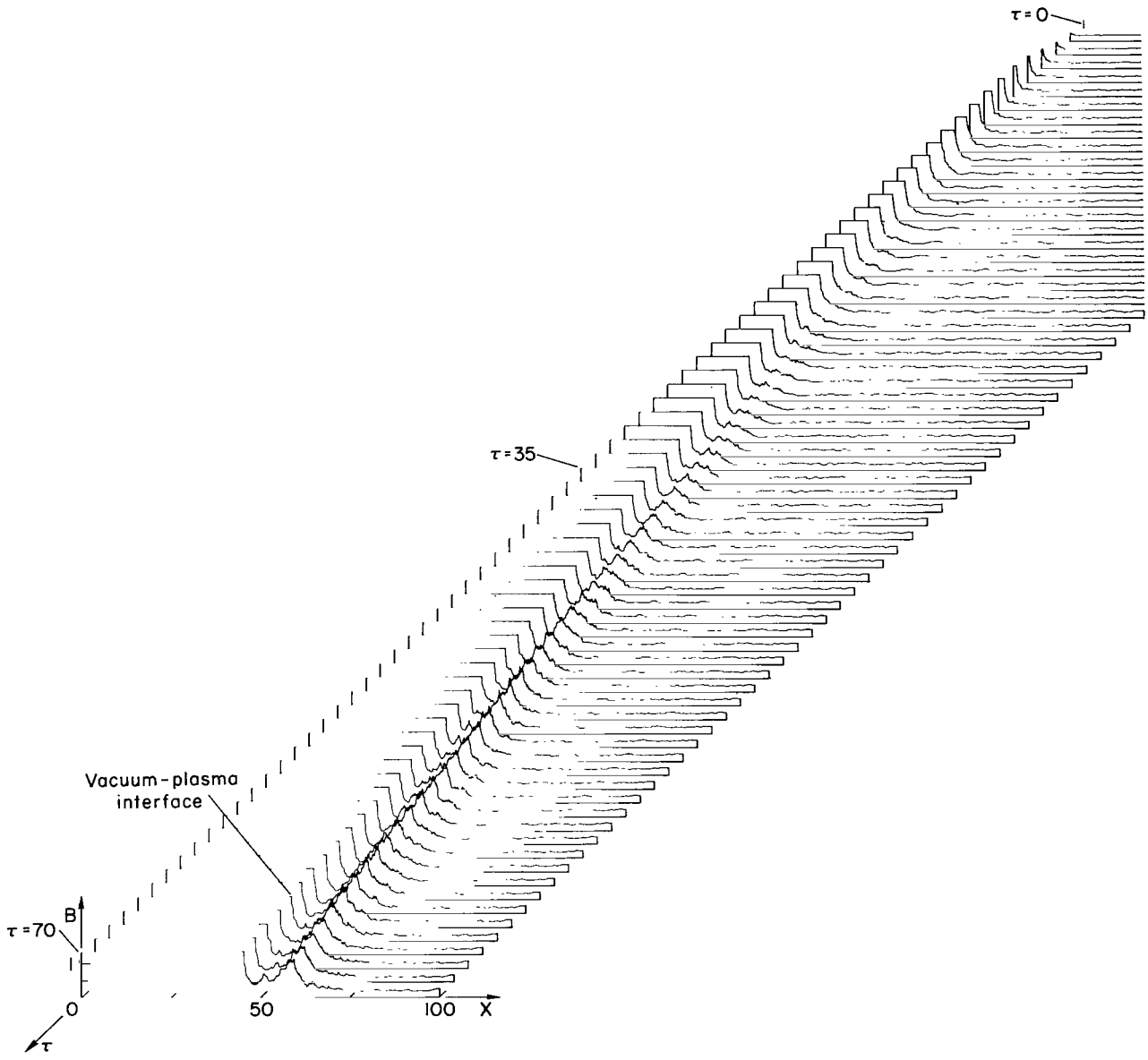

(a) Magnetic induction.

Figure 17.- Development of flow field with time for a strong disturbance moving into a warm plasma: $e_o = 1.0$, $b_o = 0.181$ ($b_o \sqrt{1 + \beta_e + \beta_i} = 0.2$; $M_A = 5.80$), $R = 25$, $\beta_g = 0.008$, $\beta_{eg} = 0.01$, $\beta_i = 0.2$, ΔX_k random, $\dot{X}_k$ random, $J_k = 0$.

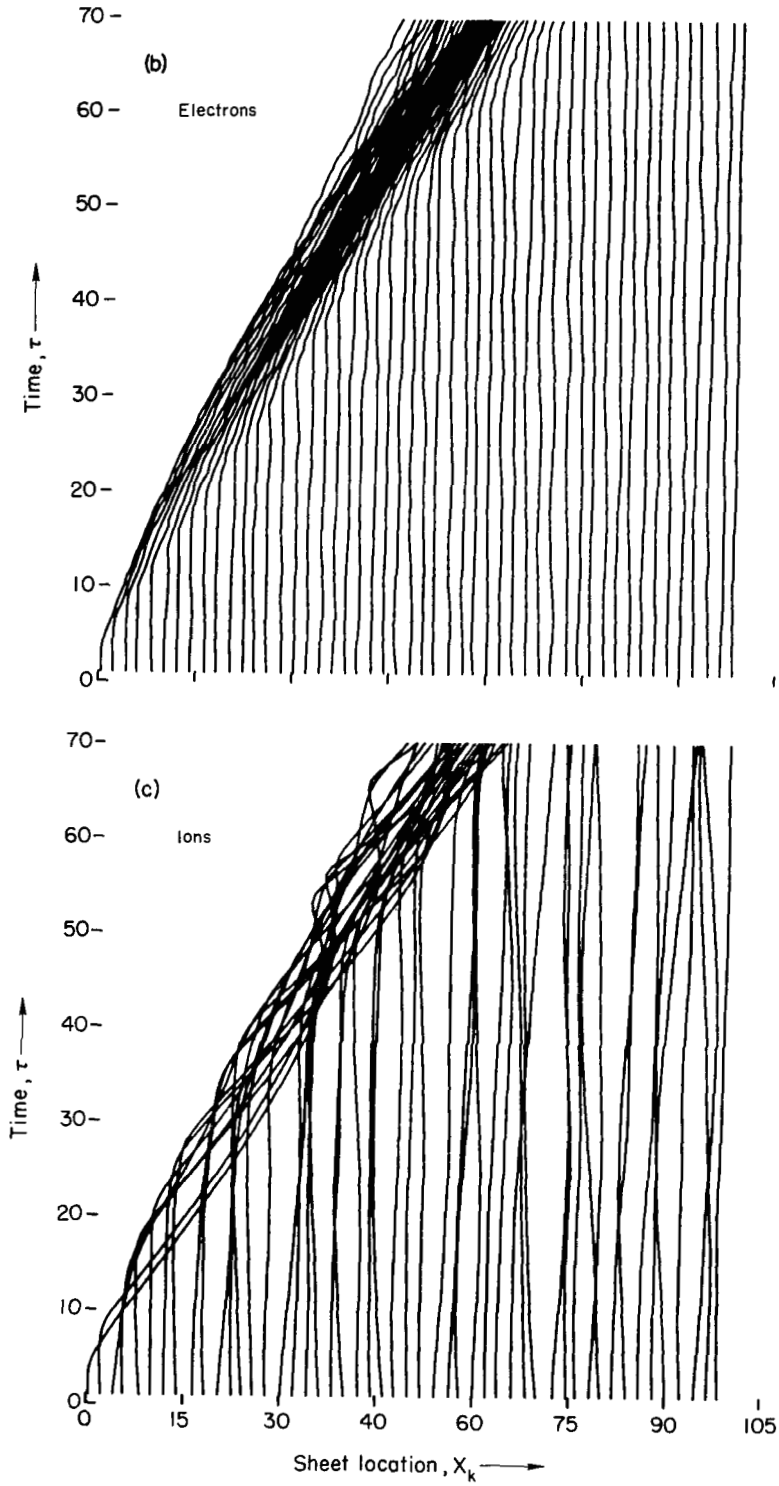

(b) Time-distance records of every tenth electron sheet; k = 1, 11, 21, . . .
(c) Time-distance records of every tenth ion sheet; k = 1, 11, 21, . . .

Figure 17.- Concluded.

NASA-Langley, 1964 A-829

"The aeronautical and space activities of the United States shall be conducted so as to contribute . . . to the expansion of human knowledge of phenomena in the atmosphere and space. The Administration shall provide for the widest practicable and appropriate dissemination of information concerning its activities and the results thereof."

—NATIONAL AERONAUTICS AND SPACE ACT OF 1958

NASA SCIENTIFIC AND TECHNICAL PUBLICATIONS

TECHNICAL REPORTS: Scientific and technical information considered important, complete, and a lasting contribution to existing knowledge.

TECHNICAL NOTES: Information less broad in scope but nevertheless of importance as a contribution to existing knowledge.

TECHNICAL MEMORANDUMS: Information receiving limited distribution because of preliminary data, security classification, or other reasons.

CONTRACTOR REPORTS: Technical information generated in connection with a NASA contract or grant and released under NASA auspices.

TECHNICAL TRANSLATIONS: Information published in a foreign language considered to merit NASA distribution in English.

TECHNICAL REPRINTS: Information derived from NASA activities and initially published in the form of journal articles.

SPECIAL PUBLICATIONS: Information derived from or of value to NASA activities but not necessarily reporting the results of individual NASA-programmed scientific efforts. Publications include conference proceedings, monographs, data compilations, handbooks, sourcebooks, and special bibliographies.

Details on the availability of these publications may be obtained from:

SCIENTIFIC AND TECHNICAL INFORMATION DIVISION

NATIONAL AERONAUTICS AND SPACE ADMINISTRATION

Washington, D.C. 20546